

**SYNTHESIS AND CATALYTIC ACTIVITY
STUDIES OF FUNCTIONALIZED
MESOPOROUS SILICA MATERIALS**

A THESIS
SUBMITTED TO THE
UNIVERSITY OF PUNE
FOR THE DEGREE OF
DOCTOR OF PHILOSOPHY
IN
CHEMISTRY

BY
LAKSHI SAIKIA

DR. D. SRINIVAS
RESEARCH GUIDE

CATALYSIS DIVISION
NATIONAL CHEMICAL LABORATORY
PUNE - 411 008, INDIA

MAY 2008

**....dedicated to my
beloved parents**



Dr. D. Srinivas
Catalysis Division
Tel: +91-20-2590 2018
Fax: +91-20-2589 3761
e-mail: d.srinivas@ncl.res.in

National Chemical Laboratory
Dr Homi Bhabha Road
Pune – 411 008, INDIA

CERTIFICATE

It is certified that the work incorporated in the thesis entitled “**Synthesis and Catalytic Activity Studies of Functionalized Mesoporous Silica Materials**”, submitted by **Mr. Lakshi Saikia**, for the degree of Doctor of Philosophy in Chemistry, was carried out by the candidate under my supervision in the Catalysis Division, National Chemical Laboratory, Pune – 411 008, India. Materials obtained from other sources have been duly acknowledged in the thesis.

Dr. D. Srinivas
Research Guide

DECLARATION

I here by declare that the thesis entitled “**Synthesis and Catalytic Activity Studies of Functionalized Mesoporous Silica Materials,**” submitted for the **Degree of Doctor of Philosophy** in Chemistry to the University of Pune, has been carried out by me at the Catalysis Division, National Chemical Laboratory, Pune - 411 008, India, under the supervision of **Dr. D. Srinivas**. The work is original and has not been submitted in part or full by me for any other degree or diploma to this or any other University.

Lakshi Saikia
Research Scholar

Acknowledgments

I find it very difficult to write something in short to acknowledge my research guide, Dr D. Srinivas. His constant inspiration, invaluable guidance and constructive criticism helped a lot to focus my views in proper perspective. I take this opportunity to express my intense reverence towards him for guiding me in the right direction throughout the course of this work. My deepest personal regards are due for him forever.

I take this opportunity to express my deepest sense of gratitude and reverence towards Dr. Paul Ratnasamy for his equally valuable discussions and suggestions throughout my research work.

I would like to express my profound gratitude to Dr. S. Sivasankar and Dr. Rajiv Kumar, former Heads of Catalysis Division for providing all facilities required for my work.

My heartfull thanks are due to Dr. C. V. V. Satyanarayana, Dr. S. B. Halligudi, Dr. S. P. Mirajkar, Dr. (Mrs.) S. A. Pardhy, Dr. (Mrs.) S. S. Deshpande, Dr. C. S. Gopinath, Dr. T. Raja, Dr. Subhangi Umberkar, Mrs. Nalini Jacob, Mr. R. K. Jha, Mrs. R. Parischa, Ms. Violet Samuel, Mr. Golap, Dr. Gaikwad, Dr. K.R. Patil and all other scientific and non-scientific staff of the Catalysis Division and NCL for their valuable help and cooperation during my tenure as a research student.

I sincerely thank all my friends especially Dr. Rajendra, Dr. Vasu, Dr. Venkatathri, Sreeprasanth, Jitendra, Rahul, Mufsir, Hamza, Dipak, Rajesh, Pranav, Sneha, Anuj, Rohit, Ganapati, Vijayraj, Maitri, Cimi, Madhu, Khirud, Manashda, Ranju, Pranjald, Ankur, Rahul, Sasankada, Gitali, Sofia, Pankaj, Nilesh, Dilip, Prasana, Srinivas, Prashant, Sangam, Swamy, Pai, Surekha, Sachin, Ganesh, Atul, Ramakant, Mahesh, Amit, Koteswer, Bhang, Pallavi, Suman, Ravindra, Baag Raghupathi, Prabhas, Sanjibda, Patil Ashish and many friends who helped me during this period of time.

It gives me great pleasure to acknowledge my parents, my brothers Munindra, Manik sisters Manisha, Pranita and sister in laws for the love, unflinching support, patience and encouragement during many years of my studies that they have shown to me in their own special way. I have no words to thank Parasha for her constant support, love and encouragement since I met her.

It is indeed my privilege to thank the Director, NCL, for allowing me this opportunity and extending all possible infrastructural facilities at NCL. Financial assistance from UGC-New Delhi is greatly acknowledged.

Lakshi Saikia

CONTENTS

Chapter–1: General Introduction	1
1.1. Mesoporous Silica Materials: General Background	2
1.2. Surface Modification of Mesoporous Silica Materials	3
1.3. Surface Modification by Grafting Techniques	5
1.3.1. Grafting with passive surface groups	6
1.3.2. Grafting with reactive groups	7
1.3.3. Site-selective grafting	7
1.3.4. Co-condensation grafting	9
1.4. Mesoporous Silicas as Supports	9
1.4.1. Immobilization of transition metal coordination compounds	10
1.4.1.1. Adsorption	10
1.4.1.2. Covalent Tethering	10
1.4.1.3. Ion Exchange (Electrostatic) Interaction	12
1.4.1.4. Direct Synthesis	13
1.5. Functionalization of Mesoporous Silica with Metal Oxides	13
1.6. A Brief Review of Catalytic Applications of Functionalized Mesoporous Silicas	13
1.7. Possible Catalytic Applications of Functionalized Mesoporous Silica Materials	14
1.7.1. Ring-opening of epoxides with amines and alcohols	14
1.7.2. Etherification of glycerol with tert-butanol	15
1.7.3. Esterification of carboxylic acid	15
1.7.4. Three-component Mannich reaction	16
1.7.5. Aerial oxidation of terpenes	16
1.7.6. Haloperoxidase activity	17
1.8. Scope of the Thesis	18
1.9. Outline of the Thesis	19
1.10. References	21
Chapter–2: Experimental Methodology	32
2.1. Introduction	33
2.2. Materials Preparation	34
2.2.1. Synthesis of SBA-15	34
2.2.2. Preparation of organo-functionalized SBA-15 materials	35
2.2.2.1. Preparation of SBA-15- <i>pr</i> -NH ₂	35
2.2.2.2. Preparation of SBA-15- <i>pr</i> -SH	35
2.2.2.3. Preparation of SBA-15- <i>pr</i> -SO ₃ H	36
2.2.3. Preparation of ‘neat’ Mn complexes	37
2.2.3.1. Preparation of Mn(Salen)Cl	37
2.2.3.2. Preparation of Mn(TPP)Cl complex	38
2.2.4. Preparation of grafted Mn(Salen)Cl	39
2.2.5. Preparation of grafted Mn(TPP)Cl	39

2.2.6.	Preparation of nanoscopic metal oxides supported on mesoporous silica	40
2.2.6.1.	Preparation of TiO _x -SBA-15	40
2.2.6.2.	Preparation of VO _x -SBA-15	40
2.2.6.3.	Preparation of MoO _x -SBA-15	41
2.2.6.4.	Preparation of WO _x -SBA-15	41
2.3.	Characterization Procedures	41
2.3.1.	X-ray powder diffraction (XRD)	41
2.3.2.	Diffuse reflectance UV-visible (DRUV-vis)	42
2.3.3.	Fourier transform infrared (FTIR)	43
2.3.4.	Laser Raman	43
2.3.5.	Electron paramagnetic resonance (EPR)	44
2.3.6.	X-ray photoelectron spectroscopy (XPS)	44
2.3.7.	Cyclic voltammetry (CV)	45
2.3.8.	Temperature-programmed desorption (TPD)	45
2.3.9.	Nitrogen adsorption/desorption	45
2.3.10.	Atomic absorption spectroscopy (AAS)	46
2.3.11.	Scanning electron microscopy (SEM)	47
2.3.12.	Transmission electron microscopy (TEM)	48
2.4.	Reaction Procedures	49
2.4.1.	Reactions over organofunctionalized SBA-15	49
2.4.1.1.	Regio- and stereoselective synthesis of β-amino alcohols	49
2.4.1.2.	Regioselective synthesis of β-alkoxy alcohols	49
2.4.1.3.	Etherification of glycerol	50
2.4.1.4.	Esterification of carboxylic acid	50
2.4.1.5.	Three-component Mannich reaction	50
2.4.2.	Chemo-, regio- and stereo-selective oxidation of terpenes over grafted Mn complexes	51
2.4.3.	Regiospecific oxyhalogenation of organics over SBA-15 supported metal oxide	51
2.4.3.1.	Oxybromination of phenol red	51
2.4.3.2.	Oxybromination of aromatics	52
2.4.3.3.	Oxyiodination of aromatics	53
2.4.3.4.	Oxychlorination of aromatics	53
2.5.	References	56

Chapter–3: SO₃H-functionalized SBA-15 as an Efficient Regio- and Stereoselective Solid Acid Catalyst **59**

3.1.	Introduction	60
3.2.	Experimental	61
3.2.1.	Material preparation and characterization	61
3.2.2.	Reaction procedure	62
3.3.	Results and Discussion	62
3.3.1.	Characterization	62
3.3.1.1.	Chemical composition	62
3.3.1.2.	XRD	63

3.3.1.3.	N ₂ adsorption-desorption	64
3.3.1.4.	FTIR spectroscopy	65
3.3.1.5.	Thermal stability	65
3.3.1.6.	²⁹ Si NMR	69
3.3.1.7.	TEM	71
3.3.1.8.	Scanning electron microscopy	72
3.3.1.9.	Acidity measurements	72
	3.3.1.9.1. NH ₃ -TPD	72
	3.3.1.9.2. Ion exchange capacity	73
3.3.2.	Catalytic activity	74
3.3.2.1.	Ring-opening of epoxides with amines and alcohols	74
	3.3.2.1.1. Aminolysis of epoxides	76
	3.3.2.1.1.A. Influence of Solvent	78
	3.3.2.1.1.B. Influence of reaction temperature	81
	3.3.2.1.1.C. Kinetic studies	82
	3.3.2.1.2. Alcoholysis of epoxides	82
	3.3.2.1.3. Mechanistic considerations	83
3.3.2.2.	Tert.-butylation of glycerol over SBA-15-pr-SO ₃ H	91
	3.3.2.2.1. Effect of temperature	94
	3.3.2.2.2. Effect of catalyst amount	95
	3.3.2.2.3. Time on steam and leaching study	95
	3.3.2.2.4. Comparative study with conventional Brønsted acidic catalysts	97
3.3.2.3.	Esterification of carboxylic acids	97
3.3.2.4.	Three-component Mannich reaction over SBA-15-pr-SO ₃ H	100
3.4.	Conclusions	103
3.5.	References	103

Chapter–4: Chemo-, Regio- & Stereoselective Oxidation of Terpenes over Mn Complexes Grafted on SBA-15 111

4.1.	Introduction	112
4.2.	Experimental	114
	4.2.1. Material synthesis and characterization	114
	4.2.2. Reaction procedure – aerial oxidation of monoterpenes	115
4.3.	Results and Discussion	116
	4.3.1. SBA-15-grafted Mn(Salen)Cl complexes	116
	4.3.1.1. Chemical analysis	116
	4.3.1.2. Low-angle XRD	117
	4.3.1.3. N ₂ adsorption/desorption	118
	4.3.1.4. TEM and SEM	121
	4.3.1.5. FTIR Spectroscopy	122
	4.3.1.6. DRUV-vis	124

4.3.1.7.	EPR	125
4.3.1.8.	Cyclic voltammetry	126
4.3.1.9.	Thermal stability	127
4.3.2.	Grafted Mn(TPP)Cl complexes	127
4.3.3.	Catalytic activity studies	135
4.3.3.1.	Oxidation of limonene	135
4.3.3.1.1.	SBA-15-grafted Mn(Salen)Cl complexes	135
4.3.3.1.2.	SBA-15-grafted Mn(TPP)Cl complexes: Oxidation of limonene	142
4.3.3.2.	Oxidation of α -pinene and carene	145
4.3.4.	Structure-activity correlations	147
4.4.	Conclusions	152
4.5.	References	153

Chapter–5: Regiospecific Oxyhalogenation of Aromatics over SBA-15-supported Nanoscopic Metal Oxides **156**

5.1.	Introduction	157
5.2.	Experimetal	158
5.3.	Results and Discussion	159
5.3.1.	Structural and spectroscopic characterization	159
5.3.1.1.	XRD	159
5.3.1.2.	N ₂ adsorption/desorption	159
5.3.1.3.	HRTEM and SEM	163
5.3.1.4.	FTIR	163
5.3.1.5.	DRUV-vis	165
5.3.1.6.	Laser Raman spectroscopy	167
5.3.1.7.	XPS	169
5.3.2.	Catalytic activity studies	171
5.3.2.1.	Oxybromination of phenol red	171
5.3.2.2.	Oxyhalogenation of aromatics	174
5.3.2.2.1.	Oxyiodination	174
5.3.2.2.2.	Oxybromination	177
5.3.2.2.3.	Oxychlorination	180
5.3.2.2.4.	Catalyst reusability	183
5.3.2.2.5.	Spectroscopic evidence for peroxidative mechanism	184
5.4.	Conclusions	186
5.5.	References	186

Chapter–6: Summary and Overall Conclusions **189**

LIST OF ABBREVIATIONS

AAS	Atomic absorption spectroscopy
acac	Acetyl acetonate
APTMS	3-Aminopropyl trimethoxysilane
BE	Binding energy
BET	Braunauer-Emmett-Teller
BJH	Barrett-Joyner-Halenda
CP-MAS	Cross polarization magic angle spinning
CPTS	3-Chloropropyltriethoxysilane
CV	Cyclic voltammetry
DMF	N,N-dimethyl formamide
DR UV-Vis	Diffuse reflectance ultraviolet visible
DTA	Differential thermal analysis
EPR	Electron paramagnetic resonance
ETBE	Ethyl tertiary-butyl ether
FSM	Folded sheet materials
FTIR	Fourier transform infrared
GC	Gas chromatography
GC-MS	Gas chromatography-mass spectroscopy
HEPES	(4-(2-Hydroxyethyl)-1-(piperazineethanesulfonic acid)
HMS	Hexagonal mesoporous silica
HRTEM	High-resolution transmission electron microscopy
IAA	Iso-amyl alcohol
ISR	Integrated sphere attachment
MAS NMR	Magic angle spinning nuclear magnetic resonance
MCM	Mobil crystalline material
MPTMS	3-Mercaptopropyl trimethoxysilane
MTBE	Methyl tertiary-butyl ether
NBA	N-bromoacetamide
NBS	N-bromosuccinimide
N-MeIm	N-methylimidazole
pr	Propyl
py	Pyridine

Salen	N, N-ethylenebis(salicylideneamine)
SBA	Santa barbara amorphous
SEM	Scanning electron microscopy
TAME	Tertiary amyl methyl ether
TEM	Transmission electron microscopy
TEOS	Tetraethyl orthosilicate
TGA	Thermogravimetric analysis
TOF	Turnover frequency
TPA	Tungstophosphoric acid
TPAOH	Tetrapropylammonium hydroxide
TPP	Tetraphenylporphyrin
TS	Titano silicate
XPS	X-ray photoelectron spectroscopy
XRD	X-ray diffraction

CHAPTER – 1
General Introduction

1.1. Mesoporous Silica Materials: General Background

In view of the industrial relevance and intrinsic scientific interest in their structural complexity and diverse chemistry, considerable efforts have been made, in the past several years, in the synthesis of templated porous solids [1 - 3]. Mesoporous silica prepared by numerous templating approaches opened a new era of solid materials that exceed the pore size limitation of zeolites and other microporous materials. The M41S type materials discovered by the researchers at Mobil Corporation, USA and FSM-16 by the Japanese researchers are first kind of well-characterized mesoporous silica materials [4]. A remarkable enhancement in the synthesis of ordered mesoporous silicas was attained when it was discovered that organic oligomers and polymers are facile supramolecular templates. Inexpensive polymeric templates, which can be readily recovered and recycled, provide vast opportunities in pore size and pore structure engineering [5].

Stucky and co-workers [6] have made a remarkable contribution to the synthesis of polymer-templated ordered porous oxides by using triblock copolymers and non-ionic oligomeric surfactants in acidic media to obtain mesoporous silicas with several different ordered porous structures. Hexagonally ordered mesoporous SBA-15 is the most prominent member of the family of block copolymer templated materials [6]. In particular, poly-(alkylene oxide) triblock copolymers are good structure directing agents due to their mesostructural ordering properties, amphiphilic character, low-cost commercial availability, and biodegradability [6]. SBA-15 can be synthesized over a range of reaction mixture compositions and conditions. It possesses adjustable large uniform pore sizes up to approximately 30 nm combined with thick hydrothermally stable

silica walls, different from the thinner-walled MCM-41 structures made with conventional cationic surfactants – alkyl trimethylammonium halide. Moreover, SBA-15 is a material that has the benefit of a combined micro and mesoporosity together evidenced by N₂ adsorption-desorption and transmission electron microscopic studies [7]. New investigations on different aspects of these materials, such as synthesis procedures and mechanisms, heteroatom insertion, stability, surface modification, physicochemical characterization, adsorption, catalytic applications etc., create an explosion in materials research [2, 8].

1.2. Surface Modification of Mesoporous Silica Materials

Surface modification allows tailoring the surface properties for potential applications in the areas of catalysis, separation technology, chemical sensors, electronic devices and drug delivery [9 – 15]. The open frameworks, controllable structures, tunable porosities and high surface areas endow mesoporous materials with accessibility to bulkier reagents. In spite of the favorable pore dimensions, the acidity of Al-substituted mesoporous materials such as Al-MCM-41 is much weaker than that of microporous zeolites [2, 12]. However, alkyl sulfonic acid functionalized mesoporous materials overcome this drawback. The inorganic part (polymeric silicate framework) of the surface modified hybrid mesoporous materials provides structural, thermal and mechanical stability whereas the pendent organic species permit flexible control of interfacial and bulk properties. Mesoporous materials are, in general, hydrophilic because of the surface hydroxyl (Si-OH) groups. Organo-functionalization modifies the surface properties making them relatively more hydrophobic. The hydrophobic nature of the

active sites' environment can be exploited to perform reactions, which are outside the reach of the other inorganic solid acid catalysts.

Organo-functionalization of the internal surfaces of mesoporous silicates can be achieved either by covalent grafting of various organic moieties onto the channel walls or by incorporating functionalities directly during the synthesis [16]. The grafting process has been widely applied to anchor desired organic functional groups via condensation with surface silanol groups of the mesoporous silicate. However, it is somewhat difficult to control the concentration and distribution of organic moieties on the silicate surface mainly due to non-uniform presence of silanol groups in different mesoporous samples. Another phenomenon to be taken into consideration is the greater accessibility of the silanol groups even on the external surface towards functionalization. This grafting on the external surface can, however, be minimized by passivating the external silanol groups before functionalization of those on the internal surface [34].

The presence of organo-functionalized moieties as part of the silica wall structure can be confirmed from solid-state ^{29}Si magic angle spin nuclear magnetic resonance (MAS NMR). Distinct resonances can be clearly observed for the siloxane $[\text{Si}(\text{OSi})_n(\text{OH})_{4-n}]$, $n = 2 - 4$; Q^3 at -100 and Q^4 at -110 ppm] and organosiloxane $[\text{Rsi}(\text{OSi})_m(\text{OH})_{3-m}]$, $m = 1 - 3$; T^3 at -65 and T^2 at -57 ppm] units. The relative integrated intensity ^{29}Si MAS NMR signals of organosiloxane and siloxane (T^m/Q^n) allows calculation of the degree of incorporation of organic moieties. The organic part of ordered sulfonic-functionalized materials can also be investigated by ^{13}C CP-MAS NMR spectroscopy [12]. The presence of amine, thiol, and sulfonic acid functionality can also be confirmed by Fourier transform infrared (FTIR) spectroscopy technique. The characteristic

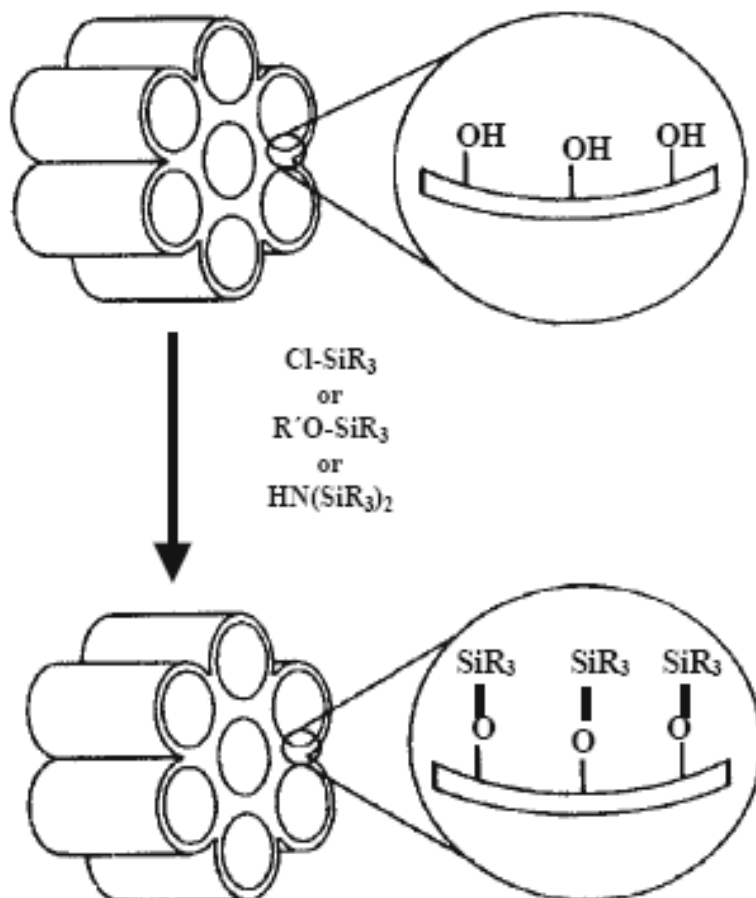
stretching frequency of the N-H of primary amines appears at 3300-3500 cm^{-1} and presence of thiol group can be confirmed from the S-H stretching band at 2575 cm^{-1} [16, 17].

The direct synthesis approach is based on the co-condensation of one tetraalkoxysilane with one or more trialkoxyorganosilane precursors in a templating environment. The tetraalkoxysilane precursor acts as a building block to create the mesoporous silicate framework, whereas the trialkoxyorganosilanes function as both framework silicate units and pendent organic functional groups [18]. The most frequently encountered problem in this method is the relatively faster hydrolysis of the organosilane precursor and its self-condensation. However, this problem can be circumvented using a suitable solvent in the synthesis gel to reduce and control the faster hydrolysis [19]. This one-step synthesis procedure can produce mesoporous silicates with high loading and homogeneous surface coverage of organic functional groups. However, in the direct synthesis approach, organic functional groups may be damaged or destroyed during the template removal process; the secondary silylation technique (grafting technique) seems to offer a better alternative for preparing mesoporous acid catalysts.

1.3. Surface Modification by Grafting Techniques

The post synthesis modification enables a stable covalent bonding between an organic functional group and the surface silanols of the mesoporous silica materials [20, 21]. In most cases, the functional group is separated from the silica surface by an organic “spacer”. This allows the active sites as stated by Prof. J.M. Thomas in his poetical words “to flutter in the molecular breeze during the process of catalytic conversion” [11]. A typical surface modification by silylation is depicted in Scheme 1.1 [9]. The

concentration of surface silanol groups required for grafting with organic functionalities altered by prior treatment of calcined mesoporous silica with boiling water [22], steam [23], or by acid hydrolysis [24].



Scheme 1.1. Grafting of organo silanes on mesoporous silica surface.

1.3.1. Grafting with passive surface groups

Organic functional groups with lower reactivity could be grafted to enhance the hydrophobicity of the surface and protecting the material towards hydrolysis. Further, the pore diameter of mesoporous materials can also be adjusted by varying the alkyl chain length of the silylating agent or by increasing the quantity of the silylating agent [26].

The commonly used surface modifying agents are the trimethyl chlorosilane (Me_3SiCl), trimethyl ethoxysilane ($\text{Me}_3\text{Si}(\text{OC}_2\text{H}_5)$) and hexamethyldisilazane [$(\text{Me}_3\text{Si})_2\text{NH}$] [20, 27]. Hexamethyldisilazane functionalization is widely used to quantify the number of surface silanols, to passivate the surface silanols and also to depolarize the surface for selective adsorption experiments [27(a, b)].

1.3.2. Grafting with reactive groups

Grafting of the mesoporous silica surfaces with organic units containing reactive functional groups like olefin, cyanide, thiol, amide, halide, etc permits further functionalization of the surface as their terminal end contains a reactive functional group. For instance, modification of these reactive materials includes hydroboration [28] and bromination of olefins [29], hydrolysis of cyanide to carboxylic acids, [30], oxidation of thiols to sulphonic acids, [31] nucleophilic substitution of amines and halides [18(a)]. After, modification of these materials with the desired functionalities, catalytically active homogenous transition metal complexes as well as organometallic complexes can be anchored over these organic-inorganic hybrid materials. For instance, the functionalization of $\text{Mn}(\text{Salen})\text{Cl}$ complex to surface-modified MCM-41 containing 3-chloro propyl silane (3-CPTS) is feasible by the nucleophilic replacement of the halogen atom [33].

1.3.3. Site-selective grafting

The external surface silanols of the mesoporous materials are kinetically more accessible than the internal surface silanols. Hence, in order to minimize the grafting of reactive surface sites on the external surface and thereby to utilize the inner pore channels, it is necessary to passivate the external silanol groups before functionalizing on

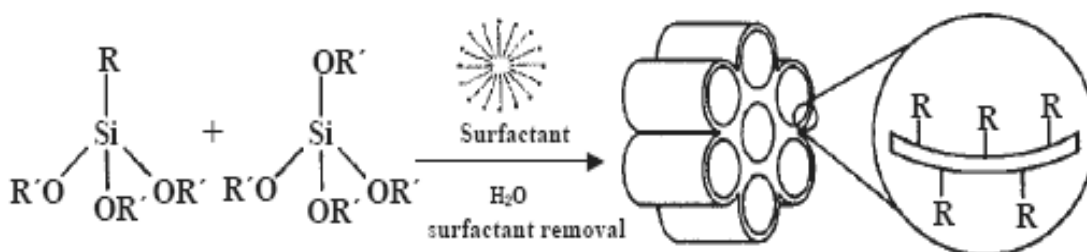
the internal surfaces [34]. Shepherd *et al.* had passivated the external surface of the MCM-41 surface with dichlorodiphenyl silane (Ph_2SiCl_2) first and then 3-aminopropyl triethoxy silane (3-APTS) was grafted over the internal channels for the heterogenization of an active ruthenium cluster. The existence of amine functional groups in the inner pore channels of MCM-41 was confirmed by the high-resolution transmission electron microscopy (HRTEM) [35].

Another approach effectively utilized was the template ion exchange property, for the grafting of Me_3SiCl , without removing the surfactants from the pore channels. The advantage of this method is that this procedure avoids the two-step synthesis and that the grafting exclusively occurs in the external surfaces due to the steric constraint of the surfactants [36]. Following solvent extraction, for the removal of surfactant groups, the internal surface of the materials is free for further modifications while the external surface is passivated.

In another way, Antochshuk and Jaroniec [37] carried out simultaneous grafting and extraction of template molecules by modification of uncalcined MCM-41 with trialkylchlorosilanes. As-synthesized MCM-41 was refluxed in neat trialkylchlorosilane, first by itself, and then with added anhydrous pyridine, followed by multiple washing with different solvents, leading to surfactant-free mesoporous products [37]. The loading of surface organic groups exceeded that on calcined supports that were otherwise treated in a similar way. The advantages of this method include the increased concentration of surface hydroxyl groups and the decreased reduction in pore size of the materials, as this procedure avoids the high temperature calcination processes for the removal of surfactant groups.

1.3.4. Co-condensation grafting

In the grafting methods, incorporation of organic groups is done by attachment of the organosiloxane precursor with surface Si-OH groups through Si-O-Si-C covalent bond formation (Scheme 1.1). Then Si-O can be cleaved at some reaction conditions as experienced by Price *et al.* [38]. Therefore, in some cases it would be desirable to have direct formation of a C-Si (surface) covalent bond. Thus, the “one-pot” co-condensation method, where condensation occurs between a tetraalkoxysilane and one or more trialkoxyorganosilanes through sol-gel chemistry, seems to have distinct advantages over the grafting methods (Scheme 1.2.) [39]. Several research groups have employed this method to prepare inorganic-organic hybrid mesoporous materials under a wide range of synthesis conditions [40]. Usually the solvent extraction technique is used to remove the surfactant from the resultant materials.



Scheme 1.2. Synthesis of organic-inorganic hybrid mesoporous silicates by co-condensation/direct synthesis approach.

1.4. Mesoporous Silicas as Supports

The ordered hexagonal SBA-15, MCM-41 and cubic MCM-48 materials possess narrow and controlled pore size distribution and large pore openings, which has stimulated fundamental research in inclusion of metal [47], metal oxide [48] and semiconductor nanoclusters [49], and metal complexes [50, 51], inside the mesoporous channels. The

reactivity of the internal surfaces of mesoporous silica has been widely exploited by anchoring of several organic functional groups on the channel walls, as discussed in the previous section. These functional groups can act as ligands to form bulky metal complexes [50], and also can act as capping agents for nanoclusters in order to stabilize them inside the network [47(e)].

1.4.1. Immobilization of transition metal coordination compounds

Several approaches have been used to immobilize coordination compounds on mesoporous silica surfaces. An outline of these approaches will be discussed below.

1.4.1.1. Adsorption

Ligands containing a sulfonic acid functional group can be adsorbed onto silica surfaces through hydrogen bonding interactions with the surface silanol groups (Fig. 1.1). Following this strategy, Bianchini et al. [52] have immobilized rhodium(I)-norbornadiene (RhI-nbd) complexes through a sulfonate-functionalized chiral diphosphine ligand hydrogen-bonded to silica surface. De Rege et al. [53] have immobilized a RhI-diphosphine complex containing a trifluoromethanesulfonate (triflate) counter ion [53]. Several research groups have reported adsorption of complexes of platinum group metals onto hexagonal mesoporous silica surfaces functionalized with propylamine moiety (Fig.1.2.) [54]. The adsorption methodologies are comparatively easier than the other strategies, but are likely to produce less stable composite materials.

1.4.1.2. Covalent tethering

The covalent tethering techniques were widely investigated to design stable hybrid materials. Ligands containing –OH, –NH₂ groups can be grafted directly onto the

silica surface, pre-functionalized with a propylhalide group, through a nucleophilic substitution mechanism (Scheme 1.3.) [55].

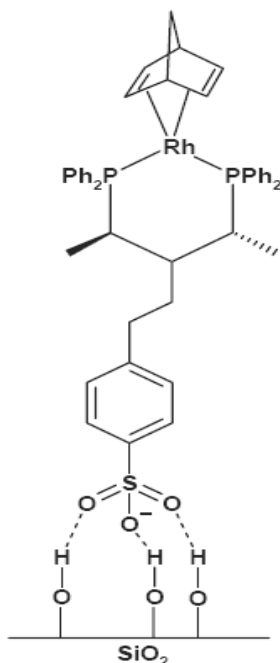


Fig. 1.1. Immobilization of RhI[(*R,R*)-BDPBzPSO₃] complex on mesoporous silica by hydrogen bonding interactions

Using this approach, several ligands such as amino alcohols [56] or diamines were anchored into the surfaces of chloropropyl-functionalized MCM-41 before complexation with the desired metal ion. A few metal–Salen complexes were also immobilized on aminopropyl-functionalized MCM-41 following similar strategy, as demonstrated by Baleizao *et al.* [57] and Kim and Park [58]. Complexes containing ligands like bisoxazoline [59], ferrocenyl [60] etc., and the Sharpless catalyst system [61] were modified by trialkoxysilane moieties, so that they could be grafted via condensation with the surface silanol groups. A similar strategy was used in the present study for the

grafting of Mn(Salen)Cl complexes on amine, thiol and sulfonic acid functionalized SBA-15.

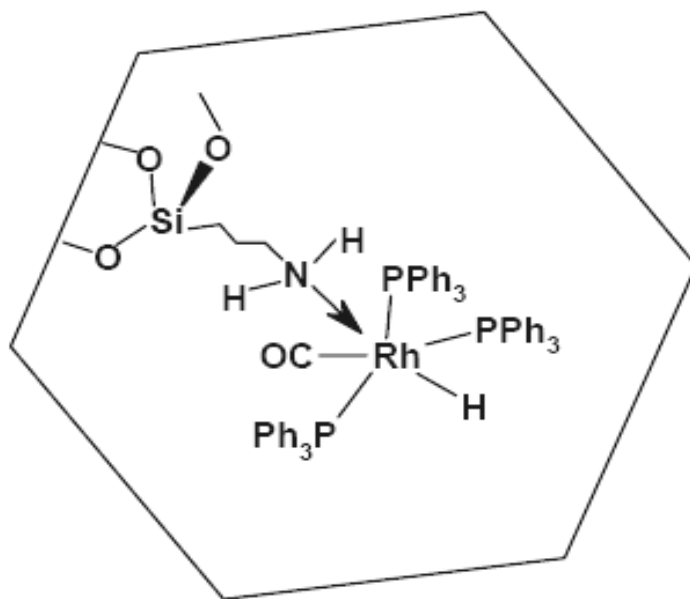
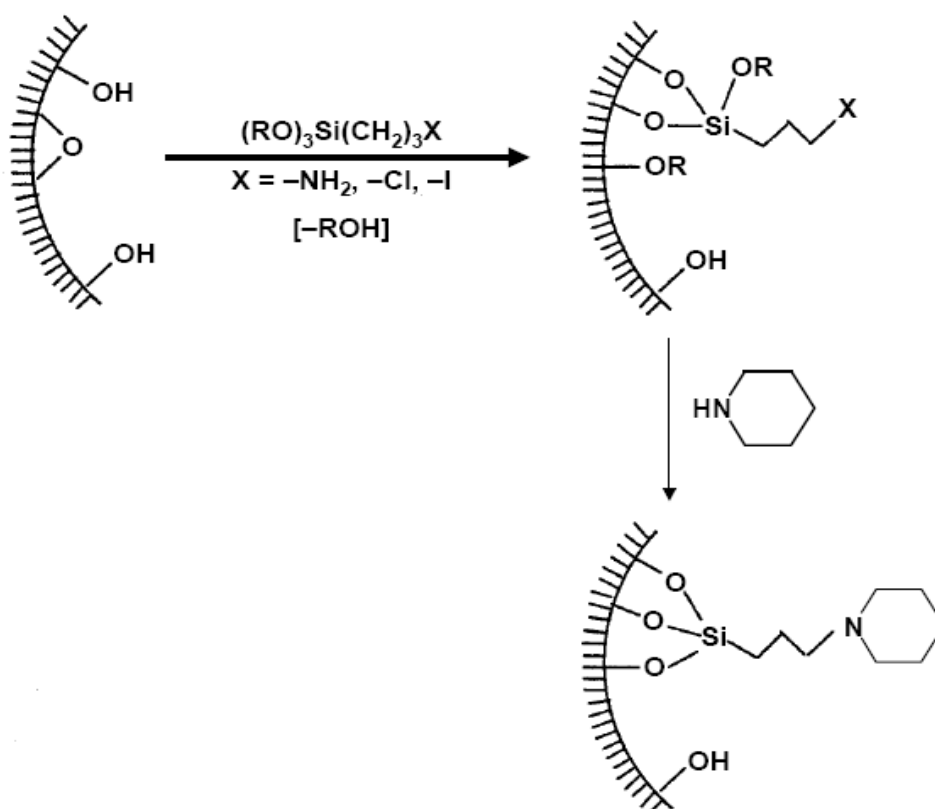


Fig.1.2. Adsorption of Wilkinson's catalyst on mesoporous silica.

1.4.1.3. Ion-exchange (electrostatic) interaction

A large number of metal complex cations can be immobilized through electrostatic interactions utilizing the existence of extraframework cations on ordered mesoporous silica materials. This ion exchange method is conceptually simple and has been observed to produce stable hybrid materials. Copper pyridine $[\text{Cu}(\text{py})_4]^{2+}$ complexes were the first to be incorporated inside the mesoporous network by ion exchange [62]. Later on, a series of cationic diphosphine [63] and bisoxazoline [64] chelate complexes were ion-exchanged inside the porous network.



Scheme 1.3. Anchoring of piperidine moiety on inner surfaces of mesoporous silica by nucleophilic substitution.

1.4.1.4. Direct synthesis

Hoppe et al. [65] were the first to introduce metal phthalocyanine complexes directly into the mesoporous MCM-41 by adding them into the synthesis gel and hydrothermal treatment thereafter.

1.5. Functionalization of Mesoporous Silica with Metal Oxides

Supported metal oxides are an important family of catalysts used in the petrochemical and refining industry. Catalytic reactions, such as ethylene polymerization, alkane oxidative dehydrogenation, alkene metathesis, and selective catalytic reduction of Nox with ammonia, occur on supported metal oxides [66-72]. Supported cobalt catalysts

have been found to be particularly efficient in the production of higher hydrocarbons from synthesis gas via Fischer-Tropsch reaction [73]. High surface area carriers lead to higher levels of metal dispersion and thereby higher catalytic activities [74].

1.6. A Brief Review of Catalytic Applications of Functionalized Mesoporous Silicas

Sulfonic acid functionalized MCM-41 and HMS showed high catalytic activity for the synthesis of 2,2-bis(5-methylfuryl)propane from 2-methylfuran and acetone [75]. Das et al [18 (a), 76] and Yang et al [77] reported that condensation of phenol and acetone at relatively low temperatures yields bis-phenol-A with very high selectivity over sulfonic acid functionalized MCM-41. Mesoporous silica supported sulfonic acids were found to be more selective than homogeneous and common solid acid catalysts. Shen et al and others [78-80] found higher catalytic activity for ether formation (dimethyl isobutyl ether and dimethyl ether) in alcohol coupling reactions at high pressures than other inorganic solid acid catalysts. These catalysts were investigated also for selective acetalization [81, 82], Prins condensation [83], Biginelli reactions [84], aromatization [85], Fries rearrangement [86] and Friedel Crafts acylation [87, 88] reactions. Esterification of fatty acids with alcohols [89-98] and synthesis of monoglycerides from fatty acids and glycerol [99, 100] were reported over these catalysts. Hydrophobic environment of the active sites in sulfonated mesoporous silicas was efficiently utilized in the dehydration of xylose into furfural [101] and hydrolysis of sugars [102]. A catalyst containing primary amine groups in combination with carboxylic acid groups (with similar chemical functionalities to proline) was reported to show superior catalytic activity in aldol condensation reaction with a number of different electrophilic components [103]. Chiral

Mn(Salen) complexes immobilized in porous silica materials via phenyl sulfonic group showed remarkably higher ee values (up to 95%) for asymmetric epoxidation of unfunctionalized olefins [104, 105].

1.7. Possible Catalytic Applications of Functionalized Mesoporous Silica Materials

1.7.1. Ring-opening of epoxides with amines and alcohols

The three-membered heterocyclic ring of an epoxide is strained and is susceptible to attack by a range of nucleophiles including nitrogen (ammonia, amines, azides), oxygen (water, alcohols, phenols, acids) and sulfur (thiol)-containing compounds leading to bifunctional molecules of great industrial value. The classical synthesis of β -amino alcohol involves the ring opening of epoxides with amines. These reactions are, conventionally, carried out with a large excess of the amine at elevated temperatures and in the presence of solvents [106]. A variety of catalyst systems such as sulfamic acid, amberlyst resin, metal triflates, transition metal halides, ionic liquids, zeolites and Lewis acids in a supercritical carbon dioxide medium have been investigated [82-89], but all those need long reaction time, elevated temperature, high pressure and stoichiometric amounts of catalysts. Garcia et al [107] reported the use of zeolite-Y for the reaction between styrene oxide and n-propanol, which gave conversions of 5-10%. In addition, many secondary products were also formed. The discovery of an efficient solid catalyst for these reactions will contribute to the eco-friendly manufacture of many pharmaceuticals and agrochemicals. Acid-functionalized SBA-15 would be ideal catalysts for the synthesis of β -amino and alkoxy alcohols by the reaction of epoxies with amines and alcohols, respectively.

1.7.2. Etherification of glycerol with tert-butanol

The preparation of the alkyl ethers of glycerol by etherification with tert-butyl alcohol (or isobutylene, C₄-fraction, respectively) in the presence of the acid catalyst is one of the possibilities of the glycerol utilization. A mixture of mono-, di-, and tri-alkyl glycerol ethers is produced and these ethers, especially the di and tri-alkyl glycerols are the most suitable as oxygenate additives to diesel and biodiesel fuels [108]. Addition of these ethers has a positive influence on the quality of final diesel fuel. Their presence decreases the particulate matter emissions, carbon oxide, and carbonyl compounds in exhaust gases [109, 110]. Moreover, glycerol ether oxygenates can decrease the cloud point (CP) when combined with biodiesel [111]. Acid-functionalized SBA-15 materials will have an edge over zeolite catalysts in glycerol etherification reactions due to the bulkier sizes of glycerol and its ether products.

1.7.3. Esterification of carboxylic acid

Esters are generally used as plasticizers, solvents, perfumery, fragrant chemicals and precursors for a wide range of pharmaceuticals, agrochemicals and fine chemicals [112]. Esterification of isoamyl alcohol with acetic acid has been studied using tungstophosphoric acid supported on different carriers such as silica, carbon, alumina, Al-MCM-41 and cation-exchange resin-Purolite CT-175 under vapor and liquid phase conditions [113-115]. Sulfonic acid-functionalized SBA-15 could be ideal alternatives to the reported catalysts for this transformation.

1.7.4. Three-component Mannich reaction

Carbon–carbon bond forming reactions continue to be the central focus of research in synthetic organic chemistry [116]. Among them, the Mannich-type reaction,

which gives β -amino carbonyl compounds in a single-step, is of considerable importance for synthesizing biologically attractive molecules containing nitrogen atom [117]. Therefore, the development of new synthetic methods leading to β -amino carbonyl compounds or their derivatives has attracted much attention. However, the classic Mannich reaction has limited applications. To overcome the drawbacks of the classical method, numerous modern versions of the Mannich reaction using preformed electrophiles, such as imines and stable nucleophiles, such as enolates, enol ethers, and enamines [118] have been developed. But the preferred route is to use a one-pot three-component strategy that gives a wide range of structural variations. However, most known catalysts suffer from drawbacks of difficult separation after the reactions and thereby they are not reusable. Furthermore, some of them are corrosive and volatile and often cause the environment problems. The application of organo-functionalized SBA-15 has not been investigated for this reaction.

1.7.5. Aerial oxidation of terpenes

Limonene is a key raw material in the synthesis of pharmaceuticals, fragrances, perfumes and food additives. Conventional manufacturing processes utilizing stoichiometric amounts of peroxides are not eco-friendly. With most of the known solid catalysts [119, 120], allylic oxidation (yielding carveol and carvone) predominates over olefinic oxidation (yielding the desired epoxides). Additionally, limonene is an ideal molecule to study chemo, region and stereoselective oxidations. One of the major challenges is develop an efficient solid catalyst for selective oxidation of organic substrates. SBA-15-functionalized Mn complexes can prove as efficient, solid catalysts for selective oxidation of terpenes via Mukaiyama type oxidation reaction.

1.7.6. Haloperoxidase activity

Haloperoxidases are enzymes that catalyze the oxidation of a halide ion by hydrogen peroxide. They are classified according to the most electronegative halogen oxidized. Thus chloroperoxidases can oxidize chloride, bromide and iodide, while bromoperoxidases oxidize only bromide and iodide. These enzymes are involved in the biosynthesis of many halogenated marine natural products like terpenes, indoles, phenols etc. Manufacture of dyes, flame-retardants, pharmaceuticals, agrochemicals, and many other products involve bromination [121]. Conventionally, bromination reactions are done using molecular bromine, which is a pollutant and hazardous reagent. Stoichiometric brominating reagents such as N-bromosuccinimide, N-bromoacetamide and bromodimethylsulfonium bromide are expensive and generate large amounts of organic waste [121]. It is postulated that bromoperoxidases generate Br^+ ions in-situ from H_2O_2 and bromide salts, which are then used in halogenation of an organic compound [122]. There have been a few reports on the use of homogeneous metal complexes and solid catalysts. However, development of an efficient, reusable solid catalyst for oxyhalogenation of aromatics is still a challenging task.

1.8. Scope of the thesis

The surface modification of SBA-15 by reactive organic and inorganic functional groups allows preparation of multifunctional molecular sieves. The objective of this study is to prepare such mesoporous, functional materials and to explore their application in selective catalytic transformation of organic molecules, at ambient conditions, in a range of reactions.

In view of the above, three-sets of surface-modified SBA-15 materials have been investigated. The first-set consists of SBA-15 modified with organo-acidic (propyl thiol and propyl sulfonic acid) and basic (propyl amine) moieties. The second-set consists of Mn complexes grafted on organo-functionalized SBA-15. The third-set composes of nanocrystalline metal oxides supported on SBA-15. Catalytic activities of the first-set have been investigated in ring-opening of epoxides with amines and alcohols, esterification, three-component-Mannich reactions and cycloaddition of CO₂ to epoxides. The second-set is evaluated for chemo-, regio- and stereoselective aerial oxidation of monoterpenes (R-(+)-limonene, α -pinene and 3-carene) at ambient conditions. TiO_x, VO_x, MoO_x and WO_x supported on SBA-15 are evaluated for oxyhalogenation of aromatic compounds at mild conditions. In all these studies emphasis is given for selective catalytic transformation over these materials. The formation, purity, characteristics and reaction mechanism have been investigated using a range of physicochemical techniques.

1.9. Outline of the thesis

The thesis is divided in six chapters. **Chapter 1** provides a general introduction and historical background to functionalized mesoporous silica materials and their catalytic application in various organic transformations.

Chapter 2 describes the synthesis methodologies of various functionalized SBA-15 materials used in this work and physicochemical characterization and reaction procedures.

Chapter 3 deals with propyl-thiol and sulfonic acid functionalized SBA-15 and their application in various acid-catalyzed reactions. These materials are prepared by the

grafting technique. They are characterized by X-ray powder diffraction, N₂ physisorption, transmission electron microscopy, thermal analysis and acidity measurements (temperature-programmed desorption of ammonia and ion-exchange studies). They are found to be efficient and selective in ring opening of epoxides with amines and alcohols, etherification of glycerol, esterification of carboxylic acid and three-component Mannich reactions at ambient temperatures and in solvent-free conditions. Possible mechanisms for regio- and stereoselective aminolysis and alcoholysis of epoxides are examined.

Chapter 4 presents the synthesis, characterization and selective catalytic oxidation properties of Mn-Salen and tetraphenylporphyrin (TPP) complexes grafted on propylamine, propylthiol and propylsulfonic acid functionalized SBA-15. The acid-basic properties of the support have influenced the molecular and electronic structure and thereby the catalytic oxidation property of the Mn complexes. Supports with acid functionalities reduced Mn ions from +3 to +2 oxidation state. Correlations between electronic properties and catalytic activity in chemo, regio and stereoselective oxidation of monoterpenes have been investigated. Also the mechanism of oxidation of terpenes over the grafted Mn complexes has been studied.

Chapter 5 describes the regioselective oxyhalogenation of aromatics over SBA-15-supported nanocrystalline tungsten, molybdenum, titanium and vanadium oxides. These materials have been prepared by the post-synthetic methodology. Nanocrystallinity and dispersion the metal oxide phase is probed by X-ray diffraction and spectroscopic techniques. These materials have exhibited efficient para-selective halogenation activity at ambient temperature and moderate pH conditions. In situ spectroscopic studies have

revealed that the halogenation by the $\text{H}_2\text{O}_2 + \text{KX}$ system occurs via the peroxidative mechanism.

Chapter 6 provides an summary and overall conclusions of the results.

By and large the work is aimed at developing efficient, selective, mesoporous solid, functionalized SBA-15 catalysts for transformation of organic molecules at mild and solvent-free conditions.

1.10. References:

- [1] (a) M. E. Davis, C. Saldarroaga, C. Montes, J. Garces, C. Crowder, *Nature* 331 (1998) 698. (b) M. E. Davis, C. Montes, P. E. Hathaway, J. P. Arhancet, D. L. Hasha, J. M. Garces, *J. Am. Chem. Soc.* 111 (1989) 3919. (c) I. W. C. E. Arends, R. A. Sheldon, M. Wallau, U. Schuchardt, *Angew. Chem. Int. Ed.* 36 (1997) 1144. (d) M. E. Davis, *Nature* 417 (2002) 813.
- [2] A. Corma, *Chem. Rev.* 97 (1997) 2373
- [3] A. Vinu, K. Zakir Hossain, and K. Ariga, *Journal of Nanoscience and Nanotechnology* 5 (2005) 347.
- [4] (a) C. T. Kresge, M. E. Leonowicz, W. J. Roth, J. C. Vartuli, J. S. Beck, *Nature* 359 (1992) 710. (b) J. S. Beck, J. C. Vartuli, W. J. Roth, M. E. Leonowicz, C. T. Kresge, K. D. Schmitt, C. T. W. Chu, D. H. Olson, E. W. Sheppard, S. B. McCullen, J. B. Higgins, J. L. Schlenker, *J. Am. Chem. Soc.* 114 (1992) 10834. (c) T. Yanagisawa, T. Shimizu, K. Kuroda, *Bull. Chem. Soc. Jpn.* 63 (1990) 988. (d) S. Inagaki, Y. Fukushima, K. Kuroda, *J. Chem. Soc., Chem. Commun.* (1993) 680
- [5] R. Ryoo, C. H. Ko, M. Kruk, V. Antochshuk, M. Jaroniec, *J. Phys. Chem. B* 104

- (2000) 11465.
- [6] (a) R. Ryoo, S. Jun, *J. Phys. Chem. B* 101 (1997) 317. (b) D. Zhao, J. Feng, Q. Huo, N. Melosh, G. H. Fredrickson, B. F. Chmelka, G. D. Stucky, *Science* 279 (1998) 548. (c) Zhao, D.; Huo, Q.; Feng, J.; Chmelka, B. F.; Stucky, G. D. *J. Am. Chem. Soc.* 120 (1998) 6024.
- [7] P. van der Voort, P. I. Ravikovitch, K. P. de Jong, A. V. Neimark, A. H. Janssen, M. Benjelloun, E. van Bavel, P. Cool, B. M. Weckhuysen, E. F. Vansant, *Chem. Commun.* (2002) 1010.
- [8] (a) A. Sayari, *Chem. Mater.* 8 (1996) 1840. (b) G. D. Stucky, Q. Huo, A. Firouzi, B. F. Chmelka, S. Schacht, I. G. V. Martin, F. Schuth, *Stud. Surf. Sci. Catal.* 105 (1997) 3. (c) J. Y. Ying, C. P. Mehnert, M. S. Wong, *Angew. Chem. Int. Ed.* 38 (1999) 56.
- [9] A. Stein, B. J. Melde, R. C. Schrodin, *Adv. Mater.* 12 (2000) 1403.
- [10] P. Selvam, S. K. Bhatia, C. G. Sonwane, *Ind Eng Chem Res* 40 (2001) 3237
- [11] M. H. Valkenberg, W. F. Hölderich, *Catal Rev Sci Eng* 44 (2002) 321
- [12] J. A. Melero, R. van Grieken, G. Morales, *Chem Rev* 106 (2006) 3790
- [13] Y. Wan, D. Zhao, *Chem Rev* 107 (2007) 2821
- [14] Y. Kubota, Y. Sugi, T. Tatsumi, *Catal Surv Asia* 11 (2007) 158
- [15] X. Feng, G. E. Fryxell, L. –Q. Wang, A. Y. Kim, J. Liu, K. M. Kemner, *Science* 276 (1997) 923.
- [16] (a) M. H. Lim, C. F. Blanford, A. Stein, *Chem. Mater.* 10 (1998) 467, (b) D. Margolese, J. A. Melero, S. C. Christiansen, B. F. Chmelka, G. D. Stucky, *Chem. Mater.* 12 (2000) 2448.

- [17] (a) F. Feng, G.E. Fryxell, L.-Q. Wang, A.Y. Kim, K.M. Kemner, *Science* 276 (1997) 923. (b) L. Mercier, T.J. Pinnavaia, *Adv. Mater.* 9 (1997) 500. (c) A. Stein, B.J. Melde, R.C. Schroden, *Adv. Mater.* 12 (2000) 1403. (d) T. Kang, Y. Park, J.C. Park, Y.S. Cho, J. Yi, *Stud. Surf. Sci. Catal.* 146 (2003) 527. (e) T. Kang, Y. Park, J. Yi, *Ind. Eng. Chem. Res.* 43 (2004) 1478. (f) C.M. Crudden, M. Sateesh, R. Lewis, *J. Am. Chem. Soc.* 127 (2005) 10045.
- [18] (a) W.M. Van Rhijn, D.E. De Vos, B.F. Sels, W.D. Bossaert, P.A. Jacobs, *Chem. Commun.* (1998) 317. (b) D. Das, J.-F. Lee, S. Cheng, *Chem. Commun.* (2001) 2178. (c) E. Cano-Serrano, J.M. Campos-Martin, J.L.G. Fierro, *Chem. Commun.* (2003) 246. (d) B.C. Wilson, C. W. Jones, *Macromolecules* 37 (2004) 9709.
- [19] (a) Lin, H. P.; Yang, L. Y.; Mou, C. Y.; Liu, S. B.; Lee, H. K. *New J. Chem.* 24 (2000) 253. (b) Lin, H. P.; Liu, Y. H.; Kao, C. P.; Liu, S. B.; Mou, C. Y. *Inter. Zeolite Confer.* 13 (2001) 29-P-16. (c) Lin, H. P.; Liu, Y. H.; Kao, C. P.; Liu, S. B.; Mou, C. Y. *Stud. Surf. Sci. Catal.* 135 (2001) 314.
- [20] K. Moller, T. Bein, *Stud. Surf. Sci. Catal.* 117 (1998) 53
- [21] P. M. Price, J. H. Clark, D. J. Macquarrie, *J. Chem. Soc., Dalton Trans.* (2000) 101.
- [22] X. S. Zhao, G. Q. Lu, *J. Phys. Chem. B* 102 (1998) 1556.
- [23] J. Liu, X. Feng, G. E. Fryxell, L. Q. Wang, A. Y. Kim, M. Gong, *Adv. Mater.* 10 (1998) 161.
- [24] K. K. Unger, *Porous Silica- Its Properties and Use as Support in Column Liquid Chromatography*, Vol. 16, Elsevier, Amsterdam, 1979.

- [25] L. Mercier, T. J. Pinnavaia, *Environ. Sci. Tech.* 32 (1998) 2749.
- [26] J. Liu, G. E. Fryxell, S. Mattigod, T. S. Zemanian, Y. Shin, L. Q. Wang, in *Proc. Nanoporous Materials II*, Banff, Canada, 2000.
- [27] T. Kimura, S. Saeki, Y. Sugahara, K. Kuroda, *Langmuir* 15 (1999) 2794.
- [28] (a) R. Anwender, C. Palm, J. Stelzer, O. Groeger, E. Engelhardt, *Stud. Surf. Sci. Catal.* 117 (1998) 135. (b) V. Antochshuk, M. Jaroniec, *J. Phys. Chem. B* 103 (1999) 6252. (c) C. P. Jaroniec, M. Kruk, M. Jaroniec, A. Sayari, *J. Phys. Chem. B* 102 (1998) 5503.
- [29] T. Asefa, M. Kruk, M. J. MacLachlan, N. Coombs, H. Grondy, M. Jaroniec, G. A. Ozin, *J. Am. Chem. Soc.* 123 (2001) 8520.
- [30] M. H. Lim, C. F. Blanford, A. Stein, *J. Am. Chem. Soc.* 119 (1997) 4090.
- [31] M. H. Lim, C. F. Blanford, A. Stein, *Chem. Mater.* 10 (1998) 467.
- [32] (a) J. H. Clark, D. J. Macquarrie, *Chem. Commun.* (1998) 853. (b) D. Brunel, *Microporous Mesoporous Mater.* 27 (1999) 329.
- [33] P. Sutra, D. Brunel, *Chem. Commun.* (1996) 2485.
- [34] M. H. Lim, A. Stein, *Chem. Mater.* 11 (1999) 3285.
- [35] D. S. Shepherd, W. Zhou, T. Maschmeyer, J. M. Maltes, C. L. Roper, S. Parsons, B. F. G. Johnson, M. J. Duer, *Angew. Chem. Int. Ed.* 37 (1998) 2719.
- [36] F. De Juan, E. R. Hitzky, *Adv. Mater.* 12 (2000) 430.
- [37] V. Antochshuk, M. Jaroniec, *Chem. Commun.* (1999) 2373.
- [38] C. Sanchez, F. Ribot, *New J. Chem.* 18 (1994) 1007.
- [39] (a) S. L. Burkett, S. D. Sims, S. Mann, *Chem. Commun.* (1996), 1367. (b) D. J.

- Macquairre, Chem. Commun. (1996) 1961. (c) Q. Huo, D. I. Margolese, G. D. Stucky, Chem. Mater. 8 (1996) 1147.
- [40] (a) S. R. Hall, C. E. Fowler, B. Lebeau, S. Mann, Chem. Commun. (1999) 201. (b) F. Babonneau, L. Leite, S. Fontlupt, J. Mater. Chem. 9 (1999) 175. (c) V. Goletto, V. Dagry, F. Babonneau, Mater. Res. Soc. Symp. Proc. 576 (1999) 229. (d) L. Mercier, T. J. Pinnavaia, Chem. Mater. 12 (2000) 188. (e) R. Richer, L. Mercier, Chem. Commun. (1998) 1775. (f) J. Brown, R. Riche, L. Mercier, Microporous Mesoporous Mater. 37 (2000) 41.
- [41] C. -Y. Chen, S. L. Burkett, H. -X. Li, M. E. Davis, Microporous Mater. 2 (1993) 27.
- [42] R. Anwander, I. Nagl, M. Widenmeyer, G. Engelhardt, O. Groeger, C. Palm, T. Roser, J. Phys. Chem. B 104 (2000) 3532.
- [43] (a) P. Mukherjee, S. Laha, D. Mandal, R. Kumar, Stud. Surf. Sci. Catal. 129 (2000) 283. (b) S. R. Hall, C. E. Fowler, B. Lebeau, S. Mann, Chem. Commun. (1999) 201.
- [44] F. Babonneau, L. Leite, S. Fontlupt, J. Mater. Chem. 9 (1999) 175
- [45] (a) L. Mercier, T. J. Pinnavaia, Chem. Mater. 12 (2000) 188. (b) M. Koya, H. Nakajima, Stud. Surf. Sci. Catal. 117 (1998) 243.
- [46] (a) R. Richer, L. Mercier, Chem. Commun. (1998) 1775. (b) J. Brown, R. Richer, L. Mercier, Microporous Mesoporous Mater. 37 (2000) 41.
- [47] (a) R. Ryoo, C. H. Ko, J. M. Kim, R. Howe, Catal. Lett. 37 (1996) 29. (b) U. Junges, F. Schuth, G. Schmid, Y. Uchida, R. Schogl, Ber. Bunsen-Ges. Phys. Chem. 101 (1997) 1631. (c) A. Jentys, N. H. Pham, H. Vinek, M. Englisch, J. A.

- Lercher, *Microporous Mater.* 6 (1996) 13. (d) C. T. Fishel, R. J. Davis, J. M. Garces, *J. Catal.* 163 (1996) 148. (e) P. Mukherjee, M. Sastry, R. Kumar, *Phys. Chem. Comm.* 3 (2000) 15.
- [48] (a) X. He, D. Antonelli, *Angew. Chem. Int. Ed.* 41 (2002) 214. (b) B. J. Aronson, C. F. Blanford, A. Stein, *Chem. Mater.* 9 (1997) 2842.
- [49] (a) R. Leon, D. Margolese, G. Stucky, P. M. Petroff, *Phys. Rev. B* 52 (1995) 2285. (b) T. Hirai, H. Okubo, I. Komasaawa, *J. Phys. Chem. B.* 103 (1999) 4228.
- [50] J. M. Thomas, *Angew. Chem. Int. Ed.* 38 (1999) 3588.
- [51] K. Moller, T. Bein, *Chem. Mater.* 10 (1998) 2950.
- [52] C. Bianchini, P. Barbaro, V. Dal Santo, R. Gobetto, A. Meli, W. Oberhauser, R. Psaro, F. Vizza, *Adv. Synth. Catal.* 343 (2001) 41.
- [53] F. M. De Rege, D. K. Morita, K. C. Ott, W. Tumas, R. D. Broene, *Chem. Commun.* (2000) 1797.
- [54] (a) K. Mukhopadhyay, B. R. Sarkar, R. V. Chaudhari, *J. Am. Chem. Soc.* 124 (2002) 124, 9692. (b) J. Jamis, J. R. Anderson, R. S. Dickson, E. M. Campi, W. R. Jackson, *J. Organomet. Chem.* 627 (2001) 37. (c) K. Mukhopadhyay, A. B. Mandale, R. V. Chaudhari, *Chem. Mater.* 15 (2003) 1766.
- [55] D. Brunel, *Microporous Mesoporous Mater.* 27 (1999) 329.
- [56] S. Abramson, N. Bellocq, M. Lasperas, *Top. Catal.* 13 (2000) 339.
- [57] C. Baleizao, B. Gigante, M. J. Sabatier, H. Garcia, A. Corma, *Appl. Catal. A:Gen.* 288 (2002) 279.
- [58] G. -J. Kim, D. -W. Park, *Catal. Today* 63 (2000) 537.
- [59] (a) D. Rechavi, M. Lemaire, *J. Mol. Catal. A: Chem.* 182-183 (2002) 239. (b) R.

- J. Clarke, I. J. Shannon, Chem. Commun. (2001) 1936.
- [60] S. A. Raynor, J. M. Thomas, R. Raja, B. F. G. Johnson, R. G. Bell, M. D. Mantle, Chem. Commun. (2000) 1925.
- [61] S. Xiang, Y. Zhang, Q. Xin, C. Li, Angew. Chem. Int. Ed. 41 (2002) 821.
- [62] W. Bohlmann, K. Schandert, A. Poppl, H. C. Semmelhack, Zeolites 19 (1997) 297.
- [63] R. Selke, M. Capka, J. Mol. Catal. 63 (1990) 319.
- [64] S. Taylor, J. Gullick, P. McMorn, D. Bethell, P. C. Bullman Page, F. E. Hancock, F. King, G. J. Hutchings, J. Chem. Soc., Perkin trans 2(2001) 1714.
- [65] R. Hoppe, A. Ortlam, J. Rathousky, G. Schulz-Ekloff, A. Zukal, Microporous Mater. 8 (1997) 267.
- [66] L. S. Wang, L.X. Tao, M.S. Xie, G.F. Xu, J.S. Huang, Y.D. Xu, Catal. Lett. 21 (1993) 35.
- [67] C. L. Thomas, Catalytic Processes and Proven Catalysts, Academic Press, New York, 1970.
- [68] J. Pasel, P. Kassner, B. Montanari, M. Gazzano, A. Vaccari, W. Makowski, T. Lojewski, R. Dziembaj, H. Papp, Appl. Catal. B: Environ. 18 (1998) 199.
- [69] A. Butler, C. Nicolaidis, Catal. Today 18 (1993) 443.
- [70] W. Z. Cheng, V. Ponec, Catal. Lett. 25 (1994) 337.
- [71] M. A. Alvarez-Merino, F. Carrasco-Marín, C. Moreno-Castilla, J. Catal. 192 (2000) 374.
- [72] C. Moreno-Castilla, M. A. Alvarez-Merino, F. Carrasco-Marín, React. Kinet. Catal. Lett. 71 (2000) 137.

- [73] A. Y. Khodakov, R. Bechara, C. Griboval, A. Appl. Catal.,A: General 254 (2003) 273.
- [74] A. M. Saib, M. Claeys, E. van Steen, Catal. Today 71 (2002) 395
- [75] R. K. Zeidan, V. Dufaud, M. E. Davis, J. Catal 239 (2006) 299
- [76] D.Das, J. F. Lee, S. J. Cheng, Catal 223 (2004) 152.
- [77] Q.Yang, J. Liu, J. Yang, M. P. Kapoor, S. Inagaki, C. Li, J. Catal 228 (2004) 265.
- [78] J. G. C. Shen, R. G. Herman, K. Klier, J Phys Chem B 106 (2002) 9975.
- [79] R. G. Herman, F. H. Khouri, K. Klier, J. B. Higgins, M. R. Galler, C. R. Terenna, J. Catal 228 (2004) 347.
- [80] R. Van Grieken, J. A. Melero, G. Morales, J Mol Catal A: Chem 256 (2006) 29
- [81] S. Koujout, D. R. Brown, Catal Lett 98 (2004) 195
- [82] K. Shimizu, E. Hayashi, T. Hatamachi, T. Kodama, T. Higuchi, A. Satsuma, Y. Kitayama, J. Catal 231 (2005) 131
- [83] S. Sreevardhan Reddy, B. David Raju, V. Siva Kumar, A. H. Padmasri, S. Narayanan, K. S. Rama Rao, Catal Commun 8 (2007) 261.
- [84] R. Gupta, S. Paul, R. Gupta, J. Mol. Catal. A: Chem 266 (2007) 50.
- [85] B. Rác, Á. Molinár, P. Forgo, M. Mohai, I. Bertóti, J. Mol. Catal. A: Chem. 244 (2006) 46.
- [86] R. Van Grieken, J.A. Melero, G. Morales, Appl Catal A: Gen 289 (2005) 143.
- [87] J. A. Melero, R. van Grieken, G. Morales, V. Nuño, Catal Commun 5 (2004) 131
- [88] M. Alvaro, A. Corma, D. Das, V. Fornés, H. García, J Catal 231 (2005) 48

- [89] W. M. Van Rhijn, D. E. De Vos, B. F. Sels, W. D. Bossaert, P.A. Jacobs *Chem Commun* (1998) 317.
- [90] E. Cano-Serrano, J. M. Campos-Martin, J. L. G. Fierro, *Chem. Commun.* (2003) 246
- [91] I. K. Mbaraka, D. R. Radu, V. S. Y. Lin, B. H. Shanks, *J. Catal.* 219 (2003) 329
- [92] Q. Yang, M. P. Kapoor, N. Shirokura, M. Ohashi, S. Inagaki, J. N. Kondo, K. J. Domen, *J Mater. Chem.* 15 (2005) 666.
- [93] Y. F. Feng, X. Y. Yang, Y. Di, Y. C. Du, Y. L. Zhang, F. S. Xiao, *J Phys Chem B* 110 (2006) 14142.
- [94] A. Karam, Y. Gu, F. Jérôme, J. P. Douliez, J. Barrault, *Chem. Commun.* (2007) 2222
- [95] I. K. Mbaraka, B. H. Shanks, *J. Catal.* 244 (2006) 78.
- [96] M. A. Jackson, I. K. Mbaraka, B. H. Shanks, *Appl Catal A: Gen* 310 (2006) 48
- [97] X. Wang, S. Cheng, J. C. C. Chan, *J Phys Chem* 111 (2007) 2156
- [98] S. Ajaikumar, A. Pandurangan, *J Mol Catal A: Chem* 266 (2007) 1
- [99] W. D. Bossaert, D. E. De Vos, W. M. Van Rhijn, J. Bullen, P. J. Grobet, P. A. Jacobs, *J Catal* 182 (1999) 156
- [100] I. Díaz, C. Márquez-Alvarez, F. Mohino, J. Pérez-Pariente, E. Sastre, *J Catal* 193 (1999) 295
- [101] A. S. Dias, M. Pillinger, A. A. Valente, *J. Catal.* 229 (2005) 414
- [102] P. L. Dhepe, M. Ohashi, S. Inagaki, M. Ichikawa, A. Fukuoka, *Catal Lett* 102 (2005) 163
- [103] R. K. Zeidan, M. E. Davis, *J. Catal.* 247 (2007) 379

- [104] H. Zhang, S. Xiang, C. Li, Chem. Commun. (2005) 1209
- [105] H. Zhang, Y. Zhang, C. Li, J. Catal. 238 (2006) 369
- [106] R. M. Hanson, Chem Rev 91 (1991) 437
- [107] R. Garcia, M. Martinez, Aracil J Chem Eng Technol 22 (1999) 12
- [108] J. Barrault, Y. Pouilloux, J. M. Clacens, C. Vanhove, and S. Bancquart, Catal. Today 75 (2002) 177.
- [109] M. Marchionna, R. Patrini, D. Sanfilippo, A. Paggini, F. Giavazzi, L. Pellegrini, Stud. Surf. Sci. Catal. 136 (2001) 489.
- [110] H. Nouredini, U.S. Patent 6,015,440 (2000).
- [111] Katarína Klepáčová, Dušan Mravec, Martin Bajus. Appl. Catal. A: Gen., 294 (2005) 141
- [112] A. Zaidi, J. L. Gainer, G. Carta, Biotechnol Bioeng 48 (1995) 601
- [113] L. R. Pizzio, P. G. V´azquez, C. V. C´aceres, M. N. Blanco, Appl Catal A: Gen 256 (2003) 125
- [114] L. R. Pizzio, M. N. Blanco, Appl Catal A:Gen 255 (2003) 265
- [115] H. T. R. Teo, B. Saha, J Catal 228 (2004) 174
- [116] Y. Kubota, Y. Sugi, T. Tatsumi, Catal Surv Asia 11 (2007) 158
- [117] S. Kobayashi, H. Ishitani, Chem Rev 99 (1999) 1069
- [118] B. M. Trost, L. R. J. Terrell, J Am Chem Soc 125 (2003) 338
- [119] (a) P. A.Villa, A. F. Taboda, C. Monte de Correa, J.Mol. Cata. A: Chem. 185 (2002) 269, (b) N.K. Kala Raj, V.G. Puranik, C. Gopinathan, A.V. Ramaswamy, Appl. Catal. A: Gen. 256 (2003) 265, (c) J. Bussi, A. L´opez, F. Pe˜na, P. Timbal, D. Paz, D. Lorenzo, E. Dellacasa, Appl. Catal. A : Gen. 253 (2003) 177.

- [120] P. A. Robles-Dutenhefner, M.J. da Silva, L.S. Sales, E.M.B. Sousa, E.V. Gusevskaya, *J. Mol. Catal. A: Chem.* 217 (2004) 139.
- [121] B. F. Sels, D. E. De Vos, P.A. Jacobs, *J Am Chem Soc* 123 (2001) 8350
- [122] R. I. De la Ross, M. J. Clague, A. Butler, *J Am Chem Soc* 114 (1992) 760

CHAPTER - 2

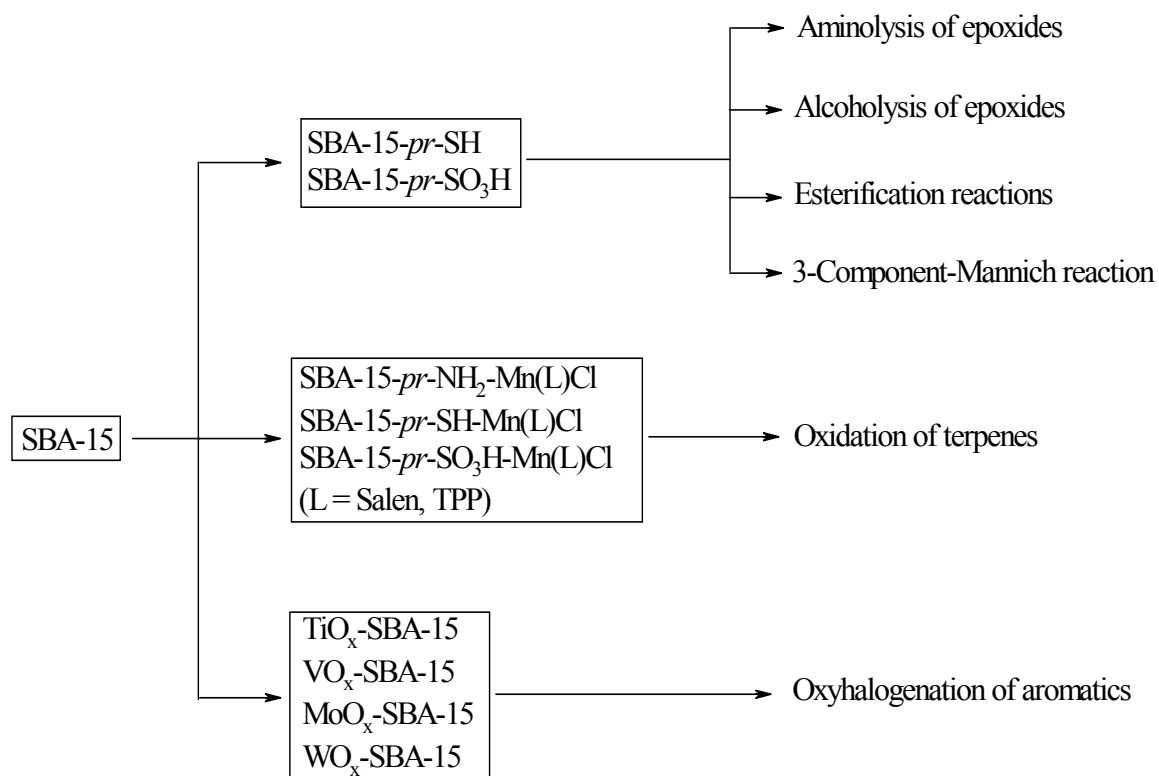
Experimental Methodology

2.1. Introduction

In recent years, surface modification of M41S type mesoporous silica materials with reactive organic and inorganic functional groups has been widely investigated [1]. Surface modification allows tailoring the surface properties of materials for potential applications in areas of catalysis, separation technology, chemical sensors, electronic devices and drug delivery [2, 3]. The open frameworks, controllable structures, tunable porosities and high surface areas endow mesoporous materials with accessibility to bulkier reagents.

This chapter describes the synthesis methodologies of various functionalized mesoporous silicas investigate in this work. It also describes the physicochemical techniques used for characterization and procedures for catalytic activity evaluation of the materials. Three-sets of surface-modified SBA-15 materials have been investigated (Scheme 2.1). The first-set consists of SBA-15 modified with organo-acidic (propyl thiol and propyl sulfonic acid) and basic (propyl amine) moieties. The second-set consists of Mn complexes grafted on organo-functionalized SBA-15. The third-set composes of nanocrystalline metal oxides supported on SBA-15. The formation, structural integrity and textural properties of the materials were investigated by various physicochemical techniques viz., atomic absorption spectroscopy (AAS), X-ray powder diffraction (XRD), N₂ physisorption measurements, temperature-programmed desorption of ammonia (NH₃-TPD), Fourier transform infrared spectroscopy (FTIR), diffuse reflectance UV-visible (DRUV-vis.) spectroscopy, electron paramagnetic resonance (EPR) spectroscopy, X-ray photoelectron spectroscopy (XPS), Laser Raman spectroscopy and cyclic voltammetry (CV). Catalytic activities of the first-set have been investigated in ring-opening of

epoxides with amines and alcohols, esterification and three-component-Mannich reactions. The second-set is efficient for chemo-, regio- and stereoselective aerial oxidation of monoterpenes at ambient conditions. TiO_x , VO_x , MoO_x and WO_x supported on SBA-15 catalyzed biomimetic haloperoxidation of aromatic compounds at mild conditions.



Scheme 2.1

2.2. Material Preparation

2.2.1. Synthesis of SBA-15

SBA-15 was prepared hydrothermally [4] using tetraethyl orthosilicate (TEOS, Aldrich Co.) as silica source, Pluronic P123 (poly(ethylene glycol)-block-poly(propylene glycol)-block-poly(ethylene glycol), $\text{EO}_{20}\text{PO}_{70}\text{EO}_{20}$; average molecular weight = 5800,

Aldrich Co.) as template and HCl as a pH controlling agent. In a typical synthesis, 10 g of P123 was dispersed in 75 g of water and 300 g of 2 M HCl solution while stirring. To it, 22 g of tetraethyl orthosilicate (TEOS, Aldrich Co.) was added over 45 min. The gel that formed was continuously stirred at 313 K for 24 h and then aged at 373 K for 48 h. Then, the solid product was separated by filtration, washed with deionized water, and dried, first at 298 K, and then at 353 K. The material was finally calcined in air at 823 K for 6 h, to decompose the triblock co-polymer P123 and to obtain a white powder, SBA-15.

2.2.2. Preparation of organo-functionalized SBA-15 materials

2.2.2.1. SBA-15-pr-NH₂

Amine-functionalization was accomplished by condensation of 3-aminopropyl trimethoxy silane (APTMS) with the surface silanol groups of SBA-15 [5]. In a typical synthesis, 4 g of calcined SBA-15 was first activated under vacuum at 423 K for 4 h. It was then dispersed in 100 ml of dry-toluene taken in a double-necked round-bottom flask (250 ml) fitted with a water-cooled condenser. To it, 4.13 g of APTMS was added slowly over 10 min. The contents of the flask were refluxed for 24 h under nitrogen. The solid was filtered, dried and Soxhlet extracted, initially with toluene (overnight) and, then, with dichloromethane (for 6 h). The amine-functionalized SBA-15 (hereafter referred to as SBA-15-pr-NH₂), thus obtained, was dried at 353 K for 6 h and used in further preparations.

2.2.2.2. Preparation of SBA-15-pr-SH

SBA-15-pr-SH was prepared [5, 6] by reacting 3-mercaptopropyl-trimethoxysilane (MPTMS) with a pre-formed SBA-15. Thiol-functionalization was accomplished by condensation of surface silanols with MPTMS. In a typical preparation,

calcined SBA-15 (4 g) was first activated under vacuum at 423 K for 4 h. It was then dispersed in dry-toluene (100 ml) and 5.42 g of MPTMS was added to it, in small amounts, over 10 min. The contents of the flask were refluxed, under nitrogen, for 24 h. Soxhlet extraction, initially with dichloromethane (for 12 h) and then with acetone (for 12 h), yielded the thiol-functionalized SBA-15 (hereafter referred to as SBA-15-*pr*-SH). It was dried at 353 K. The thiol loading estimated by sulfur analysis was 1.5 mmol/g.

Propyl thiol-functionalized SBA-15 materials were also prepared by the direct synthesis route and used in esterification reactions [7]. In a typical synthesis by this route, 10 g of Pluronic 123 (Aldrich Co.) was dissolved in 300 g of 2 M HCl while stirring at 298 K. The solution was heated to 313 K before adding TEOS (Aldrich Co.). After TEOS pre-hydrolysis, the thiol precursor (MPTMS) was added to the mixture over 10 min. The resultant solution was stirred for 20 h at 313 K, after which the mixture was aged at 373 K for 48 h under static conditions. The solid formed was recovered by filtration and air-dried at room-temperature overnight. The template was removed from the as-synthesized material by washing with ethanol under reflux for 24 h. This way, four different loadings of propyl thiol group functionalized materials were prepared.

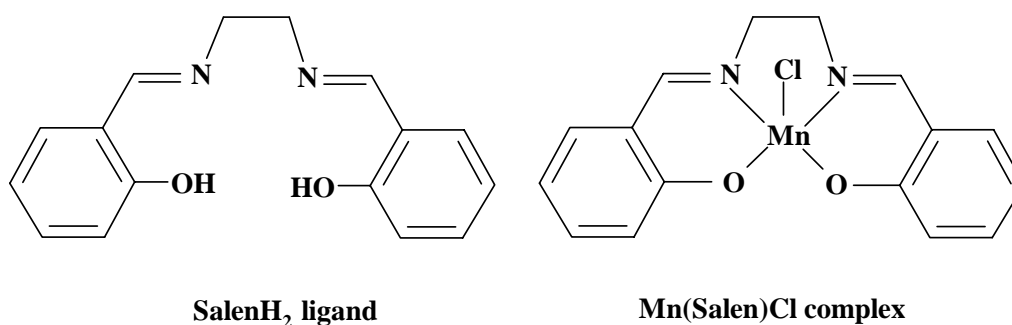
2.2.2.3. Preparation of SBA-15-*pr*-SO₃H

Sulfonic acid-functionalized SBA-15 (hereafter referred to as SBA-15-*pr*-SO₃H) was prepared [8] from SBA-15-*pr*-SH and 30% aq. H₂O₂. Sulfonation was accomplished by oxidizing the thiol-groups in SBA-15-*pr*-SH with H₂O₂. In a typical preparation, to 4 g of SBA-15-*pr*-SH (activated at 373 K), was added 65 ml of 30% aqueous H₂O₂. The mixture was then stirred for 8 h at 298 K. The solid was filtered, washed with deionized water and dried, first at 298 K for 24 h and then at 353 K for 12 h, to obtain SBA-15-*pr*-

SO₃H. The amount of -SO₃H functional group was estimated to be (sulfur analysis) 0.55 mmol/g silica. Ion exchange capacity of the solid estimated by pH measurements (0.725 meq/g silica) is in good agreement with the estimated value from the sulfur analysis.

2.2.3. Preparation of ‘neat’ Mn complexes

2.2.3.1. Preparation of Mn(Salen)Cl



Scheme 2.2

In a typical synthesis of Salen ligand (Scheme 2.2), to 10 mmol of salicylaldehyde in 100 ml of extra-pure methanol, 5 mmol of ethylenediamine was added drop-wise under nitrogen atmosphere and at reflux condition. Bright yellow crystals of N, N-ethylenebis(salicylidenaminato) (Salen) formed were isolated, recrystallized from methanol and used in further preparations.

Mn(Salen)Cl (Scheme 2.2) was prepared as follows [9]. The Salen ligand (2 mmol) was first dissolved in hot absolute alcohol. Then to this solution, 1.5 equivalents of Mn(OAc)₂·4H₂O dissolved in absolute alcohol was added over 10 min. The mixture was allowed to reflux for 1 h. To it, 3 equivalents of LiCl was added in one lot and refluxed for another 2 h. Then, it was filtered and washed with enough ice cold water and a little amount of absolute ethanol. It was dried in vacuum to get brown colored Mn(Salen)Cl complex.

of distilled water. The solid was allowed to dry in air for 15 min. It was, then, dissolved in 250 ml of methanol and the solution was filtered. The methanolic solution was poured into an equal volume of 6 M aq. HCl solution. The green precipitate formed was filtered, washed with water and dried in air as done previously. It was then, recrystallized from n-hexane. The purities of H₂TPP and Mn(TPP)Cl were confirmed by C, H & N analyses and UV-visible and FT-IR spectroscopy techniques.

2.2.4. Preparation of grafted Mn(Salen)Cl

Organo-functionalized SBA-15 materials (SBA-15-*pr*-NH₂, SBA-15-*pr*-SH and SBA-15-*pr*-SO₃H; 3 g) were first activated at 353 K, under vacuum, for 2 h and then dispersed in 50 ml of dry-toluene. “Neat” Mn(Salen)Cl (0.45 g) was added and the contents of the flask were refluxed, under nitrogen atmosphere, for 24 h. The solid was filtered, dried at 333 K and Soxhlet-extracted, initially with toluene for 12 h and then, with dichloromethane for another 12 h. The light brown, solid, Mn catalyst materials (SBA-15-*pr*-NH₂-Mn(Salen)Cl, SBA-15-*pr*-SH-Mn(Salen)Cl and SBA-15-*pr*-SO₃H-Mn(Salen)Cl, respectively), thus prepared, were dried (353 K, 12 h) and used further in characterization and catalytic activity studies.

2.2.5. Preparation of grafted Mn(TPP)Cl

The organo-functionalized SBA-15 (2 g) was, first, activated at 353 K, under vacuum, for 2 h and then, dispersed in 50 ml of dry-toluene. “Neat” Mn(TPP)Cl (0.30 g) was added and the contents of the flask were refluxed, under nitrogen atmosphere, for 24 h. The solid was filtered, dried at 333 K and Soxhlet-extracted initially, with toluene for 12 h and then, with dichloromethane for another 12 h. The solid Mn catalysts (SBA-15-*pr*-NH₂-Mn(TPP)Cl, SBA-15-*pr*-SH-Mn(TPP)Cl and SBA-15-*pr*-SO₃H-Mn(TPP)Cl,

respectively), thus prepared, were dried (353 K, 12 h) and used further in the characterization and catalytic activity studies.

2.2.6. Preparation of nanoscopic metal oxides supported mesoporous silica

2.2.6.1. Preparation of TiO_x -SBA-15

Titanium containing SBA-15 was prepared by the post synthesis method [12]. Tetrabutyl orthotitanate (0.05 g) was taken in 15 ml of glycerol and hydrolyzed with tetrapropylammonium hydroxide (20 wt% TPAOH) while stirring for 4 h. To it, calcined SBA-15 (200 mg) was added and stirred at 373 K for 72 h. The contents were filtered under vacuum and the solid obtained was dried at 393 K and calcined at 773 K for 6 h.

2.2.6.2. Preparation of VO_x -SBA-15

This material was prepared in a three steps. In the first-step, propyl amine functionalized SBA-15 was prepared as reported above. Then, in the second-step, butylammonium decavanadate was prepared: 5 g of V_2O_5 and 2.42 g of butyl amine was added to 10 ml of water taken in a 250 ml round-bottom flask equipped with a reflux condenser. The reaction mixture was heated until the contents were completely dissolved. The solution pH was adjusted to 5 by drop-wise addition of concentrated $HClO_4$. The deep orange solution was refluxed overnight. The mixture was filtered and the water was removed by evaporation, leaving brilliant orange color butylammonium decavanadate. The powder was highly soluble in water and recrystallized from acetone/water (10:1 v/v). In the third-step, SBA-15 supported vanadia was prepared using amine functionalized SBA-15 and butylammonium decavanadate as starting materials. For a 20 wt% of vanadium catalyst, 635 mg of butylammonium decavanadate was added to a suspension of 1 g of functionalized SBA-15 in 40 ml of water. The contents were stirred for 12 h,

filtered, washed with water, and dried in air, yielding an orange powder, which was then calcined at 823 K for 12 h.

2.2.6.3. Preparation of MoO_x -SBA-15

Molybdenum oxide supported on SBA-15 was prepared by the post-synthesis methodology, wherein SBA-15 (2 g) was activated at 473 K prior to use and then dispersed in a 50 ml of aqueous solution of ammonium heptamolybdate so that the molybdenum oxide loading was 20 wt%. The mixture was refluxed for 12 h, evaporated to dryness and then calcined at 823 K to get a faint blue colored supported molybdenum oxide catalyst.

2.2.6.4. Preparation of WO_x -SBA-15

Tungsten oxide supported on SBA-15 was also prepared by the post-synthesis method as described above using pre-activated SBA-15 (2 g) and ammonium tungstate solution (50 ml). The concentrations of ammonium tungstate solutions were prepared in such a way that tungsten oxide loading were 5, 10, 15 and 20 wt% of the total catalyst.

2.3. Characterization Procedures

2.3.1. X-ray powder diffraction (XRD)

XRD is an important tool, helps determining the crystallinity, phase purity, crystal structure and crystallite sizes of catalyst materials [13]. The XRD method involves interaction between the incident monochromatized X-rays (like $Cu K\alpha$ or $MoK\alpha$) with the atoms of a periodic lattice. X-rays scattered by the atoms in an ordered lattice interfere constructively as described by Bragg's law: $n\lambda = 2d \sin\theta$, where, λ is the wavelength of the X-rays, d is the distance between two lattice planes, θ is the angle

between the incoming X-rays and the normal to the reflecting lattice plane and n is an integer known as the order of reflection [13, 14].

The mesoporous materials were analyzed using an X'Pert Pro (Philips) diffractometer with Cu-K α radiation ($\lambda = 0.15406$ nm) and a proportional counter as a detector. A divergent slit of $1/32^\circ$ on the primary optics and an anti-scatter slit of $1/16^\circ$ on the secondary optics were used to measure the data in the low-angle region. The supported nanoscopic oxide were analyzed using a Rigaku Geigerflex X-ray diffractometer with Ni-filtered Cu-K α radiation (40 kV, 30 mA). The XRD patterns were measured in the 2θ range of $0.5 - 10^\circ$ in the case of mesoporous SBA-15 materials and $5 - 80^\circ$ in the case of nanoscopic oxide solids at a scan rate of 1 and $4^\circ/\text{min}$, respectively. Crystallite size of the materials was found using the Scherrer equation: $L = K\lambda/\beta\cos\theta$, where θ and λ have their usual meanings. K is a constant approximately taken as 0.9; β is the line width on the 2θ scale in radians. Unit cell parameter (a) for cubic systems was found using the equation: $a = d_{(111)}\sqrt{(h^2+k^2+l^2)}$. Here d is the inter-planar distance obtained from the Bragg's equation while considering the value of n as unity.

2.3.2. Diffuse reflectance UV-visible (DRUV-vis)

Diffuse reflectance spectroscopy is a technique based on the reflection of light in the ultraviolet (UV), visible (vis) and near-infrared (NIR) region by a powdered sample. In a DR spectrum, the ratio of the light scattered from a thick closely packed catalyst layer and the scattered light from an infinitely thick layer of an ideal non-absorbing (white) reference sample is measured as a function of the wavelength, λ . DRUV-vis spectroscopy is a highly sensitive and powerful technique for identification and

characterization of the metal ion's coordination and location (framework or extra-framework) in metal-containing solid catalysts [15].

The measurements were conducted on a Shimadzu UV-2550 spectrophotometer equipped with an integrating sphere attachment (ISR 2200). In general, spectral grade BaSO₄ was used as the reference material. In the case of “neat” metal complexes, the UV-vis spectra were recorded in liquid mode by dissolving the complex in a suitable solvent. The solvent in which the complex was dissolved was used as a reference solvent.

2.3.3. Fourier transform infrared (FTIR)

The formation of silicate framework and metal ion incorporation were determined using FTIR spectroscopy [16]. The spectra were recorded on a Shimadzu FTIR-8201 PC spectrophotometer in the wave number range of 400 – 4000 cm⁻¹. The samples were made into KBr pellets (1% wt). In general, neat KBr was used as a reference material.

2.3.4. Laser Raman

Raman spectroscopy is based on the inelastic scattering of photons, which lose energy by exciting vibrations in the sample. A vibration is Raman active only if there is a change in the polarizability. Raman spectroscopy is widely used for the investigation of supported and bulk metals and metal oxides [17]. All characteristic vibrational features of oxides of the transition metals like V, Cr, Mo and W fall in the frequency range below 1100 cm⁻¹ and these oxides have high Raman scattering cross sections because of their relatively high covalent bond character. Various studies have demonstrated that the simultaneous use of reference compounds and the correlation between Raman frequency and bond length make Raman Spectroscopy well suited to study the molecular structures of supported metal oxides. The usual support materials (silica and alumina) have very

low Raman scattering cross sections and show weak absorption bands in the 1100-700 cm^{-1} region. Hence, Raman spectroscopy has the advantage that the normal modes of the minority components, viz., the transition metal oxides dispersed on the supports can most frequently be detected with relative ease. A disadvantage of this technique is the small cross section for Raman scattering, that most of the scattered intensity goes into the Rayleigh band, which is typically about three orders of magnitude greater than the Stokes bands.

2.3.5. Electron paramagnetic resonance (EPR)

Electron paramagnetic resonance (EPR) spectroscopy is a technique for studying chemical species that have one or more unpaired electrons, such as organic and inorganic free radicals or transition metal ions. EPR spectroscopy provides information on the structure and reducibility of metal ions in various catalyst systems [18, 19]. The spectra were recorded on a Bruker EMX spectrometer operating at X-band frequency ($\nu \approx 9.4$ GHz) and 100 kHz field modulation. Spectral calculations and manipulations were done using the Bruker WIN-EPR software package.

2.3.6. X-ray photoelectron spectroscopy (XPS)

The nature, oxidation state and dispersion of surface metal species were estimated by XPS [20]. The spectra of calcined powder samples were acquired on a VG Microtech Multilab ESCA 3000 instrument with a non-monochromatized Mg $K\alpha$ radiation ($h\nu = 1253.6$ eV). Base pressure in the analysis chamber was maintained at $3 - 6 \times 10^{-10}$ mbar range. The energy resolution of the spectrometer was set at 0.8 eV at pass energy of 20 eV. Binding energy (BE) was calibrated with respect to Au $4f_{7/2}$ core level (83.9 eV). The error in all the BE values reported is ± 0.1 eV.

2.3.7. Cyclic voltammetry (CV)

Cyclic voltammetry (CV) enabled determination of the redox behavior of metal ions in solid catalysts investigated in the present study [21]. Cyclic voltammetry measurements were performed at 298 K using a three-electrode system (Solatron SI-1287 electrochemical interface). The immobilized Mn complex (60 wt%) and graphite powder were mixed with 0.1 ml of Teflon powder. The slurry was then pasted onto a Pt disc (1.5 mm diameter) and dried under an infrared (IR) lamp. This modified Pt disc was used as a working electrode. Pt foil was used as a counter electrode and a Pt wire was used as a reference electrode. All these three-electrodes were placed in a glass compartment containing DMF. LiClO₄ (0.1 M) was used as a supporting electrolyte. Prior to cyclic voltammetric experiments (scan speed = 25 mV/sec), the electrolytic solutions were deoxygenated by purging with argon gas.

2.3.8. Temperature-programmed desorption (TPD)

Acidity or basicity of solid catalysts can be investigated by adsorption/desorption technique of basic or acidic probe molecule respectively. NH₃ was used as a probe molecule for measuring the acidity of organo acid-functionalized SBA-15. From the amount of adsorption/desorption of the corresponding probe molecule, total acidity of the catalyst was estimated.

2.3.9. Nitrogen adsorption/desorption

The most common method of measuring surface area and textural characteristics of catalyst materials is that based on the theory developed by Brunauer, Emmett and Teller (BET), considering the multilayer adsorption. The BET equation can be represented as: $P/V(P_0-P) = 1/cV_m + [(c-1)/cV_m] (P/P_0)$, where P is adsorption

equilibrium pressure, P_o is saturation vapor pressure of the adsorbate at the experimental temperature, V is volume of N_2 adsorbed at a pressure P , V_m is the volume of adsorbate required for monolayer coverage, and c , a constant that is related to the heat of adsorption and liquefaction [22]. A linear relationship between $P/V(P_o-P)$ and P/P_o is required to obtain the quantity of nitrogen adsorbed. The monolayer volume, V_m is given by $1/(S+I)$, where S is the slope and is equal to $(c-1)/cV_m$ and I is the intercept equal to $1/cV_m$.

The surface area of the catalyst (S_{BET}) is related to V_m , by the equation: $S_{BET} = (V_m/22414)N_a\sigma$, where N_a is Avagadro number and σ is mean cross sectional area covered by one adsorbate molecule. The value of σ generally accepted for N_2 is 0.162 nm^2 . Several computational procedures are available for the derivation of pore size distribution of mesoporous samples from physisorption isotherms. Most popular among them is the Barrett-Joyner-Halenda (BJH) model, which is based on speculative emptying of the pores by a stepwise reduction of P/P_o , and allowance being made for the contraction of the multilayer in those pores already emptied by the condensate [23]. The mesopore size distribution is usually expressed as a plot of $\Delta V_p/\Delta r_p$ versus r_p , where V_p is the mesopore volume, and r_p is the pore radius. Adsorption of nitrogen measured by Brunauer-Emmett-Teller (BET) equation at low pressure (10^{-4} Torr) and liquification temperature of N_2 (77 K) is the standard method for determination of surface area, pore volumes and pore size distribution of molecular sieves. All these measurements were conducted on a Coulter (Omnisorb 100 CX) instrument.

2.3.10. Atomic absorption spectroscopy (AAS)

The metal ion content in the catalyst samples was determined by atomic absorption spectroscopy (AAS). The sample solution required for the AAS analysis was prepared by dissolving 200 mg of catalyst in conc. H_2SO_4 and HF (about 2-3 drops) and it was then diluted with deionized water (100 ml). The sample solutions thus prepared were injected into the sample port of the spectrometer. The metal ion content (in ppm) was estimated from the optical absorption values and calibration plot (made using standard solutions of different concentrations).

2.3.11. Scanning electron microscopy (SEM)

SEM probes the morphological characteristics of materials. SEM scans over a sample surface with a probe of electrons (5-50 eV) and detects the yield of either secondary or back-scattered electrons as a function of the position of the primary beam. Contrast is generally caused by the orientation that part of the surface facing the detector appears brighter than parts of the surface with their surface normal pointing away from the detector. The interaction between the electron beam and the sample produces different types of signals providing detailed information about the surface structure and morphology of the sample [24]. When an electron from the beam encounters a nucleus in the sample, the resultant Coulombic attraction leads to a deflection in the electron's path, known as Rutherford elastic scattering. A fraction of these electrons will be completely backscattered, re-emerging from the incident surface of the sample. Since the scattering angle depends on the atomic number of the nucleus, the primary electrons arriving at a given detector position can be used to produce images containing topological and compositional information [25]. A major advantage of SEM is that bulk samples can also

be directly studied by this technique. SEM of the catalyst samples in this work were recorded using a SEM Leica 440 instrument operating at 100 kV.

2.3.12. Transmission electron microscopy (TEM)

TEM is typically used for high resolution imaging of thin films of a solid sample for micro structural and compositional analysis. The technique involves: (i) irradiation of a very thin sample by a high-energy electron beam, which is diffracted by the lattices of a crystalline or semi crystalline material and propagated along different directions, (ii) imaging and angular distribution analysis of the forward scattered electrons (unlike SEM where backscattered electrons are detected), and (iii) energy analysis of the emitted X-rays [26]. In detail, a primary electron beam of high energy and high intensity passes through a condenser to produce parallel rays, which impinges on the sample. As the attenuation of the beam depends on the density and thickness, the transmitted electrons form a two-dimensional projection of the sample mass, which is subsequently magnified by the electron optics to produce the so-called bright field image. The dark field image is obtained from the diffracted electron beams, which are slightly off angle from the transmitted beam. Typical operating conditions for TEM instruments are 100-200 keV electrons, 10^{-6} mbar vacuum, 0.5 nm resolution and a magnification of about 105. The topographic information obtained by TEM in the vicinity of atomic resolution can be utilized for structural characterization and identification of various phases of mesoporous materials, *viz.*, hexagonal, cubic or lamellar [27]. TEM also provides real space image on the atomic distribution in the bulk and surface of a nanocrystal [28]. TEM of the samples were recorded using a JEOL-model 1200 EX instrument operating at 100 kV.

2.4. Reaction Procedures

2.4.1. Reactions over organofunctionalized SBA-15

2.4.1.1. Regio- and stereoselective synthesis of β -amino alcohols

A known quantity of the catalyst (SBA-15-*pr*-SO₃H or SBA-15-*pr*-SH), epoxide and equimolar amount of amine were taken in a double-necked round-bottom flask (50 ml) placed in a temperature-controlled oil bath and fitted with a water-cooled condenser. The reaction was conducted at a specified temperature and for a desired period of time. The progress of the reaction was monitored by taking out aliquots of the sample, diluting it with a known quantity of dichloromethane, separating the catalyst by centrifugation and subjecting the diluted liquid to gas chromatographic analysis (Varian 3400; CP-SIL8CB column; 30 m-long and 0.53 mm-i.d.). The products were identified using GC-MS (Varian CP-3800; 30 m-long, 0.25 mm-i.d., and 0.25 μ m-thick CP-Sil8CB capillary column). In some cases, the products were isolated by column chromatography (eluent: petroleum ether – ethyl acetate mixture) and characterized by ¹H NMR (Bruker AC 200) spectroscopy.

2.4.1.2. Regioselective synthesis of β -alkoxy alcohols

Ring opening of epoxide with alcohol was carried out by taking equimolar amounts of styrene oxide and alcohol and a known quantity of the catalyst in a double-necked round-bottom flask (50 ml) placed in a temperature-controlled oil bath and fitted with a water-cooled condenser. The progress of the reaction and analysis of the products were determined as described in section 2.4.1.1.

2.4.1.3. Etherification of glycerol

Etherification of glycerol with tert-butanol was carried out using SBA-15-*pr*-SO₃H catalyst. In a typical reaction, a known quantity of catalyst, pure glycerol (99%) and tert-butanol were taken in a Teflon-lined steel-autoclave. The reaction was carried out in hydrothermal rotating reactor (HIRO Co.) at 363 K (50 rpm). After 8 h of the reaction, it was cooled down to room temperature, catalysts were separated by filtration and the liquid sample was injected in gas chromatograph (Carvowex). The formation of product was confirmed by FTIR and ¹H NMR spectroscopy. The etherification reaction was also carried out using conventional solid acid catalysts like zeolite-β and amberlyst resins. The influence of reaction parameters on catalytic activity and product selectivity was studied.

2.4.1.4. Esterification of carboxylic acid

Esterification of carboxylic acid was carried out in a double-necked round bottom flask fitted with a water-cooled condenser. 0.05 gm of SBA-15-*pr*-SO₃H catalyst, 100 mmol of alcohol and 20 mmol of acid were taken and the reaction was conducted at 373 K. The progress of the reaction was monitored by GC analysis. The product was also isolated by column chromatography, characterized by ¹H NMR and FTIR spectroscopies and the isolated yield of ester was determined. The influence of sulfonic acid loading (0.3-1.6 mmol/g) and method of preparation (post synthetic vs direct synthesis) were investigated on the esterification of acetic acid with benzyl alcohol.

2.4.1.5. Three-component Mannich reaction

Mannich reaction of aldehyde, ketone and amine by Brønsted acidic organosulfonic acid functionalized SBA-15 was done at moderate conditions. In a typical

reaction, 0.05 gm of the catalyst, 10 mmol of aldehyde, 10 mmol of amine and 10 mmol of ketone having α -hydrogen were taken in a double-necked round-bottomed flask fitted with a water-cooled condenser at 298 K for 1 h. After completion of the reaction the catalyst was filtered, washed and extracted with ethanol. The ethanol layer was collected, and the product was allowed to recrystallize. Some of the isolated products were confirmed by ^1H NMR technique.

2.4.2. Chemo-, regio- and stereo-selective oxidation of terpenes over grafted Mn complexes

In a typical reaction, 0.1 g of immobilized Mn complexes, 3.75 mmol of mono-terpene [*R*-(+)-limonene, α -pinene or 3-carene], 9 mmol of iso-butyraldehyde, 1.7 mmol of *N*-methylimidazole (*N*-MeIm) and 20 ml of solvent were taken in a double-necked round-bottom flask (50 ml) fitted with a gas-purging unit. The reactions were conducted by bubbling air (1 atm) for 8 h, at 298 K. The catalyst was separated by filtration and the liquid portion was analyzed by gas chromatography (Varian 3400; CP-SIL8CB column; 30 m-long and 0.53 mm-i.d.). The products were identified using standard samples and by GC-MS (Shimadzu QP-5000; 30 m-long, 0.25 mm-i.d., and 0.25 μm -thick capillary column DB-1). In some experiments, the influence of solvent (polar and non-polar) and additives (*N*-methyl imidazole, 2-methyl imidazole and imidazole) on catalytic activity was investigated.

2.4.3. Regiospecific oxyhalogenation of organics over SBA-15 supported metal oxide

2.4.3.1. Oxybromination of phenol red

Oxybromination of phenol red to bromo-phenol blue was performed over nanoscopic tungsten oxide, molybdenum oxide, titanium oxide and vanadium oxide

supported on SBA-15. In a typical reaction, 20 ml of 0.05 M phenol red solution ($\text{H}_2\text{O} + \text{CH}_3\text{OH}$, 4 : 1) was taken in a double-necked round bottom flask. To it, 2 mmol of KBr and 2 mmol of H_2O_2 (30% aqueous) were added. After addition of 0.025 g of catalyst, the pH of the reaction mixture was adjusted to ~ 5 by adding HEPES (4-(2-hydroxyethyl)-1-piperazineethanesulfonic acid) buffer drop-wise. The progress of the reaction conducted at 298 K was monitored by taking out small aliquots of samples at equal interval (15 min), separating the catalyst by centrifugation and then by recording the UV-vis spectrum which shows the decrease in absorbance at $\lambda_{\text{max}} = 430\text{-}450$ nm corresponding to phenol red and increase in absorbance at $\lambda_{\text{max}} = 590 - 600$ nm corresponding to bromo phenol blue. The reaction was also carried out with different loadings of tungsten oxide under similar conditions. Effect of temperature on the conversion of phenol red was studied $\text{WO}_x\text{-SBA-15}$ (20%) catalyst.

2.4.3.2. Oxybromination of aromatics

In a typical bromination reaction, 0.05 g of supported oxide catalysts (WO_x , MoO_x , TiO_x or VO_x), 2 mmol of the substrate, 5 mmol of KBr, 5 mmol of H_2O_2 (30% aq.), and 10 ml of solvent ($\text{CH}_3\text{CN} + \text{H}_2\text{O}$; 1:1) were taken in a double-necked round-bottom flask (50 ml). The pH of the reaction was controlled at 4.4-5 by adding requisite amount of HNO_3 . The reaction was conducted at 298 K for 4 h. At the end of the reaction, catalyst was separated. The liquid portion was extracted with water and dichloromethane, the organic layer was collected, concentrated and analyzed by gas chromatography and the products were identified using standard samples and by GC-MS and ^1H NMR spectroscopy.

2.4.3.3. *Oxyiodination of aromatics*

Oxidative iodination of aromatics was carried out in a similar manner as described for the bromination reaction, except that KI was used as iodinating agent and the pH of the reaction medium was maintained at ~ 4.

2.4.3.4. *Oxychlorination of aromatics*

Oxychlorination of aromatics was also carried out in a similar manner as described for bromination and iodination reactions. The chlorinating agent used was HCl and the pH of the reaction medium was adjusted to ~ 3.

Table 2.1 provides the list of chemicals used in the present study, their quality and source of procurement.

Table 2.1. Chemicals and starting materials used in the present work

Chemical	Grade	Remarks
Acetone “dry”	AR, 99%	S.D. fine-Chem. Ltd., India
Acetonitrile	GR, 99%	Loba Chemie, Pvt. Ltd. India
Cetyltrimethyl ammonium bromide	98%	S.D. fine-Chem. Ltd., India
Cyclohexene	99%	S.D. fine-Chem. Ltd., India
5,5-Dimethyl-1-pyrroline-N-oxide	97%	Aldrich (purified)
Ethanol Absolute “Omnis”	99.9%	S.D. fine-Chem. Ltd., India
n-Hexane	AR 99%	S.D. fine-Chem. Ltd., India
Hydrogen peroxide solution (30% aq.)	GR (100 Volume)	Loba Chemie Pvt. Ltd. India (standardized)
Hydrogen peroxide 50%	145 w/w	Loba Chemie Pvt. Ltd. India (standardized)
Methanol Extra Pure	99%	Loba Chemie Pvt. Ltd. India

		(purified)
Poly(ethylene glycol)-block-poly(propylene glycol)-block-poly(ethylene glycol)	Avg. M_n ca. 5800	Sigma-Aldrich
2-Propanol	GR, 99.7%	Merck Ltd., India
Styrene monomer	99%	Encore Chemicals (Distilled)
3-Aminopropyl trimethoxysilane	97%	Aldrich
3-Mercaptopropyl trimethoxysilane	95%	Aldrich
Tetrabutylorthotitanate	99%	Acros Organics, USA (used as recieved)
Tetraethylorthosilicate	99%	Sigma-Aldrich, Germany
Tetramethylammonium hydroxide, 25 wt% solution in water		S.D. Fine-Chem. Ltd., India
Tetrapropylammonium hydroxide, 20 wt%	< 10 ppm Na^+	Catalysis Pilot Plant, NCL, Pune
Salicylaldehyde	99 %	Merck India Ltd.
Ethylenediamine	99.9 %	Meerck India Ltd
Benzaldehyde	99.5 %	Merck India Ltd.
Pyrrole	99 %	Spectrochem
Propionic acid	98 %	S.D. Fine-Chem. Ltd., India
Manganese acetate tetrahydrate	99 %	Merck India Ltd.
N, N- dimethyl formamide	99 %	Merck India Ltd.
Ammonium tungstate	99 %	Merck India Ltd.
Ammonium heptamolybdate	99 %	Merck India Ltd.
Vanadium pentoxide		Merck India Ltd.
Vanadyl sulfate trihydrate		Aldrich, USA

Dichloromethane	99%	Merck India Ltd.
Methanol	99%	Merck India Ltd.
Toluene	99%	Merck India Ltd.
R-(+)-Limonene	98%	Aldrich
α -Pinene	96%	Aldrich
3-Carene	98%	Aldrich
Phenol red	99%	S.D. Fine-Chem. Ltd., India
4-(2-hydroxyethyl)-1-piperazineethane sulfonic acid	99%	Aldrich
Potassium bromide	99.9%	Merck
Potassium iodide	99.9%	Merck
Hydrochloric acid	34.5% V/V	S.D. Fine-Chem. Ltd., India
Styrene oxide	99%	Aldrich
Cyclohexene oxide	99%	Aldrich
Epichlorohydrin	99.5%	Spectrochem
Aniline	99.9%	Merck India Ltd.
4-Choloro aniline	99.9%	Loba Chemie Pvt. Ltd. India (standardized)
<i>p</i> -Anisidine	99%	S.D. Fine-Chem. Ltd., India
<i>o</i> -Toluidine	99.5%	S.D. Fine-Chem. Ltd., India
<i>m</i> -Toluidine	99.5%	S.D. Fine-Chem. Ltd., India
Butyl amine	99%	Loba Chemie Pvt. Ltd. India (standardized)
Cyclohexyl amine	99%	Merck
Anisole	99.9%	Spectrochem
Phenol	99%	S.D. Fine-Chem. Ltd., India
Iso-butyaldehyde	99.9%	Aldrich

Imidazole	99%	Spectrochem
2-Methyl Imidazole	99%	Spectrochem
N-Methyl Imidazole	99.9%	Flüka
Benzyl alcohol	99%	Merck
Glycerol	98%	Merck India Ltd.

2.5. References

- [1] A. Stein, B. J. Melde, R. C. Schrodén, *Adv. Mater.* 12 (2000) 1403.
- [2] A. P. Wight, M. E. Davis, *Chem. Rev.* 102 (2002) 3589.
- [3] K. Møller, T. Bein, *Chem. Mater.* 10 (1998) 2950.
- [4] (a) D. Zhao, J. Feng, Q. Huo, N. Melosh, G. H. Fredrickson, B. F. Chmelka, G. D. Stucky, *Science* 279 (1998) 548. (b) Zhao, D.; Huo, Q.; Feng, J.; Chmelka, B. F.; Stucky, G. D. *J. Am. Chem. Soc.* 120 (1998) 6024.
- [5] (a) F. Feng, G.E. Fryxell, L.-Q. Wang, A.Y. Kim, K.M. Kemner, *Science* 276 (1997) 923. (b) L. Mercier, T.J. Pinnavaia, *Adv. Mater.* 9, (1997), 500. (c) A. Stein, B.J. Melde, R.C. Schrodén, *Adv. Mater.* 12 (2000) 1403.
- [6] C.M. Crudden, M. Sateesh, R. Lewis, *J. Am. Chem. Soc.* 127 (2005) 10045.
- [7] D. Margolese, J. A. Melero, S. C. Christiansen, B. F. Chmelka, and G. D. Stucky, *Chem. Mater.* 12 (2000) 2448
- [8] (a) W.M. Van Rhijn, D.E. De Vos, B.F. Sels, W.D. Bossaert, P.A. Jacobs, *Chem.*

- Commun. (1998) 317. (b) D. Das, J.-F. Lee, S. Cheng, Chem. Commun. (2001) 2178. (c) E. Cano-Serrano, J.M. Campos-Martin, J.L.G. Fierro, Chem. Commun. (2003) 246. (d) B.C. Wilson, C. W. Jones, Macromolecules 37 (2004) 9709.
- [9] K. Srinivasan, P. Michaud, J.K. Kochi, J. Am. Chem. Soc. 108 (1986) 2309
- [10] A. D. Alder, F.R. Longo, F. Kampas, J. Kim, J. Inorg. Nucl. Chem. 32 (1970) 2443.
- [11] M. S. Morey, S. O'Brien, S. Schwarz, G.D. Stucky, Chem. Mater. 12 (2000) 898.
- [12] V. Pârvulescu, C. Anastasscu, B.L. Su, J. Mol. Catal. A: Chemical 198 (2003) 249.
- [13] W. H. Bragg, W. L. Bragg, The Crystalline State, Vol. 1, McMillan, New York, 1949.
- [14] G. Bergeret, in: Handbook of Heterogeneous Catalysis, Vol. 2, Eds: G. Ertl, H. Knozinger, J. Weitkamp, Wiley-VCH, Weinheim, 1997, pp. 464
- [15] C. N. Banwell, "Fundamentals of Molecular Spectroscopy" Tata McGraw-Hill Pub. Co. Ltd. New Delhi, 1979
- [16] V. B. Kartha, "Spectroscopic Methods in Heterogeneous Catalysis" Eds N.M. Gupta, V.B. Kartha and R.A. Rajadhyaksha, Tata McGraw Hill, 1991, p.1.
- [17] P. L. Villa, F. Trifiro, I. Pasquon, React. Kinet. Catal. Lett. 1 (1974) 341.
- [18] J. E. Wertz, J.R. Bolton, "Electron Spin Resonance" McGraw-Hill, New York, 1972.
- [19] A. Abragam, B. Bleaney, "Electron Paramagnetic Resonance of Transition Ions" Clarendon, Oxford, 1970.

- [20] J. Wolstenholme, “An Introduction to Surface Analysis by XPS and AES” John Wiley & Sons, New York, 2003.
- [21] D. K. Gosser, “Cyclic Voltammetry Simulation and Analysis of Reaction Mechanisms” Wiley-VCH, Germany, 1993.
- [22] S. Brunauer, P. H. Emmett, E. Teller, *J. Am. Chem. Soc.* 60 (1938) 309.
- [23] E. P. Barrett, L. G. Joyner, P. P. Halenda, *J. Am. Chem. Soc.* 73 (1951) 373.
- [24] J. I. Goldstein, H. Yakowitz (Eds.), *Practical Scanning Electron Microscopy*, Plenum Press, New York, 1975.
- [25] G. Lawes, *Scanning Electron Microscopy and X-Ray Microanalysis*, John Wiley and Sons Ltd., Chichester, 1987.
- [26] J. R. Fryer, *Chemical Applications of Transmission Electron Microscopy*, Academic Press, San Diego, 1979.
- [27] J. M. Thomas, O. Terasaki, P. L. Gai, W. Zhou, J. Gonzalez-Calbet, *Acc. Chem.Res.* 34 (2001) 583.
- [28] S. Brunauer, P. H. Emmett, E. Teller, *J. Am. Chem. Soc.* 60 (1938) 309.

CHAPTER – 3

SO₃H-functionalized SBA-15 as an Efficient Regio- and Stereoselective Solid Acid Catalyst

3.1. Introduction

The discovery of mesoporous silica of FSM and MCM-type materials in early nineties has opened a new era in the field of heterogeneous solid catalysts because of the unique properties of these materials like high uniform surface area, large pore size and thick pore walls [1]. The pore sizes of these materials can be tailored depending on the synthesis method used, ranging from 1.5-10 nm. Larger pore sizes are also shown by SBA family e.g. SBA-15 making them superior to MCM type mesoporous materials [2, 3]. The ordered mesostructured materials can serve as better-defined supports, in comparison to non-ordered, amorphous solids, onto which organic groups can be anchored. Hence, the attachment of organic functionalities to the surface of the silica mesoporous supports has been an interesting research area in heterogeneous catalysis and green chemistry during the last few years [4]. These hybrid mesoporous solids have been considered for a wide range of catalytic transformations [5]. Heterogenization of active species can result in an improvement of the overall efficiency of the process because of several features such as easier separation of the catalyst from the reaction medium, catalyst regeneration and reuse, and confinement of the active species within the mesopores which provides a way to introduce shape selectivity and thus, greater specificity to a reaction product. Basically, two strategies have been described to anchor organic groups to a mesostructured silica surface via formation of covalent bonds: grafting methods (post-synthesis procedure) and co-condensation (direct synthesis). Grafting procedures are based on modification of the silica surface with organic groups through silylation reactions occurring on isolated ($\equiv\text{Si-OH}$) and geminal ($=\text{Si}(\text{OH})_2$) silanol groups using trichloro- or trialkoxyorganosilane and silylamines as organic precursors. In contrast, direct synthesis consists of the co-condensation of siloxane and organosiloxane precursors in

the presence of the corresponding structure-directing agent, SDA. Each functionalization pathway has certain advantages. Direct method usually yields a uniform surface coverage with organic groups and also provides better control over the amount of organic groups incorporated to the structure. However, products obtained by post-synthesis grafting are often structurally better defined and hydrolytically more stable than samples obtained from the direct synthesis method. In this chapter, ordered, mesoporous SBA-15 have been functionalized with propyl thiol and propyl sulfonic acid groups and their catalytic activities in a variety of acid-catalyzed reactions is reported.

3.2. Experimental

3.2.1. Material preparation and characterization

Neat and propyl thiol and sulfonic acid functionalized SBA-15 materials were prepared as reported in Chapter – 2. X-ray diffractograms were recorded on an X'Pert Pro (Philips) diffractometer using Cu K α radiation and a proportional counter as detector. Transmission electron micrographs (TEM) of the samples were scanned on a JEOL (model 1200 EX) microscope operating at 100 kV. The C, H, N & S composition was determined by a Carlo-Erba 1106 analyzer. The specific surface area (BET) of the samples was determined using NOVA 1200 Quanta Chrome equipment. The data points of p/p_0 in the range of about 0.05 to 0.3 were used in the calculations. The micropore volume was estimated from the t-plot and the pore diameter was estimated using the Barret-Joyner-Halenda (BJH) model. Thermogravimetric analysis was done on a Seiko DTA-TG 320 instrument under air (50 ml/min), at a ramp rate of 10 K/min, in the temperature range of 308 – 1078 K. FTIR spectra were recorded on a Shimadzu 8201 PC spectrophotometer in the region 400 – 4000 cm⁻¹. Diffuse-reflectance UV-visible (DRUV-vis) spectra were obtained with a Shimadzu UV-2500

PC spectrophotometer in the range 200 – 850 nm. Acidity of the catalysts was measured by NH₃-TPD measurements. It was also estimated based on ion exchange capacity. About 50 mg of SBA-15-*pr*-SO₃H was dispersed in 10 ml of 0.01 M NaCl solution. It was allowed to equilibrate for about 30 min. The solid was separated out and the liquid portion was titrated with 0.01 M NaOH solution. The ion exchange capacity of the catalyst was determined from the titration value [6]. In some studies, SBA-15-*pr*-SO₃H was initially adsorbed with different amounts (0.25 – 1.5 mmol) of styrene oxide or aniline. Ion exchange capacities of these modified catalysts were determined in the same manner as described above. Thus the influence of substrate adsorption on the ion exchange capacity of SBA-15-*pr*-SO₃H was determined.

3.2.2. Reaction procedure

The activity of the catalysts were investigated in various acid-catalyzed reactions: (1) regio- and stereo selective ring opening of epoxides with amines to produce β-amino alcohols, (2) regio-selective ring opening of epoxides with alcohols to produce β-alkoxy alcohols, (3) etherification of glycerol with tert.-butyl alcohol to produce glycerol alkyl ethers, (4) esterification of acids, and (5) 3-component Mannich condensation reactions. Details of the reaction procedures are provided in Chapter – 2. Purity of some β-amino alcohols was confirmed by NMR ([Appendix-I](#)).

3.3. Results and Discussion

3.3.1. Characterization

3.3.1.1. Chemical composition

Sulfonic acid-functionalized SBA-15 molecular sieves were prepared by the secondary synthesis route, wherein, in the first step, thiol-functionalized SBA-15 (SBA-15-*pr*-SH) was prepared by silylation/condensation of pre-formed, vacuum-dried SBA-15 with MPTMS, which was then, in the second step, oxidized with

aqueous H₂O₂ to the sulfonic acid functionality (SBA-15-*pr*-SO₃H). Chemical analysis (Table 3.1) revealed that SBA-15-*pr*-SO₃H contained 0.6 mmol of -*pr*-SO₃H groups per g. silica whereas the initial loading of propyl thiol functional group was about 1.5 mmol per g of silica. The organic functional groups have three potential sites (-Si(OCH₃)₃), which can bind to the silica surface. While the entire three -Si-OCH₃ can, in principle, react with surface silanol groups to form Si-O-Si bonds, it is also possible that only one or two of the alkoxy groups would react with surface silanol groups. In addition, two of the SH-propyltrimethoxysilane molecules may also react with each other forming direct Si-O-Si bonds between the organic functional molecules. However, at the low concentration of functional groups utilized in the present case such a possibility and formation of disulfide bonds are unlikely and spectral analysis did not indicate the presence of such disulfide bonds.

3.3.1.2. XRD

The SBA-15 materials showed XRD pattern (Fig. 3.1) corresponding to a 2D hexagonal *p6mm* symmetry [7, 8]. Well-resolved (100), (110) and (200) reflections, consistent with a long-range, mesopore ordering for SBA-15, appeared at 2 θ values of 0.919, 1.570 and 1.809°, respectively. Upon organo-functionalization these peaks shifted to higher 2 θ values – 1.019, 1.755 and 2.035° for SBA-15-*pr*-SH and 1.034, 1.779, 2.059° for SBA-15-*pr*-SO₃H (Fig. 3.1). Shift in peaks position to higher 2 θ values was observed also by other researchers when transition metal ions and metal complexes were introduced into mesoporous architectures [7, 8]. The d-spacing (d_{100}) and unit cell parameters (Table 3.1) agree well with the reported values [7, 8].

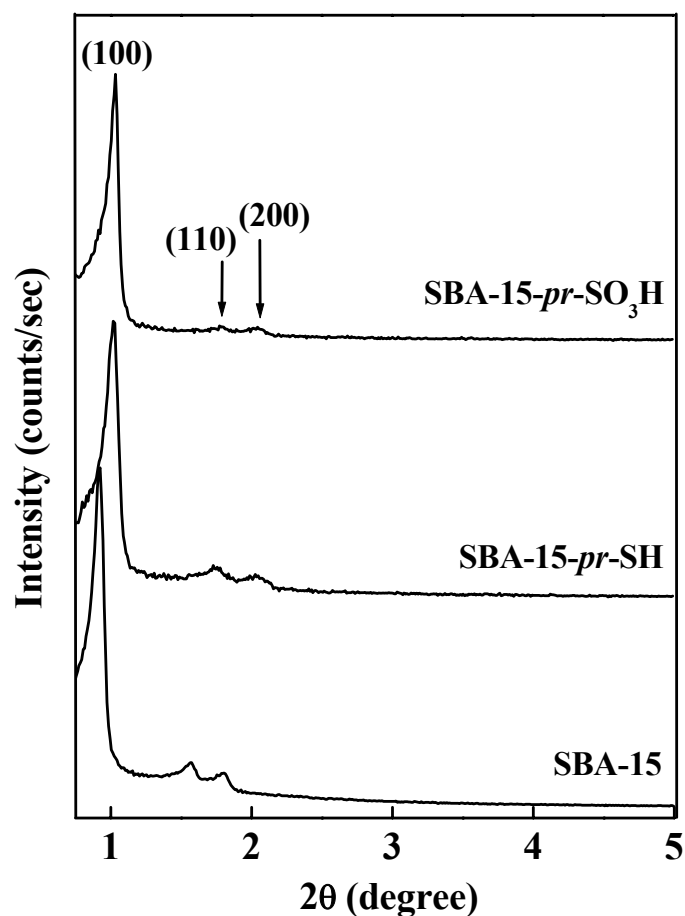


Fig. 3.1. X-ray diffractograms of “neat” and organo-functionalized SBA-15.

3.3.1.3. N_2 adsorption-desorption

Organic-functionalization did not alter the long-range mesoporous arrangement (Fig. 3.2). The catalysts, in general, showed type IV nitrogen adsorption/desorption isotherms with H1 hysteresis. Upon organic-functionalization, a marked decrease in BET surface area (from 692 to 533 m^2/g) and total pore volume (from 1.13 to 0.83 cm^3/g) was detected (Table 3.1). The pore diameters were in the range of 6.2 – 6.5 nm, corresponding to mesopores [7, 8]. The value of the C constant of the BET equation decreased from 1.05×10^2 (for SBA-15) to 0.78×10^2 and 0.83×10^2 for SBA-15-pr-SH and SBA-15-pr- SO_3H , respectively. This is because of the

elimination of acidic surface OH upon silylation. In such a case the BET theory does not apply. However, the surface area determined by BJH theory using the cumulative area of the pores also showed a similar decrease as a consequence of organofunctionalization (Table 3.1). Thus, this large decrease in surface area on functionalization with a few molecules of modifier (*-pr-SH* and *-pr-SO₃H*) is, rather, surprising. Apparently some reconstruction of the solid, which we have not been able to detect, is occurring.

3.3.1.4. FTIR spectroscopy

SBA-15 showed characteristic IR peaks at around 1040 – 1260, 820 and 500 cm^{-1} due to Si-O-Si stretching vibrations and a broad, asymmetric feature at 2900 – 3800 cm^{-1} due to the O-H of silanols and water (Fig. 3.3) [7]. Functionalization with *-pr-SH* showed additional features at 2928 and 2852 cm^{-1} due to C-H stretching vibrations and a weak peak at 2776 cm^{-1} , confirming the presence of SH functionality in the solid [7]. In the case of SBA-15-*pr-SO₃H*, the band at 2776 cm^{-1} was completely absent, indicating that the *-SH* groups originally present in SBA-15-*pr-SH*, were all oxidized to *-SO₃H* groups. The sulfonic acid group showed bands at 650 and 1060 cm^{-1} in SBA-15-*pr-SO₃H* [8].

3.3.1.5. Thermal stability

Thermal analysis (TG-DTA) of SBA-15 (Fig. 3.4) showed three stages of weight loss in agreement with the earlier reports [9]. Stage I (313 – 475 K; exothermic) corresponds to the loss of physically held water; stage II (475 – 815 K, exothermic) corresponds to the loss of water present within the micropore walls. Stage III (815 – 1273 K, endothermic) is due to silanol condensation ($2 \text{ Si-OH} \rightarrow \text{Si-O-Si} + \text{H}_2\text{O}$).

Table 3.1. Chemical composition and structural properties of functionalized SBA-15 materials

System	Elemental analysis			Organic functional group	XRD		N ₂ adsorption			Wall thickness (nm)	
	(wt%)				(mmol/g) ^a	d ₁₀₀ (nm)	Unit cell parameter (nm)	Pore diameter (nm)	Specific surface area (m ² /g)		Total pore volume (cm ³ /g)
	C	H	S	BET					BJH		
SBA-15	0.4	0.9	0	0	9.5	11.0	6.5	692	686	1.13	4.5
SBA-15- <i>pr</i> -SH	6.3	1.8	4.7	1.5 (1.7)	9.9	11.5	6.5	534	554	0.87	5.0
SBA-15- <i>pr</i> -SO ₃ H	4.8	1.8	1.8	0.6 (0.7)	9.7	11.3	6.2	533	546	0.83	5.1

^aDetermined from the S-content. Values in parentheses are those estimated from the thermo-gravimetric analysis data.

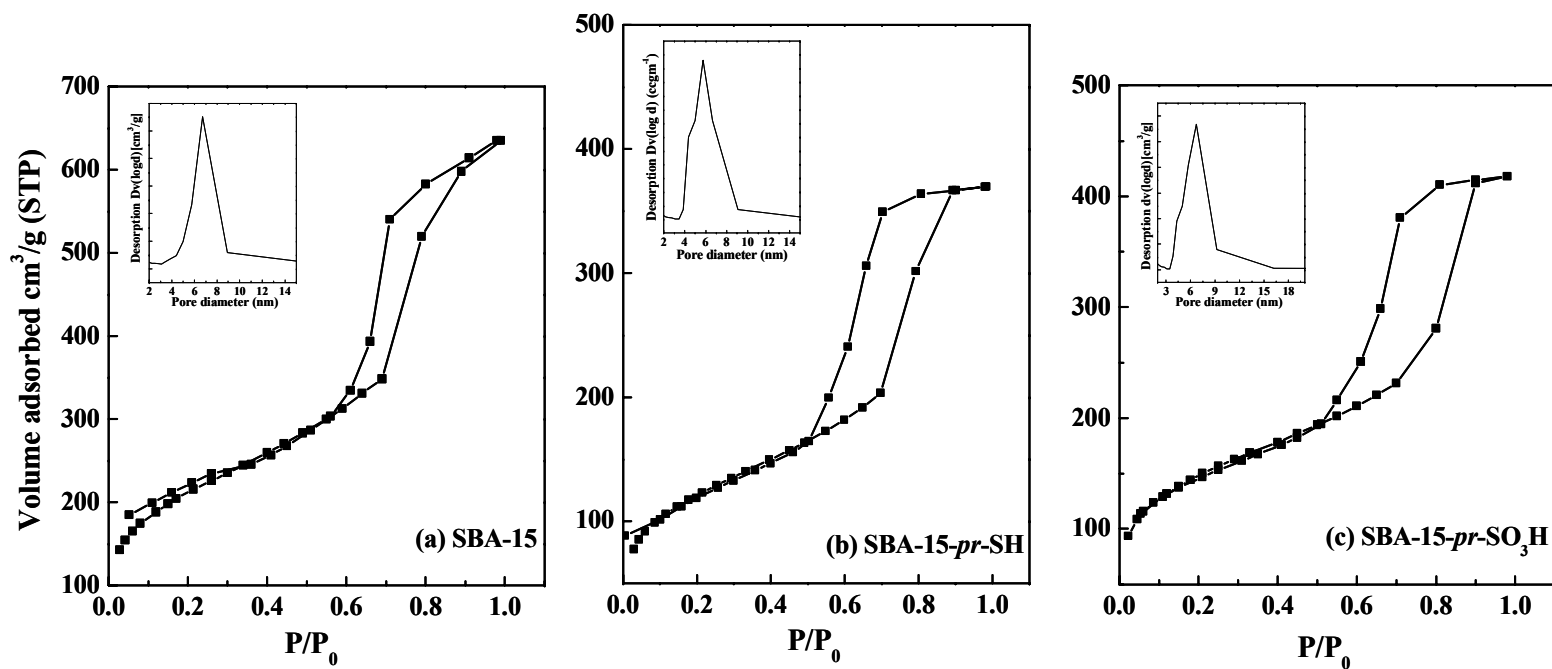


Fig. 3.2. Nitrogen adsorption/desorption isotherms and pore size distribution of SBA-15 molecular sieves.

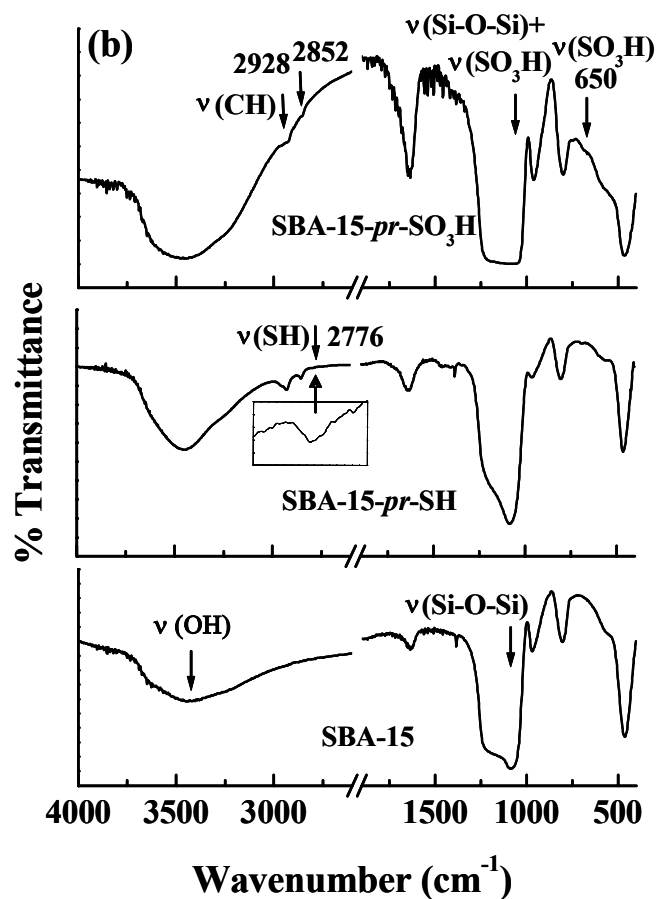


Fig. 3.3. FTIR spectra of “neat” and organo-functionalized SBA-15. Characteristic IR peaks are indicated by arrows.

SBA-15-*pr*-SH and SBA-15-*pr*- SO_3H showed four stages of weight loss: stages I, IIA, IIB and III, respectively. Stages IIA (475 – 661 K) and IIB (661 – 815 K) are due to desorption of water from the micropore walls as well as decomposition of the organic functional group (*-pr*-SH and *-pr*- SO_3H) [10].

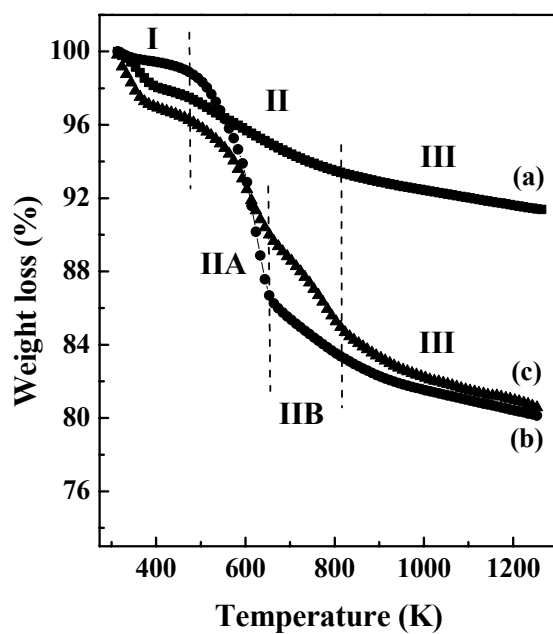
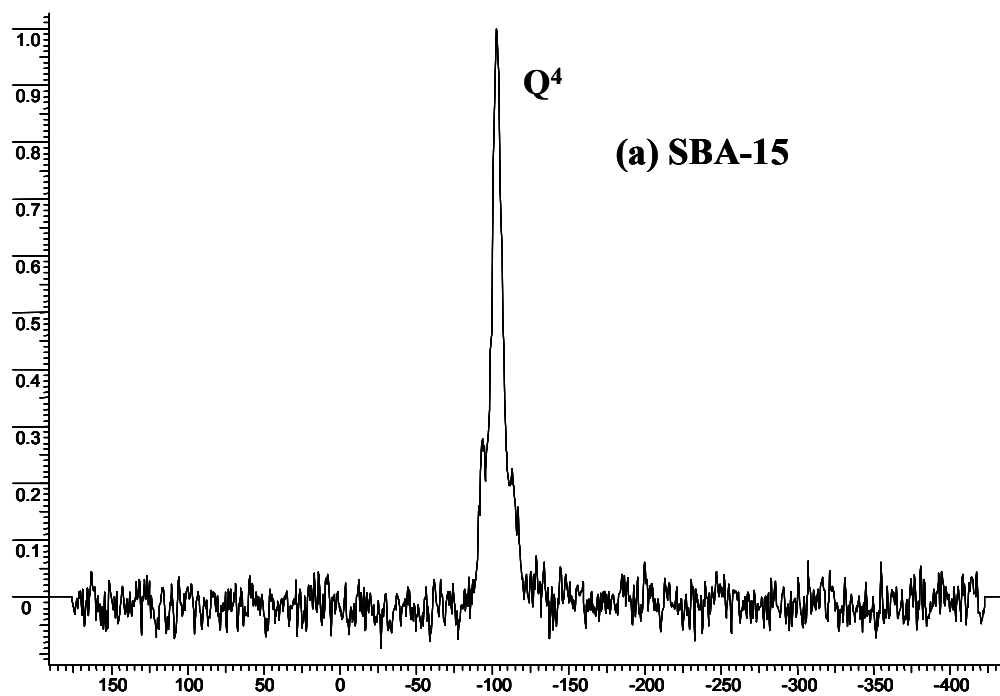


Fig. 3.4. TG profiles (a)SBA-15, (b) SBA-15-*pr*-SH, (c) SBA-15-*pr*-SO₃H

3.3.1.6. ²⁹Si NMR



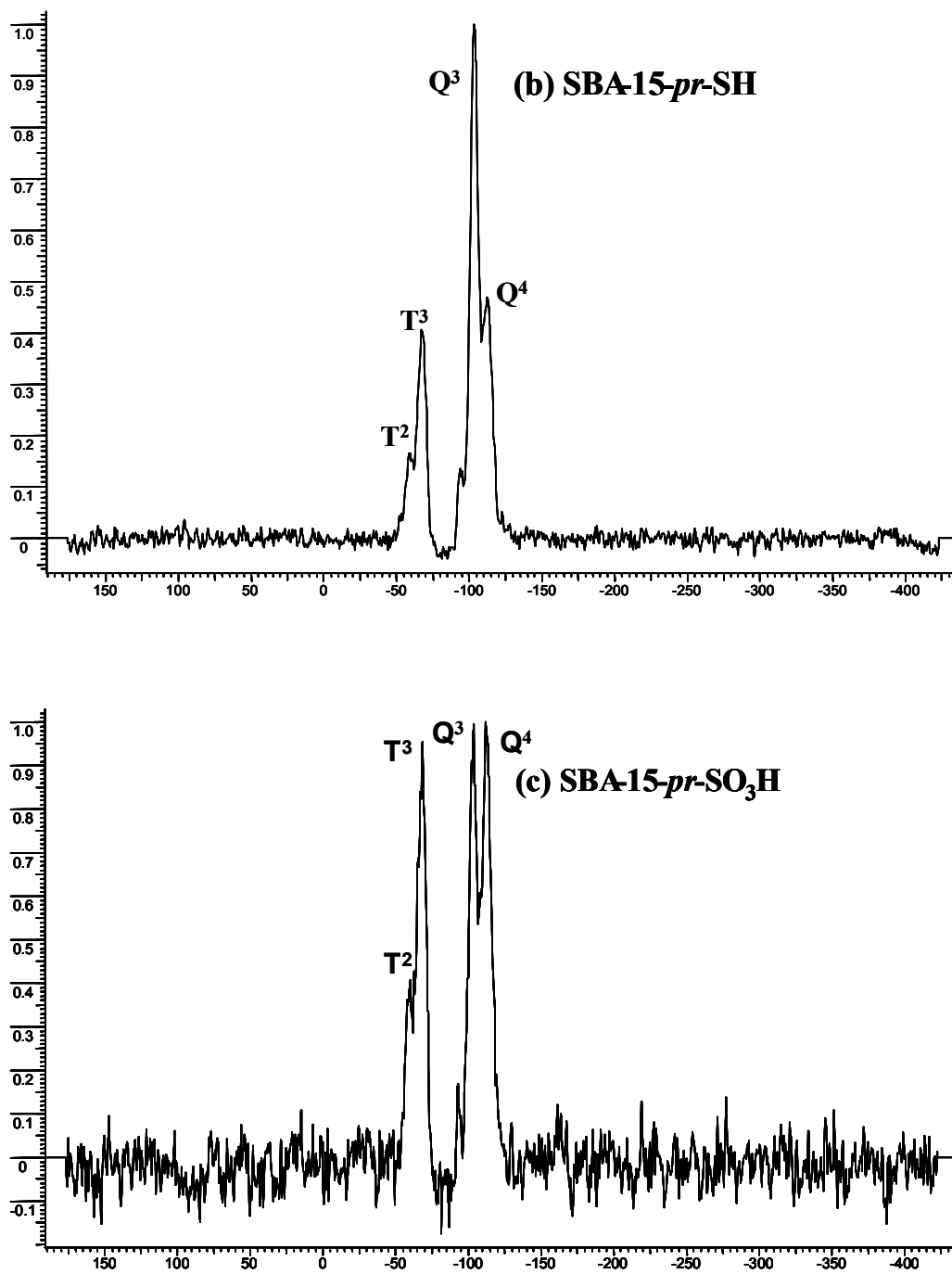


Fig. 3.5. ^{29}Si NMR of (a) ‘neat’ SBA-15, (b) SBA-15-*pr*-SH and (c) SBA-15-*pr*-SO₃H

'Neat' SBA-15 showed mainly a signal due to Q^4 and a shoulder due to Q^3 species. Propyl thiol functionalized SBA-15 contained Q^3 type silicon as the major species. Two additional type silicon species T^2 and T^3 were also detected (Fig. 3.5). These changes in the NMR spectra provide a clear evidence for the presence of different types (Q^3 , T^3 and T^2) of surface functionalized silanol group. Propyl sulfonic acid functionalized SBA-15 showed spectral features similar to that of SBA-15-*pr*-SH.

3.3.1.7. TEM

Transmission electron microscopy (TEM) has been used to obtain topographic information about the mesoporous matrices at near atomic resolution. Fig 3.6 shows the TE micrographs of (a) 'bare' SBA-15, (b) SBA-15-*pr*-SH and (c) SBA-15-*pr*- SO_3H respectively. The parallel TEM pattern showed the uniform channels while the perpendicular TEM pattern showed clear hexagonal pores of the mesoporous silica. Hence, it can be stated that the long range mesoporous ordering didn't get affected due to organo-functionalization. These figures support conclusions based on the low-angle XRD patterns.

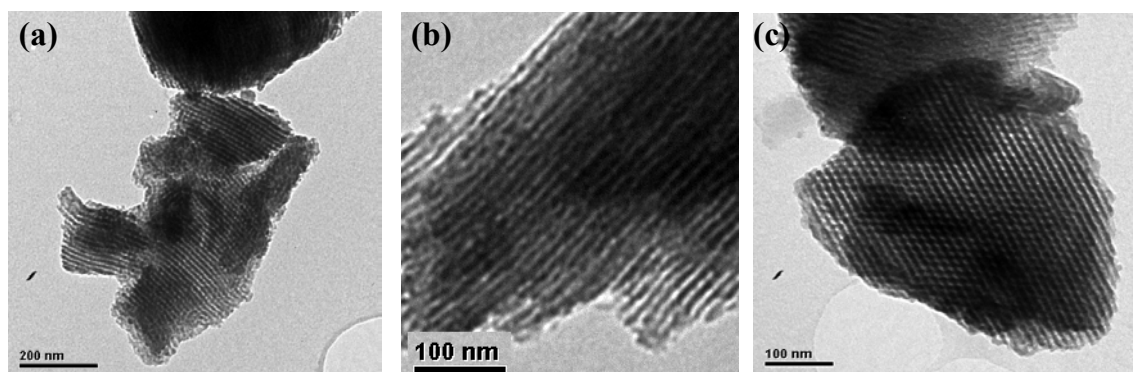


Fig. 3.6. Transmission electron micrographs of (a) SBA-15, (b) SBA-15-*pr*-SH and (c) SBA-15-*pr*- SO_3H .

3.3.1.8. Scanning Electron microscopy

The morphology and particle size of ‘bare’ and organo-functionalized SBA-15 mesoporous silica have been determined from scanning electron microscopy. Fig 3.7 depicts the SEM micrographs of (a) ‘bare’ SBA-15, (b) SBA-15-*pr*-SH and (c) SBA-15-*pr*- SO_3H respectively. Morphology of the particles was in general elliptical.

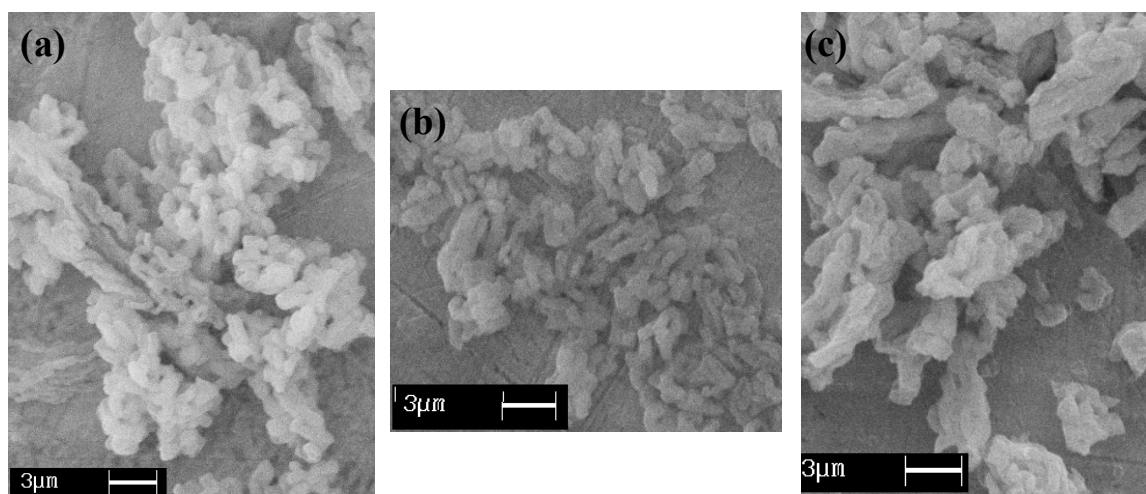


Fig. 3.7. SEM of (a) SBA-15, (b) SBA-15-*pr*-SH and (c) SBA-15-*pr*- SO_3H .

3.3.1.9. Acidity measurements

3.3.1.9.1. NH_3 -TPD

Temperature-programmed desorption (TPD) of ammonia was performed on a Micromeritics Autochem 2910 instrument. SBA-15-*pr*- SO_3H (50 mg), sample was initially activated at 423 K for 1 h in He-flow (5 ml/min). It was then cooled to 298 K and 10% NH_3 in He was adsorbed for 1 h. The sample was flushed with He (10 ml/min) for 30 min at 373 K and the desorption of NH_3 was measured raising the temperature from 373 to 923 K at a ramp rate of 10 K/min and held at 923 K for 20 min.

The organic functional groups on SBA-15-*pr*-SO₃H are thermally unstable beyond 475 K. So, acidity estimation from NH₃-TPD may not be an accurate method for sulfonic acid functionalized SBA-15 samples. Neat SBA-15 did not desorb NH₃ in the temperature range 373 – 473 K (Fig. 3.8). SBA-15-*pr*-SO₃H showed a desorption peak with maximum at 470 K. The amount desorbed was 0.26 mmol/g catalyst.

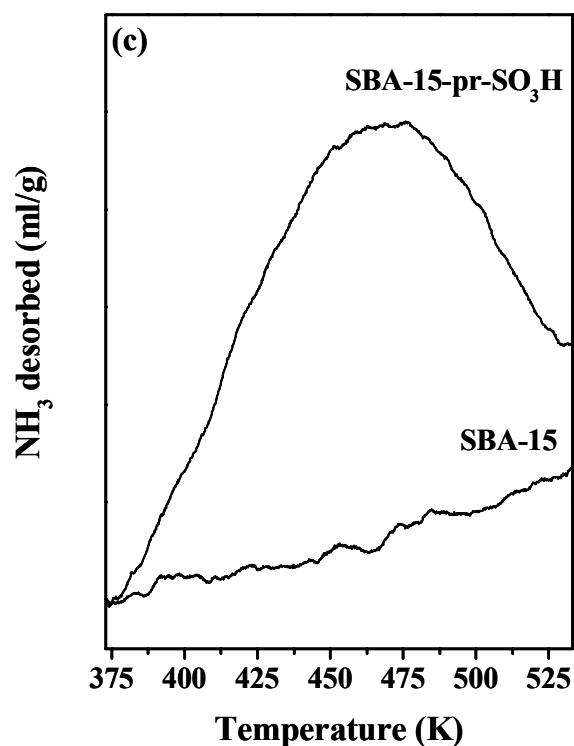


Fig. 3.8. NH₃-TPD of ‘bare’ SBA-15 and SBA-15-*pr*-SO₃H.

3.3.1.9.2. Ion exchange capacity

Based on titrimetric method, it was found that the ion exchange capacity of SBA-15-*pr*-SO₃H was 0.7 meq/g catalyst, which is in good agreement with the expectation from thermal and elemental analyses (of –SO₃H groups). This suggests that in SBA-15-*pr*-SO₃H almost all the protons of sulfonic acid can be exchanged with sodium ions.

Titrimetric studies were conducted also for thiol-functionalized SBA-15 (SBA-15-*pr*-SH) and “bare” SBA-15. Ion exchange capacities of these materials were 0.2 and 0.04 meq/g catalyst respectively. It may be noted that the ion exchange capacity of SBA-15-*pr*-SH is much lower than the actual thiol content in the catalyst (Table 3.1). Hence, only a fraction of surface SH protons is replaced by Na⁺. The thiol group is a weaker acid than sulfonic acid. Hence, the dissociation of S-H protons and consequent ion exchange with Na⁺ are lower for SBA-15-*pr*-SH than for SBA-15-*pr*-SO₃H.

3.3.2. Catalytic activity

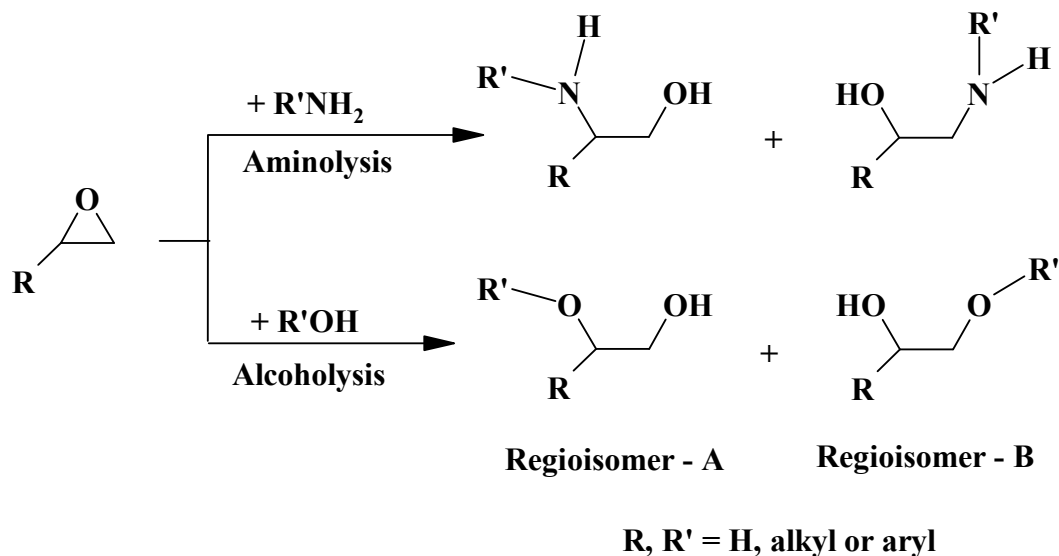
3.3.2.1. Ring-opening of epoxides with amines and alcohols

Epoxides are versatile and important intermediates in pharmaceutical and agrochemical industries. The three-membered heterocyclic ring is strained and offers an uncommon combination of reactivity, synthetic flexibility and atom economy. It is susceptible to attack by a range of nucleophiles including nitrogen (ammonia, amines, azides), oxygen (water, alcohols, phenols, acids) and sulfur (thiol)-containing compounds leading to bifunctional molecules of great industrial value. β -Amino alcohols (Scheme 3.1), for example, are used in the synthesis of β -blockers, insecticidal agents, oxazolines and as chiral ligands in asymmetric synthesis [11-15]. The classical synthesis of β -amino alcohol involves the ring opening of epoxides with amines. These reactions are, conventionally, carried out with a large excess of the amines at elevated temperatures and in the presence of solvents. This method is less effective for weakly nucleophilic amines and yields low regioselectivity [16, 17]. A variety of catalyst systems such as sulfamic acid, amberlyst resin, metal triflates, transition metal halides, ionic liquids, zeolites and Lewis acids in a supercritical carbon dioxide medium have been investigated [18-25]. All

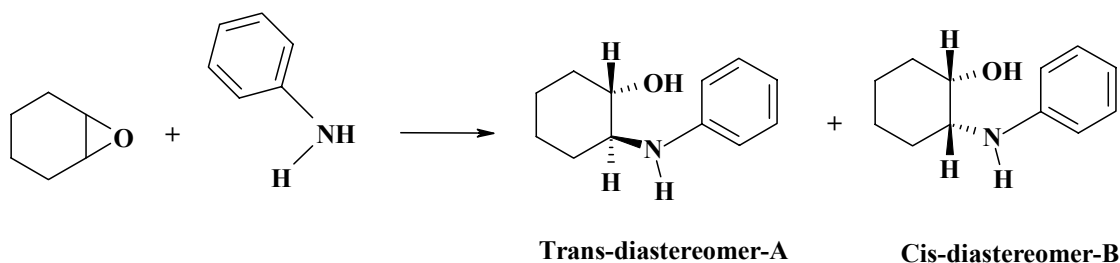
these catalysts need long reaction times, elevated temperatures, high pressures, stoichiometric amounts of catalysts and use of expensive reagents or catalysts. Recently, the ring opening of epoxides in water in the absence of any catalyst was reported, but it also required a long reaction time. The product yield was also low [26]. Even though, heterogeneous catalysts have been used in the ring opening addition of nucleophiles like amines and alcohols to epoxides, their activity and selectivity were also low. Garcia et al [27], for example, reported that zeolite Y, in the reaction between styrene epoxide and n-propanol, gave conversions only in the range of 5-10%. In addition, many secondary products were also formed. Robinson et al [28] reported that mesoporous aluminosilicates catalyze the alcoholysis of epoxides to give β -alkoxyalcohols in high yields at room temperature and in short reaction times (1 – 4.5 h). In this chapter the application of solid, Brønsted acidic, sulfonic acid-functionalized SBA-15 for the activation and ring opening of epoxides with amines and alcohols is reported.

Sulfonic acid-functionalized mesoporous silica [29, 30] has been used as a catalyst for the esterification of carboxylic acid with alcohols [31-33], synthesis of polycaprolactone [34] and oxidation reactions [35, 36]. The aims of the present study are: (1) to study the activity and, especially, the selectivity of sulfonated SBA-15 for the aminolysis of epoxides, and (2) to delineate the dominant structural, adsorption and other kinetic parameters that control the rates and selectivity in this reaction. In contrast to the alcoholysis of epoxides, not much information is available on the use of solid Brønsted acids for the aminolysis of epoxides. A range of β -amino and alkoxy alcohols, respectively, was synthesized using these solid catalysts in very high yields from

symmetrical and unsymmetrical epoxides (with aromatic as well as aliphatic amines/alcohols) at *ambient temperatures* and *under solvent-free* conditions



Scheme 3.1.A. Regioselective ring opening of epoxides with amines and alcohols



Scheme 3.1.B. Stereoselective ring opening of cyclohexene oxide with aniline

3.3.2.1.1. Aminolysis of epoxides

β -Amino alcohols were synthesized by the ring opening of epoxides with amines over SBA-15-*pr*-SO₃H catalyst, at ambient temperatures, and solvent-free conditions (Table 3.2). Both steric hindrance and nucleophilicity of the amine influenced the reactivity.

The reaction of styrene oxide with aniline yielded two types of regio-isomers: A and B (Scheme 3.1.). Selectivity for the A-isomer was always higher (Table 3.2). The intrinsic catalytic activity (turnover frequency; TOF) of SBA-15-*pr*-SO₃H is higher than all the hitherto known catalysts for this reaction [18-26]. For example, for the reaction between styrene oxide and aniline, TOF values over sulfamic acid, amberlyst-15, Sc(OTf)₃ and NaY catalysts were 32, 2, 7 and 0.8 h⁻¹, respectively [18-26]. The corresponding value for SBA-15-*pr*-SO₃H was found to be 68 h⁻¹ (Table 3.2).

Very high conversion (92.6 mol %) and selectivity of product-A (100 mol %) were obtained when epichlorohydrin instead of styrene oxide was reacted with aniline (Table 3.2, Run No. 1). In spite of the fact that epichlorohydrin has many reactive positions and it can, in principle lead to some other products, no products other than the amino alcohols, A and B were observed by gas chromatography. Moreover, the conversions estimated based on the disappearance of either of the two reactants (epoxide/amine), were about the same. The reactivity (% conversion) decreased in the order: epichlorohydrin > propene oxide > styrene oxide > cyclohexene oxide. Cyclohexene oxide is a symmetrical epoxide. Reaction with aniline yields cis- and trans-diastereomeric products (Scheme 3.1.A). Only the trans-diastereo isomer formed (product characterization by ¹H NMR study) with 100% selectivity over these catalysts (Table 3.2, Run No. 15).

A range of β-amino alcohols was produced with high regio-selectivity from styrene oxide and different amines. The reactivity (epoxide conversion and turnover frequency), however, depended on the nature and type of the amine molecule. The product yield was low when cyclohexyl amine instead of aniline was used. High

conversions were obtained with aliphatic amines like n-butyl amine (Table 3.2, Run No. 3). With a secondary amine, piperidine, a conversion of 89.1 mol% and product isomer-A selectivity of 99.4 mol% was obtained (Table 3.2, Run No. 13). However, with morpholine, containing an additional oxygen atom in the hexa-cyclic saturated ring, the conversion was only 44.6 mol% (Run No. 14).

The reaction of styrene oxide with aniline at 298 K in the presence of thiol-functionalized SBA (SBA-15-*pr*-SH) and “bare” SBA-15 was also conducted. Conversions of styrene oxide in those experiments were found to be only 29 and 24.6 mol%, in contrast to 38.1 mol% in the presence of SBA-15-*pr*-SO₃H (Table 3.2, Run No. 6). These variations in catalytic activity follow changes in the ion exchange capacities/acid strengths of these SBA-15 materials. While isomers – A and B with product selectivity of 89.8 and 10.2 mol%, respectively, formed over SBA-15-*pr*-SO₃H, only the isomer-B formed over SBA-15-*pr*-SH and SBA-15 catalysts.

3.3.2.1.1.A. *Influence of Solvent*

Use of solvents suppressed the catalytic activity (Table 3.3). Solvent molecules compete with the substrate molecules for adsorption on the surface. The conversion was higher in non- or weakly-polar solvents (dichloromethane, toluene) than in polar solvents (acetonitrile, ethyl acetate) (Table 3.3).

Table 3.2. Aminolysis of epoxides over SBA-15-*pr*-SO₃H^a

Run No.	Epoxide	Amine	Epoxide conversion, mol %	Product selectivity, %		TOF ^b , h ⁻¹
				A	B	
1	Epichlorohydrin	Aniline	92.6	100	0	165
2	Epichlorohydrin	m-Toluidine	58.0	87.0	13.0	103
3	Epichlorohydrin	n-Butyl amine	87.5	87.0	13.0	156
4	Epichlorohydrin	Dibutyl amine	36.3	92.6	7.4	65
5	Propene oxide	Aniline	59.7	100	0	107
6	Styrene oxide	Aniline	38.1	89.8	10.2	68
6a			(54.2) ^c	(92.6) ^c	(7.4) ^c	(24) ^c
6b			(4.6) ^d	(100) ^d	(0) ^d	
7	Styrene oxide	p-Chloroaniline	34.0	94.4	5.6	61
8	Styrene oxide	p-Anisidine	15.0	100	0	27
9	Styrene oxide	m-Toluidine	32.3	88.2	11.8	58
10	Styrene oxide	o-Toluidine	19.1	100	0	34
11	Styrene oxide	Cyclohexylamine	10.0	85.0	15.0	18
12	Styrene oxide	n-Butyl amine	7.2	100	0	13
13	Styrene oxide	Piperidine	89.1	99.4	0.6	159
14	Styrene oxide	Morpholine	44.6	94.8	5.2	80
15	Cyclohexene oxide	Aniline	23.8	100	0	43

^aReaction conditions: SBA-15-*pr*-SO₃H - 25 mg (-*pr*-SO₃H loading was 0.56 mmol/g), epoxide - 10 mmol, amine - 10 mmol, temperature - 298 K, reaction time - 4 h.

^bTurnover frequency (TOF) = moles of epoxide converted per mol of -SO₃H in the catalyst per hour.

^cReaction conducted with 100 mg of the catalyst. ^dReaction conducted in the absence of a catalyst.

Table 3.3. Influence of solvent on the adsorption characteristics and reaction of styrene oxide with aniline over SBA-15-*pr*-SO₃H^a

Solvent (dielectric constant)	One substrate		Epoxide conv. mol%	Product selectivity, mol%		TOF (h ⁻¹) ^b
	Styrene oxide	Aniline		A	B	
			No solvent	0.20	0.21	38.1
Dichloromethane (9.1)	0.20	0.21	33.7	62.0	38.0	30
Toluene (2.4)	0.17	0.20	26.4	100	0	24
Acetonitrile (37.5)	0.06	0.13	4.1	100	0	4
Ethyl acetate (6.0)	0.04	0.11	3.9	100	0	3

^aReaction conditions: SBA-15-*pr*-SO₃H (*pr*-SO₃H loading is 0.56 mmol/g) - catalyst, 25 mg; styrene oxide, 5 mmol (with solvent) or 10 mmol (without solvent); reaction temperature, 298 K. reaction time, 4 h.

^bTurnover frequency (TOF) = moles of epoxide converted per mol of –SO₃H

The adsorption of reactants on the catalyst was performed in different solvent medium which were used as reaction solvent also. For this purpose, activated (393 K for 4 h) SBA-15-*pr*-SO₃H (50 mg) was dispersed, for 1 hr, in 0.5 mmol of styrene oxide or aniline substrate dissolved in 5 ml of solvent. The solid catalyst was, then, separated and the concentration of the substrate in the liquid portion was determined by gas

chromatography. The amount adsorbed on the catalyst surface was determined by difference of gas chromatographic peak area for corresponding reactant after and before adsorption. It was observed that, the adsorption of reactant was significantly higher in the absence of solvent than in the presence of solvent.

3.3.2.1.1.B. Influence of reaction temperature

Temperature had a notable effect on catalytic activity but only a marginal effect was found on selectivity (Table 3.4). The conversion increased with reaction time but the product selectivity was unaffected. At near-ambient conditions, complete conversion of styrene oxide and very high selectivity of the A-type regio-isomer (89.8 mol%) were obtained.

Table 3.4 Influence of temperature on the reaction of styrene oxide with aniline over SBA-15-*pr*-SO₃H^a

Reaction temperature (K)	Epoxide conversion, mol%	Product selectivity, %		TOF (h ⁻¹) ^b
		A	B	
298	38.1	89.8	10.2	68
308	68.5	86.3	13.7	122
323	88.7	87.1	12.9	158
343	91.3	83.6	16.4	163

^aReaction conditions: Catalyst, 25 mg; styrene oxide, 10 mmol; styrene oxide : aniline (molar ratio), 1 : 1; reaction time, 4 h, ^bTurnover frequency (TOF) = moles of epoxide converted per mol of –SO₃H

3.3.2.1.1.C. Kinetic studies

The kinetic rate constants and apparent activation energies for the aminolysis of styrene oxide with aniline over SBA-15-*pr*-SO₃H catalyst was determined using different molar ratios of the reactants and at different temperatures. The reaction was found to be first order with respect to both styrene oxide and aniline. The apparent activation energies (E_a) were calculated using the Arrhenius equation ($k = A \exp(-E_a/RT)$). These values for the catalyst are listed in Table 3.5. Brønsted-acidic SBA-15-*pr*-SO₃H possibly protonates the amines instead of activating the epoxide molecules.

Table 3.5. Kinetic data for aminolysis of styrene oxide with aniline over SBA-15-*pr*-SO₃H catalyst^a

Catalyst	Reaction temperature (K)	Rate constant (lit.mol ⁻¹ .sec ⁻¹)	Activation Energy (E_a) (KJ.mol ⁻¹)
SBA-15- <i>pr</i> -SO ₃ H	298	7.96×10^{-4}	59
	308	2.70×10^{-3}	
	313	2.75×10^{-3}	
	318	3.58×10^{-3}	

^aReactions were conducted taking 1:1 molar ratio of styrene oxide to aniline. Amount of the catalyst: 25 mg (SBA-15-*pr*-SO₃H)

3.3.2.1.2. Alcoholysis of epoxides

SBA-15-*pr*-SO₃H showed catalytic activity for the reaction of styrene oxide with different alcohols at ambient temperature and solvent-free conditions (Table 3.6). Selectivity of product A (Scheme 3.1.A) is 100%. The intrinsic catalytic activity of SBA-

15-*pr*-SO₃H is significantly higher than the hitherto known catalysts [28]. Alcohols having lower molecular weight have shown better activity as compared to higher molecular weight alcohols.

Table 3.6. Alcoholysis of styrene oxide over SBA-15-*pr*-SO₃H^a

Run No.	Alcohol	Styrene oxide conversion (mol%)	Selectivity of Product - A	TOF (h ⁻¹) ^b
1	Methanol	25.6	100	23
2	Ethanol	16.8	100	15
3	Propanol	10.4	100	9
4	n-Butanol	9.2	100	8
5	Benzyl alcohol	6.2	100	5
6	Cyclohexanol	7.2	100	6

^aReaction conditions: SBA-15-*pr*-SO₃H: Catalyst, 25 mg; styrene oxide and alcohol, 5 mmol each; temperature, 298 K; reaction time, 4 h.

^bTurnover frequency (TOF) = moles of styrene oxide converted per mol of –SO₃H in the catalyst per hour.

3.3.2.1.3. Mechanistic considerations

Most of the reactions of epoxides involve the opening of the oxirane ring, the addition of a proton to the epoxide oxygen and the deprotonated molecule of the substrate to one of the carbon atoms of the oxirane ring [37]. The reaction can occur under neutral, basic or acidic conditions. Reaction under neutral or basic conditions, involves the attack of a nucleophile on one of the epoxide carbon atoms. Under acidic conditions, the addition of the nucleophile is considerably accelerated due to the reversible formation of

the more reactive conjugate acid of the epoxide. The ring-opening reactions of epoxides take place by ionic mechanisms. The bond, which is broken, is the highly polar carbon-oxygen bond, which would be expected to break ionically. Possible exceptions are the reactions with hydrogen and a metal catalyst, which may take place by a free-radical mechanism [37]. To understand the interactions between the epoxide and substrate molecules with the active sites of the catalyst and draw conclusions on the reaction mechanism, the adsorption of these molecules on the catalyst surface have been investigated.

Adsorptions of one substrate (epoxide or amine) as well as competitive adsorption of both were investigated. In the adsorption studies of one substrate, a known quantity of SBA-15-*pr*-SO₃H catalyst (50 mg) was initially activated at 393 K for 4 h and then dispersed in a known concentration of the substrate (0.5 mmol) dissolved in a solvent (5 ml). After an hour, the concentration of the substrate in the liquid portion was estimated by gas chromatography and the amount adsorbed, in separate experiments, on the catalyst surface was determined. When dichloromethane was used as a solvent, the amount of styrene oxide and aniline adsorbed on the catalyst surface were found to be 0.204 and 0.210 mmol/g catalyst, respectively (Table 3.3). Similar values were obtained also when toluene was used as a solvent (Table 3.3). However, in the polar-aprotic acetonitrile, the amounts of epoxide as well as the amine adsorbed on the catalyst were considerably lower (0.055 and 0.13 mmol/g catalyst, respectively). Polar solvents compete with the substrate molecules for adsorption (on sulfonic acid groups) on the catalyst surface and thereby lower the catalytic activity.

The influence of substrate adsorption on ion exchange capacity of the catalyst was investigated by the titrimetric method as described in the experimental section. When different amounts (0.25 – 1.5 mmol) of styrene oxide or aniline were adsorbed on the sulfonic acid functionalized SBA-15, the ion exchange capacity of the catalyst decreased from 0.725 meq/g for SBA-15-*pr*- SO_3H to about 0.3 meq/g for the epoxide or amine adsorbed catalyst (Fig. 3.9). Hence, both the epoxide and aniline adsorb on the sulfonic acid functionality reducing thereby the ion-exchange capacity of the catalysts (and proton concentration).

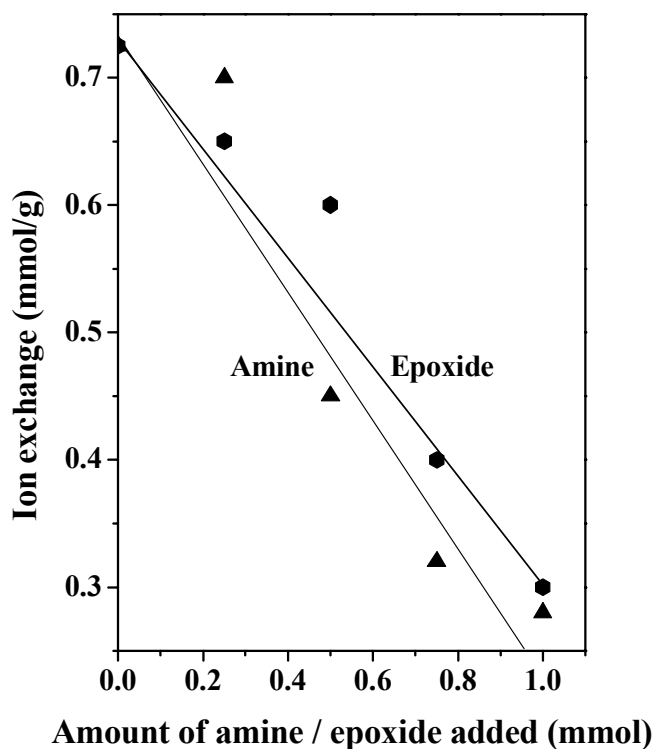


Fig. 3.9. Variation in ion-exchange capacity with the amount of pre-adsorbed epoxide or amine on SBA-15-*pr*- SO_3H .

In some experiments, aniline was pre-adsorbed on SBA-15-pr-SO₃H. Styrene oxide was, then, adsorbed. The catalytic activities of these aniline-pre-adsorbed catalysts were also, simultaneously, determined. The amount of epoxide adsorbed as well as catalytic activity decreased with increasing amounts of pre-adsorbed amine indicating that the pre-adsorbed amine molecules poison the active, acidic site. Epoxide adsorption on the acid site is apparently, essential for the reaction to occur (Fig. 3.10 (a)).

In another set of experiments, different amounts of styrene oxide were initially added onto the SBA-15-pr-SO₃H surface. Thereafter, the amine adsorption capacity and catalytic activity of those modified catalysts were determined. The amount of aniline adsorption and catalytic activity increased with increasing amount of epoxide added (Fig. 3.10 (b)). Aniline is consumed due to reaction with the epoxide already activated on the acidic site, yielding the product β -amino alcohol. There is a correlation between styrene oxide conversion and the amount of epoxide pre-adsorbed (Fig. 3.10 (c)). The amounts of different epoxides or amines adsorbed per gram of SBA-15-pr-SO₃H (in one-substrate adsorption experiments) are listed in Table 3.7. Adsorptions were done also on “bare” SBA-15. The amount of substrate adsorbed on catalyst surface varied with the nature of the substrate molecule. Diffusion constraints are not expected over these mesoporous catalysts. Both epoxide and amine adsorb even on “bare” SBA-15, the former more than the latter (Table 3.7). Functionalization of SBA-15 surface with propylsulfonic acid moieties enhanced the adsorption of epoxide as well as amine substrates, the latter more than the former (Table 3.7). The amount of substrate adsorbed increased with its concentration in the solution. However, it was always lower than the molar equivalent of propylsulfonic acid moieties present on the catalyst surface.

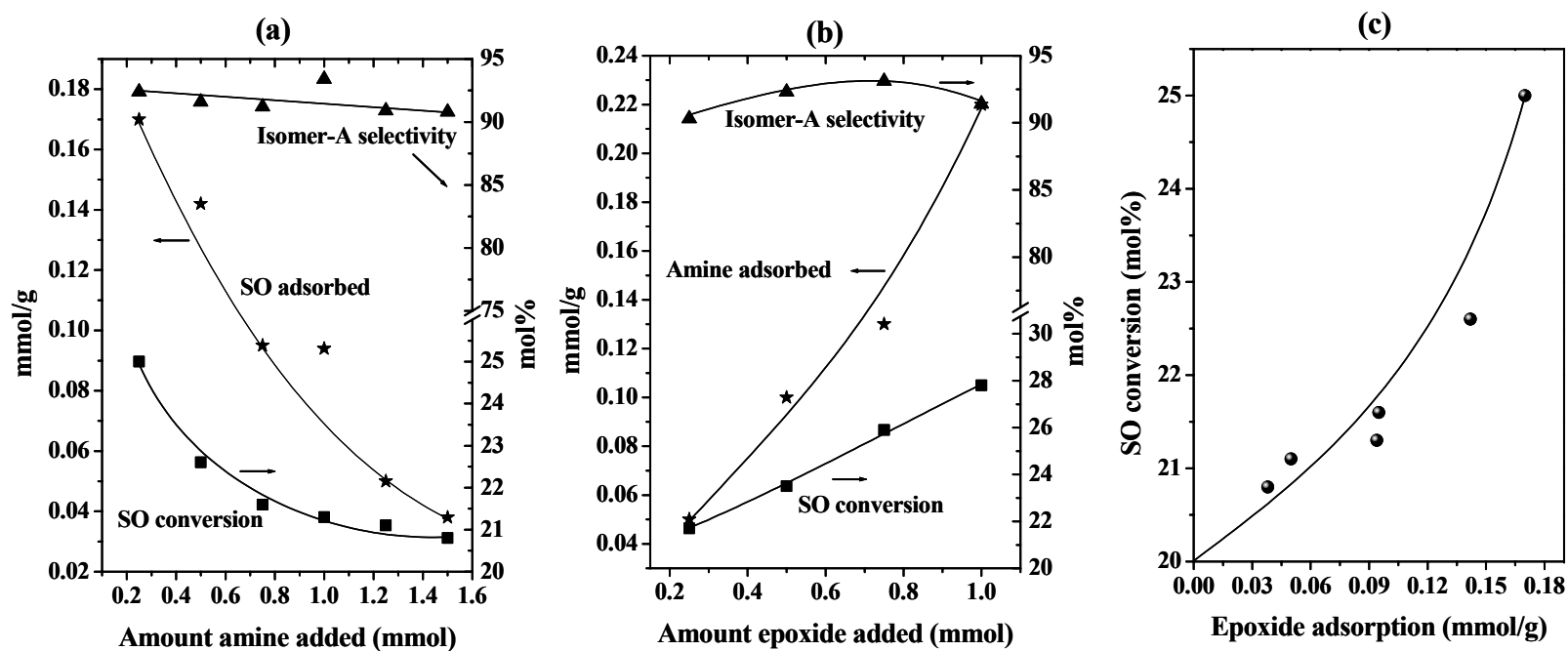


Fig. 3.10. (a) Variation in styrene oxide adsorption and conversion with pre-adsorbed aniline. (b) Variation in aniline adsorption and styrene oxide conversion with pre-adsorbed styrene oxide. (c) Influence of pre-adsorbed amine on epoxide adsorption and catalytic activity in the reaction of styrene oxide (SO) with aniline.

Table 3.7. Epoxide and amine adsorptions on SBA-15 materials^a

Material	Amount of epoxide adsorbed (mmol/g)			Amount of amine adsorbed (mmol/g)		
	Epichloro- hydrin	Styrene oxide	Cyclo- hexene oxide	Piperidine	Aniline	4-Cl- aniline
SBA-15	0.093	0.037	0.168	0.017	0.005	0.085
SBA-15- <i>pr</i> -SO ₃ H	0.168	0.204	0.340	0.033	0.210	0.230

^a50 mg of activated SBA-15 material was dispersed, for 1 hr, in 0.5 mmol of styrene oxide or aniline substrate dissolved in 5 ml of solvent. The solid was, then, separated and the concentration of the substrate in the liquid portion was determined by gas chromatography. The amount adsorbed on the catalyst surface was determined by difference.

Since adsorption is an essential prerequisite in many of the liquid phase bimolecular reactions between epoxides and amines [37], competitive adsorption experiments were performed wherein the sulfonic acid functionalized SBA-15 catalyst (50 mg) was suspended in equimolar (0.5 mmol) amounts of epoxide (cyclohexene oxide, epichlorohydrin or styrene oxide) and amine (aniline or o-toluidine) dissolved in dichloromethane (5 ml). The adsorption of both the epoxide and amine were estimated. Table 3.8 compares the relative adsorption values of the various epoxides and amines. The corresponding turnover frequencies of the reaction are also given. The importance of carrying out competitive adsorption of the reactants (in addition to their independent adsorption data) is brought out by comparing the data in Tables 3.7 and 3.8. In independent adsorption experiments, the amount of epoxides adsorbed on SBA-15-*pr*-SO₃H varies as epichlorohydrin (0.168) < styrene oxide (0.204) < cyclohexene oxide

(0.34) (Table 3.7). However, in the presence of an amine (aniline) a *reverse* variation is observed: epichlorohydrin > styrene oxide > cyclohexene oxide (relative adsorption ratios of 1.75, 1.14 and 0.82, respectively) (Table 3.8). The corresponding relative rates (TOF of 165, 68 and 43 h⁻¹) correlate better with data from the competitive adsorption experiments and illustrate the perils involved in drawing conclusions from adsorption of individual reactants without taking into account the competition from the others or the solvent.

Table 3.8. Competitive adsorption of epoxide and amine over SBA-15-pr-SO₃H^a

Adsorbate substrates	Amount adsorbed (mmol/g catalyst)		Relative adsorption ratio	TOF (h ⁻¹) ^b
	Epoxide	Amine	Epoxide/amine	
Epichlorohydrin + aniline	0.10	0.06	1.8	165
Styrene oxide + aniline	0.08	0.07	1.1	68
Cyclohexene oxide + aniline	0.10	0.13	0.8	43
Styrene oxide + o- toluidine	0.03	0.04	0.8	34

^a50 mg of sulfonic acid functionalized SBA-15 was suspended for 1 h in equimolar amounts (0.5 mmol) of epoxide and amine dissolved in 5 ml of dichloromethane. The catalyst was, then, separated and the concentration of the substrate in the liquid portion was determined by gas chromatography. The amount adsorbed on the catalyst surface was determined by difference.

^bTurnover frequency (TOF) = moles of epoxide converted per mol of $-\text{SO}_3\text{H}$ in the catalyst per hour.

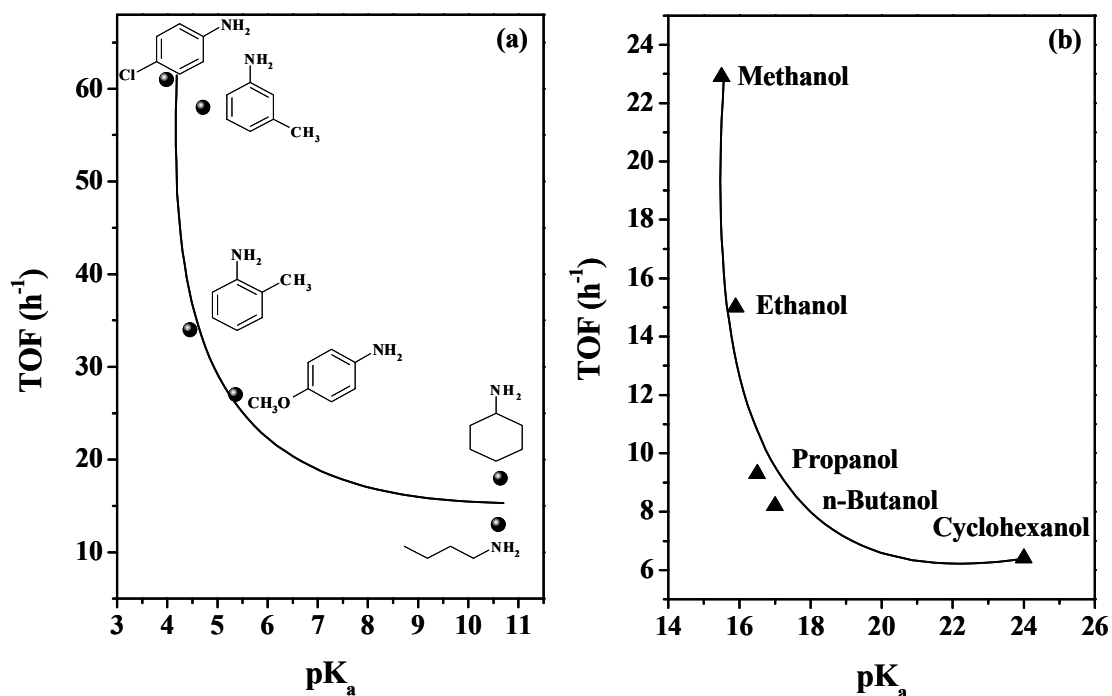


Fig. 3.11. (a) Correlation between catalytic activity (turnover frequency; TOF) and pK_a of amine in aminolysis of styrene oxide and (b) correlation between TOF and pK_a of alcohols in alcoholysis of styrene oxide over SBA-15-*pr*- SO_3H .

Fig. 3.11 illustrates, further, the competition between the epoxide (styrene oxide) and the amine or alcohol for the active site. The rate of the reaction decreases when the basicity of the amine or alcohol increases. A decrease of the styrene oxide conversion was observed in solvents of high dielectric constant. Highly polar solvents compete with the epoxide for adsorption on the acidic site. It is, hence, not surprising that the highest conversions are observed in the absence of any solvent (Table 3.3, row 1). Another

interesting feature of relevance to the mechanism of this reaction is the orientation of the epoxide ring opening.

As shown in [Scheme 3.1](#), two regioisomers are theoretically possible. In almost all studies, the A isomer predominates. Substituent groups on the epoxide (like R in [Scheme 3.1](#)) influence the orientation of the incoming moiety (R'NH and R'OH) by steric as well as electronic effects [37]. Bulky R groups favor the B isomer. Similarly, under basic or neutral conditions, when an S_N2 attack of the reagent molecule (like R'NH₂ or R'OH) on the epoxide ring carbon atom leads to products, the B isomer is dominant. Under acidic conditions, on the other hand, electronic effects (inductive and conjugative) determine the orientation [37]. These effects can stabilize a positive charge on the carbon atom (of the epoxide ring) adjacent to R. This is facilitated if the reaction occurs by a S_N1 mechanism in which the transition state for the rate determining step carries a partial positive charge on the carbon atom adjacent to R. Protonation of the epoxide oxygen by the –SO₃H group over SBA-15-*pr*-SO₃H apparently favors the S_N1 mechanism and the consequent predominance of the A isomer. This picture is supported by the results over SBA-15-*pr*-SH and SBA-15, mentioned earlier, wherein the B-isomer predominated over the A-isomer. Propyl thiol and silanol are weakly acidic and nearly neutral functional groups, respectively, compared to propyl sulfonic acid (refer to the ion exchange capacities in [section 3.3.1.9.2](#)). Hence, the significant formation of the B isomer over SBA-15-*pr*-SH and bare SBA-15 is understandable.

3.3.2.2. *Tert.-butylation of glycerol over SBA-15-*pr*-SO₃H*

Biodiesel is produced from renewable sources, especially from vegetable oils. These fuels are typically not based on petroleum and are desirable because they provide

environmental benefits. Biodiesel is manufactured by transesterification of natural oils with methanol. Glycerol is formed as a by-product in this reaction [38]. The steeply growing production of biodiesel will eventually produce huge amounts of glycerol by-product. Preparation of alkyl ethers of glycerol by etherification with tert-butyl alcohol (or isobutylene, C₄-fraction, respectively) in the presence of an acid catalyst is one of the possibilities of glycerol utilization. A mixture of mono-, di-, and tri-alkyl glycerol ethers is produced and these ethers, especially the di and tri-alkyl glycerols are most suitable as oxygenate additives to diesel fuels [39]. Higher glycerol ethers (di- and tri-ethers, due to their solubility in diesel fuel) possess similar properties as the current commercial oxygenate additives (MTBE, ETBE, TAME applied in gasoline) [40] used as oxygenates to diesel fuel, biodiesel or their mixture [41–44]. Addition of these ethers has a positive influence on the quality of final diesel fuel [41, 45]. Moreover, glycerol ether oxygenates can decrease the cloud point (CP) of diesel fuel when combined with biodiesel [46]. The limitation factor of vegetable oil methyl esters is cloud Point. This value for diesel fuel is –16°C and for biodiesel is around 0°C. The addition of glycerol alkyl ethers to diesel or biodiesel fuel decreases cloud point.

The mixture of alkyl ethers of glycerol is prepared [47] by etherification of glycerol by alkenes and preferentially by isobutylene at a molar ratio of glycerol/isobutylene = 1:2 and temperature from 323 to 423 K on a strongly acidic catalyst. Amberlyst. The mixture of alkylethers is added to original diesel fuel with biodiesel or separately. The reduction of carbon oxide, hydrocarbons, aldehydes and particulate matters after addition of alkyl ethers of glycerol to diesel fuel was already proved. p-Toluene sulfonic acid was also used as a catalyst for etherification of glycerol

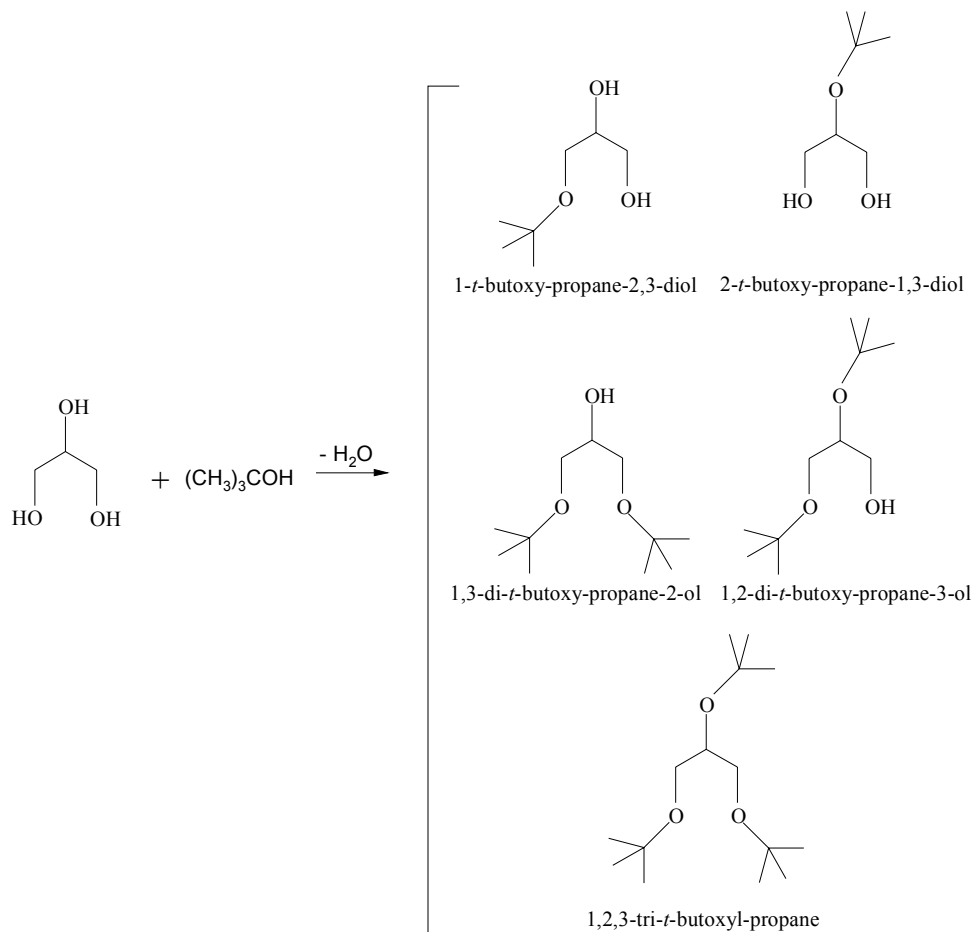
[48]. *Tert*-butyl ethers of glycerol were reported to be formed by etherification of glycerol with isobutylene in the liquid phase in the presence of large-porous zeolite catalyst at a temperature in the range of 353 – 393 K, pressure between 0.6 to 2.1 MPa and molar ratio of glycerol/alkene = 1:1 to 1:5 [47]. The conversion of glycerol was nearly 99%. Macho et al. [54] studied possibilities of utilization of isobutylene from C₄-fraction for etherification of hydroxylic aliphatic compounds.

A number of studies on the preparation of glycerol ethers by using different catalyst systems have been reported [47-50]. The etherification of polyols can be catalyzed by homogeneous [48] and preferentially by heterogeneous acid catalysts and especially by strong acid ion exchange resins generally used for production of commercial ethers [48-53]. The utilization of large-pore zeolites as etherification catalysts was also published [44, 54]. Homogeneous catalysts are not suitable because of the known technical problems and environmental reasons.

Mesoporous sulphonic acid functionalized silica materials have been used in various organic transformations such as esterification of carboxylic acid [31-33], synthesis of polycaprolactone [34], regioselective ring opening of epoxide with amines and alcohols and etherification of 1-butanol [10, 55], etc. Here, the application of mesoporous SBA-15-*pr*-SO₃H is reported for the etherification of glycerol with *tert*-butanol to synthesize mono-, di- and tri-ethers of glycerol.

Etherification of glycerol is a type of O-alkylation reaction (Scheme 3.2). The formation of 1- and 1,3-ethers (primary —OH groups) is more probable against 2- and 1,2-ethers. Moreover, primary —OH groups of glycerol are preferred for *tert*-butylation due to steric reasons. Etherification reactions were carried out in the liquid phase without

any solvent at autogenous pressure (Chapter-2). *Tert*-butyl alcohol was used as etherification agent.



Scheme 3.2. Etherification of glycerol with *t*-butanol

The conversion of glycerol over SBA-15-*pr*- SO_3H was found to be as high as 83.3% at 393 K. The selectivity of di- and tri-ethers was found to be 29% with 7.5 wt % of catalyst.

3.3.2.2.1. Effect of temperature

Etherification of glycerol with *tert*-butanol was carried out in the temperature range of 333-393 K (Table 3.9). A maximum conversion 83.3% was achieved at 393 K. The selectivity for di- and tri-ethers was found to be 29.6%.

Table 3.9. Effect of temperature on t-butylation of glycerol

Reaction temperature (K)	Gly : t-butanol	Glycerol conversion (mol %)	Product Selectivity (%)	
			Mono ether	Di- & tri- ether
333	1:4	31.4	96.0	4.0
348	1:4	49.8	95.2	4.8
363	1:4	75.8	84.4	15.6
373	1:4	83.5	81.6	18.4
393	1:4	80.5	70.4	29.6

Reaction conditions: Glycerol (54.3 mmol), t-butanol (217.4 mmol), catalyst (SBA-15-*pr*-SO₃H) (5 wt%), time (8h).

3.3.2.2.2. Effect of catalyst amount

While the conversion was about the same (Table 3.10), di- and tri-ethers selectivity was found higher at high catalyst concentrations.

Table 3.10. Effect catalyst amount on t-butylation of glycerol

Catalyst amount (wt %)	Gly : t-butanol	Glycerol conversion (mol %)	Product Selectivity (%)	
			Mono ether	Di- & tri- ether
5	1:4	76.3	88.7	11.3
7.5	1:4	75.8	84.4	15.6
10	1:4	79.3	83.4	16.6
15	1:4	83.3	77.3	22.7

Reaction conditions: Glycerol (54.3 mmol), t-butanol (217.4 mmol), time (8h), temp. (363 K).

3.3.2.2.3 Time on stream and leaching study

Conversion verses time plot (Fig 3.12) revealed that an optimum conversion of glycerol could be obtained in about 4 hr. Activity of the catalyst decreased in recycling experiments indicating a possible deactivation of the active sites.

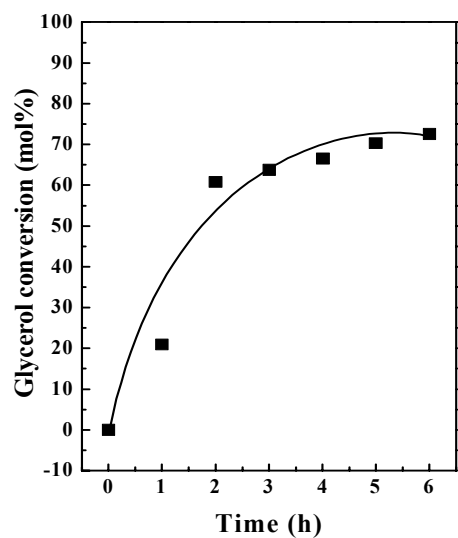


Fig. 3.12. Glycerol conversion with respect to time

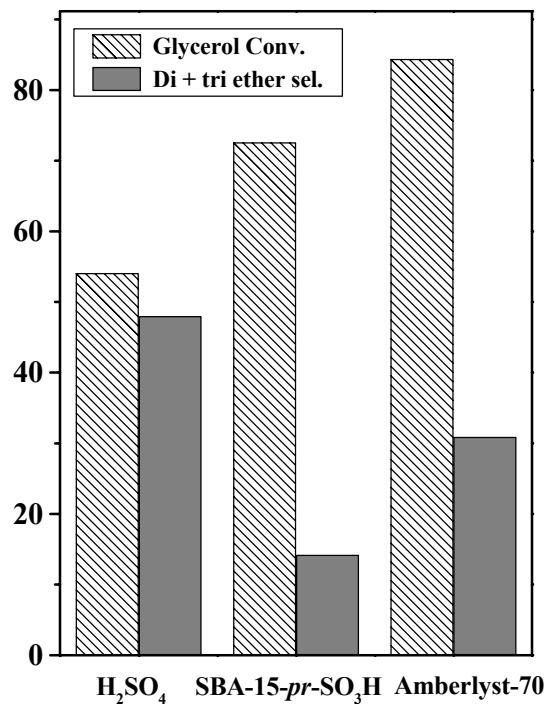


Fig. 3.13. Comparison of SBA-15-*pr*- SO_3H with conventional acid catalysts for etherification of glycerol with tert-butanol

3.3.2.2.4. *Comparative study with conventional Brønsted acidic catalysts*

For comparison, etherification reaction was carried out with homogeneous conc. sulphuric acid and acidic resin Amberlyst-70. SBA-15-*pr*-SO₃H showed better activity than conc. sulphuric acid (Fig 3.13).

3.3.2.3. *Esterification of carboxylic acids.*

Esterification of carboxylic acids is a fundamental reaction in organic chemistry [56]. Esters are generally used as plasticizers, solvents, perfumery, fragrant chemicals and precursors for a wide range of pharmaceuticals, agrochemicals and fine chemicals [57]. The reaction of carboxylic acid with alcohol is limited by equilibrium that is established between the reactants and the products. This necessitates the use of an excess amount of one of the reactants or elimination of water from products to attain higher conversions. Homogeneous catalysts such as sulfuric acid and *p*-toluene sulphonic acid suffer from the problem of side reactions, corrosion of the equipment and additional steps needed for catalyst separation from the reaction mixture [58]. Esterification has been investigated over many solid acid catalysts such as immobilized lipase [69-62], Y-type zeolite [63] and immobilized *Rhizomucor miehei* [64]. Particularly the esterification of isoamyl alcohol (IAA) with acetic acid (AA) in gaseous phase has been studied using tungstophosphoric acid (TPA) supported on different carriers such as silica materials, carbon, alumina, Cs or K salts, Al-MCM-41, cation-exchange resin Purolite CT-175 under vapour and liquid phase conditions. Use of silicotungstic acid supported on hydrous zirconia for esterification with primary and secondary alcohols have also been reported [65-69]. Herein, Brønsted acidic sulphonic acid functionalized mesoporous

SBA-15 (SBA-15-*pr*-SO₃H) is used for the esterification acetic acid with various alcohols (Table 3.11). High conversion of acetic acid is achieved even at moderate temperatures.

Table 3.11. Esterification of acetic acid with alcohols over SBA-15-*pr*-SO₃H

Alcohol	Reaction temperature (K)	Reaction time (h)	Acetic acid conversion (mol%)
Ethanol	333	1	42.5
n-Butanol	383	1	98.5
n-Hexanol	383	2	77.9
n-Octanol	383	4	97.2
Benzyl alcohol	383	1	93.8
	353	1	76.1
	333	1	68.2
Isoamyl alcohol	373	3	92.7

Reaction conditions: Catalyst (50 mg; -SO₃H loading was 1.56 mmol/g. catalyst), acetic acid (50 mmol), alcohol (100 mmol). Product selectivity is 100 mol%. Catalyst was prepared by in-situ condensation instead of post-grafting technique.

For comparative studies we have prepared catalysts with different loading of sulfonic acid. Also catalysts were prepared by both the post-synthesis and co-condensation techniques. It may be noted that those catalysts prepared by the latter method showed superior activity in esterification reaction. Catalytic activity increased with increasing sulfonic acid content (Table 3.12).

Table 3.12. Esterification of acetic acid with benzyl alcohol: Influence of the method of catalyst preparation

Catalyst (SO ₃ H mmol/g catalyst)	Method of catalyst preparation	Acid conversion (mol%)
SBA-15- <i>pr</i> -SO ₃ H(0.29)	Post-synthesis	13.3
SBA-15- <i>pr</i> -SO ₃ H(0.87)	Post-synthesis	15.0
SBA-15- <i>pr</i> -SO ₃ H(1.38)	Post-synthesis	40.4
SBA-15- <i>pr</i> -SO ₃ H(1.56)	Post-synthesis	54.8
SBA-15- <i>pr</i> -SO ₃ H(0.29)	Co-condensation	33.3
SBA-15- <i>pr</i> -SO ₃ H(0.87)	Co-condensation	49.2
SBA-15- <i>pr</i> -SO ₃ H(1.38)	Co-condensation	65.9
SBA-15- <i>pr</i> -SO ₃ H(1.56)	Co-condensation	68.0

Reaction conditions: Catalyst (50 mg; -SO₃H loading was 1.56 mmol/g. catalyst), acetic acid (50 mmol), benzyl alcohol (100 mmol), reaction time = 1 h, reaction temperature = 333 K. Product selectivity is 100 mol%.

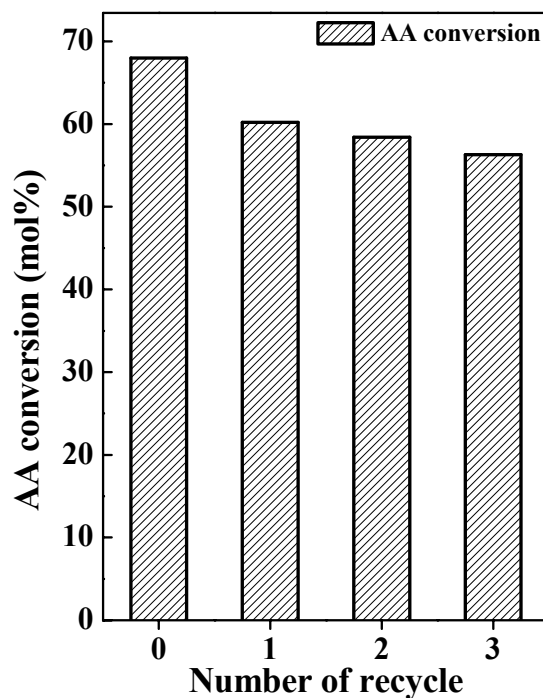


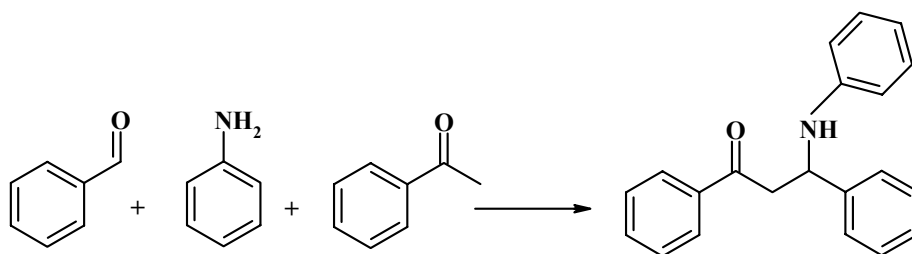
Fig. 3.14. Catalyst reusability study in esterification of acetic acid with benzyl alcohol.

Reusability of SBA-15-*pr*-SO₃H (20) catalyst was studied in the esterification of acetic acid with benzyl alcohol at 333 K. The catalyst was filtered, washed with alcohol and acetone and dried at 363 K prior to use in the next run. The activity of the catalyst decreased in subsequent recycling experiments (Fig. 3.14).

3.3.2.4. *Three-component Mannich reaction over SBA-15-*pr*-SO₃H*

Carbon–carbon bond forming reactions continue to be the central focus of research in synthetic organic chemistry [70]. Among them, the Mannich-type reaction, which gives β-amino carbonyl compounds in a single-step, is of considerable importance for synthesizing biologically attractive molecules containing nitrogen atom [71]. Therefore, the development of new synthetic methods leading to β-amino carbonyl compounds or their derivatives has attracted much attention. However, the classic Mannich reaction has limited applications. To overcome the drawbacks of the classical method, numerous modern versions of the Mannich reaction using electrophiles, such as imines and stable nucleophiles, enolates, enol ethers, and enamines [72] have been developed. But the preferred route is to use a one-pot three-component strategy (Scheme 3.3.) that gives a wide range of structural variations. However, most known catalysts suffer from the drawbacks of difficulty in separation after the reactions. Furthermore, some of them are corrosive and volatile and often cause the environment problems. It is found here that SBA-15-*pr*-SO₃H is highly efficient for three-component Mannich reaction yielding selectively (100%) β-amino carbonyls (Table 3.13). The catalysts were prepared with different amounts of functionalized SO₃H groups. Catalytic activity for the reaction of benzaldehyde, aniline and acetophenone increased with increasing amounts of acid functionalities on the catalyst surface. The reaction occurs at even 298 K and with

out use of any solvent. The catalysts prepared by the post-synthesis method showed superior activity to those prepared by the co-condensation method.



Scheme 3.3. Three components Mannich reaction

Table 3.13. Mannich reaction of Aniline, aldehyde and acetophenone with SBA-15-pr-SO₃H catalysts

Catalyst (SO ₃ H mmol/g catalyst)	Method of catalyst preparation	Aldehyde	Ketone	Yield (%)
SBA-15- <i>pr</i> -SO ₃ H(0.29)	Post-synthesis	Benzaldehyde	Acetophenone	83.2
SBA-15- <i>pr</i> -SO ₃ H(0.87)	Post-synthesis	Benzaldehyde	Acetophenone	85.9
SBA-15- <i>pr</i> -SO ₃ H(1.38)	Post-synthesis	Benzaldehyde	Acetophenone	87.2
SBA-15- <i>pr</i> -SO ₃ H(1.56)	Post-synthesis	Benzaldehyde	Acetophenone	90.0
SBA-15- <i>pr</i> -SO ₃ H(0.29)	Co-condensation	Benzaldehyde	Acetophenone	71.5
SBA-15- <i>pr</i> -SO ₃ H(0.87)	Co-condensation	Benzaldehyde	Acetophenone	84.6
SBA-15- <i>pr</i> -SO ₃ H(1.38)	Co-condensation	Benzaldehyde	Acetophenone	88.6
SBA-15- <i>pr</i> -SO ₃ H(1.56)	Co-condensation	Benzaldehyde	Acetophenone	90.1
SBA-15- <i>pr</i> -SO ₃ H(1.56)	Co-condensation	4-Cl Benzaldehyde	Acetophenone	77.9
SBA-15- <i>pr</i> -SO ₃ H(1.56)	Co-condensation	3-NO ₂ benzaldehyde	Acetophenone	22.1
SBA-15- <i>pr</i> -SO ₃ H(1.56)	Co-condensation	Benzaldehyde	Cyclohexanone	50.5

Reaction conditions: Catalyst (50 mg), aldehyde, aniline and ketone (5 mmol each), reaction temperature (298 K), reaction time (1 h), no solvent

Mannich reaction of aniline, benzaldehyde and acetophenone was performed in different protic polar and non-polar solvents. It may be noted that the highest activity was

achieved when no solvent was used (Table 3.14). As discussed earlier, solvent molecules compete with the reactants for adsorption on the active sites and thereby suppress the catalytic activity (Section 3.3.2.1.3.).

Table 3.14. Effect of solvent on aldehyde conversion in Mannich reaction over SBA-15-*pr*-SO₃H (1.56) prepared by post-synthesis method

Solvent	Toluene	Tetrahydrofuran	Chloroform	Dichloromethane	Acetonitrile	<i>t</i> -Butanol	Ethanol	No Solvent
Aldehyde conv. (mol %)	10	16	35.3	44.2	46.2	49.8	53	90.1

Reaction conditions: Catalyst (50 mg), benzaldehyde, aniline and acetophenone (5 mmol each), solvent (10 ml), reaction temperature (298 K), reaction time (1 h).

Different substituted amines were used to investigate the reaction with benzaldehyde and acetophenone. *p*-Chloro aniline was found to be more active than aniline and other substituted amines like *p*-anisidine. The higher activity in the case of *p*-Cl-aniline may be attributed to the electron withdrawing nature of chlorine which makes the aromatic ring of amine ready for nucleophilic attack.

Table 3.15. Effect of substituents on amine groups on the Mannich reaction

Amine	Aniline	<i>p</i> -Cl-aniline	<i>o</i> -Toluidine	<i>m</i> -Toluidine	<i>p</i> -Anisidine	Cyclohexyl amine
Aldehyde conv. (mol %)	63.6	70.1	52.4	53.0	46.0	22.2

Reaction conditions: Catalyst (SBA-15-*pr*-SO₃H (1.56) prepared by post-synthesis method, 50 mg), benzaldehyde, aniline and acetophenone (5 mmol each), solvent (10 ml), reaction temperature (298 K), reaction time (1 h).

3.4. Conclusions

The surface of SBA-15 was modified with acidic functionalities like propyl thiol and propyl sulfonic acid. The materials were characterized by a range of structural and spectroscopic techniques. Acidic properties of those materials were determined by NH₃-TPD and ion-exchange capacity. The studies reveals that propyl sulfonic acid functionalization on SBA-15 (SBA-15-*pr*-SO₃H) is an efficient solid acid catalyst for a range of acid catalyzed reactions. A range of β-amino alcohols was synthesized with high regio- and stereoselectivity by reacting symmetric or unsymmetric epoxides with aromatic as well as aliphatic amines. Both amine and epoxide compete for adsorption on the catalyst surface. Etherification of glycerol with *tert*-butanol forming mono-, di- and tri- *tert*-butyl ether of glycerol was achieved at mild conditions over these catalysts. These ethers find application as additives to diesel fuel. These catalysts also showed good activity for esterification, and 3-component Mannich reactions.

3.6. References

- [1] Kresge, C. T.; Leonowicz, M. E.; Roth, W. J.; Vartluti, J. C.; Beck, J. S. *Nature* 359 (1992) 710
- [2] Zhao, D.; Feng, J.; Huo, Q.; Melosh, N.; Fredrickson, G. H.; Chmelka, B. F.; Stucky, G. D. *Science* 279 (1998) 540.
- [3] Zhao, D.; Huo, Q.; Feng, J.; Chmelka, B. F.; Stucky, G. D. *J. Am. Chem. Soc.* 120 (1998) 6024.
- [4] Juan A. Melero, Rafael van Grieken, Gabriel Morales, *Chem. Rev.* 106 (2006) 3790
- [5] Clark, J. H.; Macquarrie, D. J. *Chem. Commun.* (1998) 853.
- [6] D. Margolese, J.A. Melero, S.C. Christiansen, B.F. Chmelka, G.D. Stucky, *Chem. Mater.* 12 (2000) 2448.
- [7] (a) F. Feng, G.E. Fryxell, L.-Q. Wang, A.Y. Kim, K.M. Kemner, *Science* 276 (1997) 923. (b) L. Mercier, T.J. Pinnavaia, *Adv. Mater.* 9 (1997) 500. (c) A. Stein, B.J. Melde, R.C. Schroden, *Adv. Mater.* 12 (2000) 1403.
- [8] (a) W.M. Van Rhijn, D.E. De Vos, B.F. Sels, W.D. Bossaert, P.A. Jacobs, *Chem. Commun.* (1998) 317. (b) D. Das, J.-F. Lee, S. Cheng, *Chem. Commun.* (2001) 2178. (c) E. Cano-Serrano, J.M. Campos-Martin, J.L.G. Fierro, *Chem. Commun.* (2003) 246.
- [9] B. Sow, S. Hamoudi, M.H. Zahedi-Niaki, S. Kaliaguine, *Microporous Mesoporous Mater.* 79 (2005) 129.
- [10] (a) B. Sow, S. Hamoudi, M.H. Zahedi-Niaki, S. Kaliaguine, *Micropor. Mesopor. Mater.* 79 (2005) 129, (b) L.M. Yang, Y.J. Wang, G.S. Luo, Y.Y. Dai, *Micropor.*

- Mesopor. Mater. 84 (2005) 275.
- [11] O. Mitsunobu in “Comprehensive Organic Synthesis,” E. Winterfeldt (Ed.), Pergamon Press, New York (1996), Vol. 6, pat 1.3.4.1.
- [12] E. J. Corey, F.-Y. Zhang, Angew. Chem. Int. Ed. Engl. 38 (1999) 1931.
- [13] D. J. Ager, I. Prakash, D.R. Schaad, Chem. Rev. 96 (1996) 835.
- [14] P. O’Brien, Angew. Chem. Int. Ed. Engl. 38 (1999) 326.
- [15] G. Li, H.-T. Chang, K.B. Sharpless, Angew. Chem. Int. Ed. Engl. 35 (1996) 451.
- [16] R. M. Hanson, Chem. Rev. 91 (1991) 437.
- [17] P. A. Crooks, R. Szyudler, Chem. Ind. (London) (1973) 1111.
- [18] A. Kamal, B. Rajendra Prasad, A. Malla Reddy, M. Naseer, A. Khan, Catal. Commun. 8 (2007) 1876.
- [19] M. Vijender, P. Kishore, P. Narender, B. Satyanarayana, J. Mol. Catal. A. Chem. 266 (2007) 290.
- [20] A.T. Placzek, J.L. Donelson, R. Trivedi, R.A. Gibbs, S.K. De, Tetrahedron Lett. 46 (2005) 9029.
- [21] J. Iqbal, A. Pandey, Tetrahedron Lett. 31 (1990) 575.
- [22] R.I. Kureshy, S. Singh, N.H. Khan, S.H.R. Abdi, E. Suresh, R.V. Jasra, J. Mol. Catal. A: Chem. 264 (2007) 162.
- [23] F. Carrée, R. Gil, J. Collin, Org. Lett. 7 (2005) 1023.
- [24] J.S. Yadav, B.V.S. Reddy, A.K. Basak, A.V. Narasaiah, Tetrahedron Lett. 44 (2003) 1047.
- [25] P.-Q. Zhao, L.-W. Xu, C.G. Xia, Synlett 2004 (2004) 245.
- [26] N. Azizi, M.R. Saidi, Org. Lett. 7 (2005) 3649

- [27] R. Garcia, M. Martinez, J. Aracil, *Chem. Eng. Technol.* 22 (1999) 12.
- [28] M.W.C. Robinson, R. Buckle, I. Mabbett, G.M. Grant, A.E. Graham, *Tetrahedron Lett.* 48 (2007) 4723.
- [29] A. Vinu, K.Z. Hossain, K. Ariga, *Nanosci. Nanotech.* 5 (2005) 347.
- [30] J. A. Melero, R. van Grieken, G. Morales, *Chem. Rev.* 106 (2006) 3790.
- [31] I. K. Mbraka, D.R. Radu, V.S.Y. Lin, B.H. Shanks, *J. Catal.* 219 (2003) 329.
- [32] W.D. Bossaert, D.E. De Vos, W.M. Van Rhijin, J. Bullen, P.J. Grobet, P.A. Jacobs, *J. Catal.* 182 (1999) 156.
- [33] I. Diaz, C. Márquez-Alvarez, F. Mohino, J. Pérez-Pariente, E. Saste, *Microporous Mesoporous Mater.* 44–45 (2001) 295.
- [34] B.C. Wilson, C.W. Jones, *Macromolecules* 37 (2004) 9709.
- [35] L. Saikia, D. Srinivas, P. Ratnasamy, *Appl. Catal. A Gen.* 309 (2006) 144.
- [36] L. Saikia, D. Srinivas, P. Ratnasamy, *Microporous and Mesoporous Materials* 104 (2007) 225.
- [37] Parker RE, Isaacs NS *Chem Rev* 59 (1959) 737
- [38] J. Barrault, Y. Pouilloux, J. M. Clacens, C. Vanhove, and S. Bancquart, *Catal. Today* 75 (2002) 177.
- [39] V. P. Gupta, U.S. 5,476,971 (1995).
- [40] F. Ancillotti, V. Fattore, *Fuel Proc. Technol.* 57 (1998) 163.
- [41] S. Kesling, L.J. Karas, F.J. Liotta, U.S. Patent 5,308,365 (1994) to ARCO Chem. Technology, L.P.
- [42] D. S. Bradin, U.S. Patent 5,578,090 (1996) to BRI, Macon.
- [43] A. Behr, H. Schmidke, C. Lohr, M. Schneider, DE Patent 4222183 (1994) to Henkel

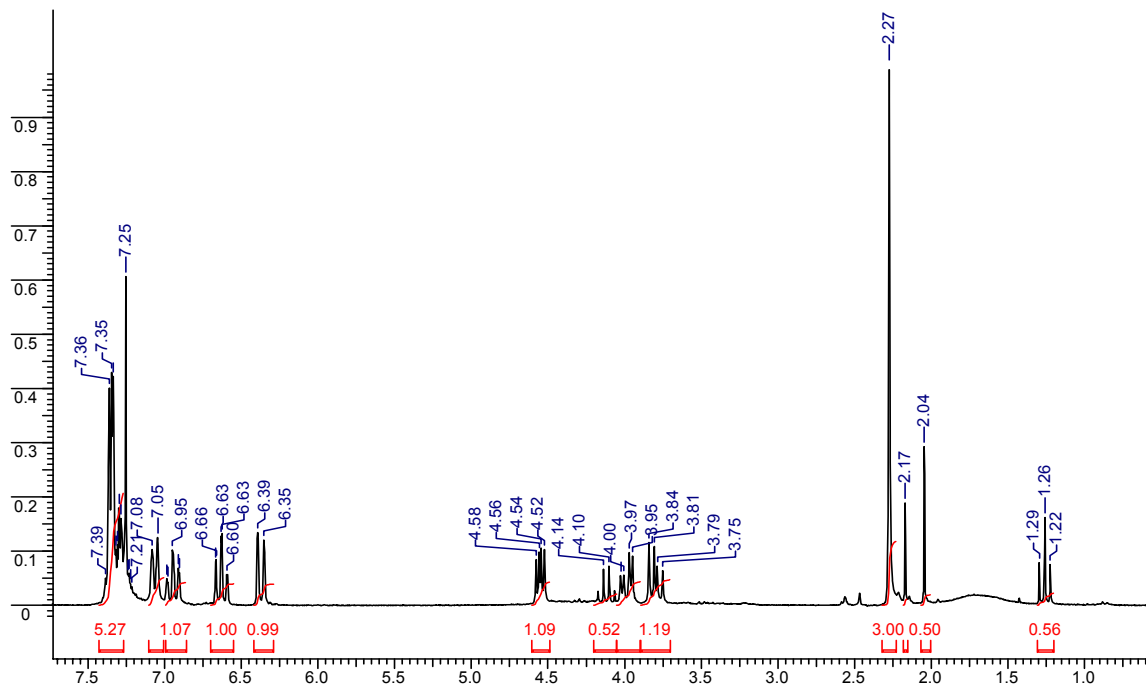
KGaA.

- [44] C. Dewattines, H. Hinnekens, BE Patent 9301097 (1993) to FINA RESEARCH S.A.
- [45] M. Marchionna, R. Patrini, D. Sanfilippo, A. Paggini, F. Giavazzi, L. Pellegrini, *Stud. Surf. Sci. Catal.* 136 (2001) 489.
- [46] H. Nouredini, U.S. Patent 6,015,440 (2000).
- [47] Katarína Klepáčová, Dušan Mravec, Martin Bajus. *Appl. Catal. A: Gen.*, 294 (2005) 141
- [48] A. Behr, L. Obendorf, *Chem. Ing. Tech.* 73 (2001) 1463.
- [49] Katarína Klepáčová, Dušan Mravec , Alexander Kaszonyi, Martin Bajus *Appl. Catal. A: Gen.* 328 (2007) 1
- [50] R. S. Karinen, A.O.I. Krause, *Appl. Catal.* 306 (2006) 128.
- [51] S. S. Jayadeokar, M.M. Sharma, *React. Polym.* 20 (1993) 57.
- [52] A. Chakrabarti, M.M. Sharma, *React. Polym.* 20 (1993) 1.
- [53] R. Alca'ntara, L. Canoira, C. Ferna'ndez-Marti'n, M.J. Franco, J.I. Martinez-Silva, A. Navarro, *React. Funct. Polym.* 43 (2000) 97.
- [54] V. Macho, M. Kavala, M. Mat'as', C'. Hy' bl, CS Patent 189,071 (1978)
- [55] Bineta Sow, Safia Hamoudi, M. Hassan Zahedi-Niaki, Serge Kaliaguine. *Microporous and Mesoporous Materials* 79 (2005) 129
- [56] R.C. Larock, *Comprehensive Organic Transformations*, second ed., VCH, New York, 1999
- [57] A. Zaidi, J.L. Gainer, G. Carta, *Biotechnol. Bioeng.* 48 (1995) 601
- [58] M.F. Malone, F. Doherty, *Ind. Eng. Chem. Res.* 39 (2000) 3953.
- [59] S. Hari Krishna, B. Manohar, S. Divakar, S.G. Prapulla, N.G. Karanth,

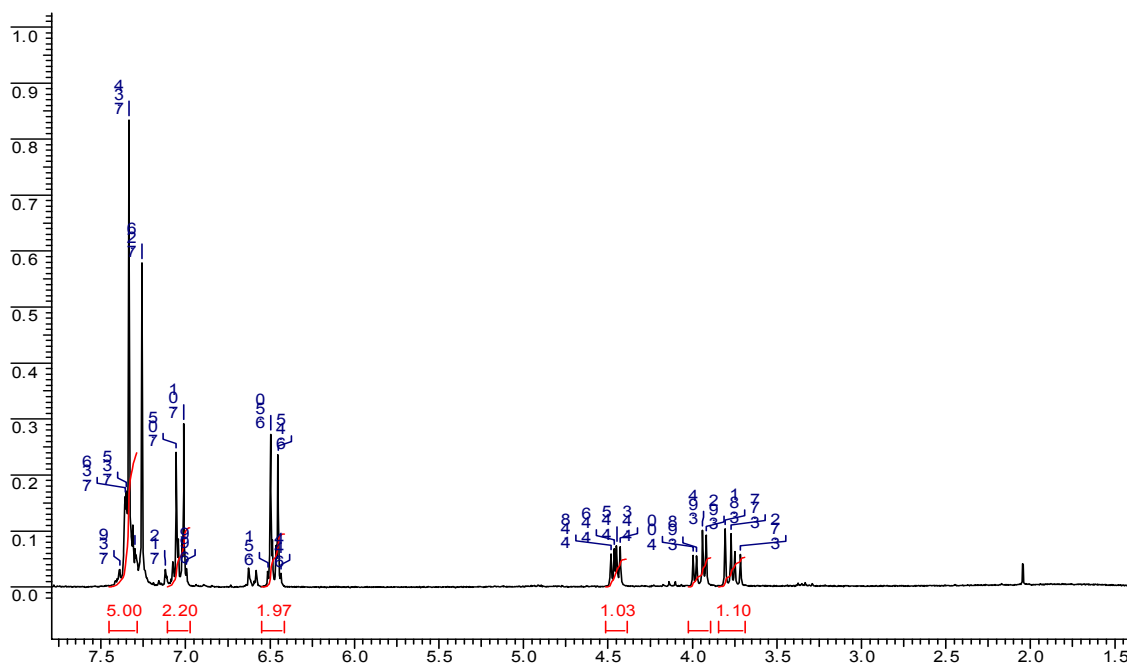
- Enzyme Microb. Technol. 26 (2000) 131.
- [60] H. Ghamgui, M. Karra-Cha[^]abouni, S. Bezzine, N. Miled, Y. Gargouri, Enzyme Microb. Technol. 38 (6) (2006) 788.
- [61] M.D. Romero, L. Calvo, C. Alba, M. Habulin, M. Prim^ozi^č, Z. Knez, J. Supercrit. Fluids 33 (2005) 77.
- [62] M. Rizzi, P. Stylos, A. Riek, M. Reuss, Enzyme Microb. Technol. 14 (1992) 709.
- [63] L. Lian-sun, L. Ren-guey, Fluid Phase Equilib. 165 (1999) 261
- [64] A. G^uvens, N. Kapucu, M. ^Ulk^u, Process Biochem. 38 (2002) 379.
- [65] L. R. Pizzio, P.G. V^azquez, C.V. C^aceres, M.N. Blanco, Appl. Catal. A: Gen. 256 (2003) 125.
- [66] L. R. Pizzio, M.N. Blanco, Appl. Catal. A: Gen. 255 (2003) 265.
- [67] A. Palani, A. Pandurangan, J. Mol. Catal. A: Chem. 226 (2004) 129
- [68] H.T.R. Teo, B. Saha, J. Catal. 228 (2004) 174.
- [69] N. Bhatt, A. Patel, J. Mol. Catal. A: Chem. 238 (2005) 223.
- [70] Kleinman, E. F. In Comprehensive Organic Synthesis; Trost, B. M., Fleming, I., Eds.; Oxford: Pergamon, 1991; Vol. 2, p 893
- [71] S. Kobayashi, H. Ishitani Chem. Rev. 99 (1999) 1069
- [72] (a) B. M. Trost, L. R. Terrell, J. Am. Chem. Soc. 125 (2003) 338; (b) S. Matsunaga, N. Kumagai, S. Harada, M. J. Shibasaki, Am. Chem. Soc. 125 (2003) 4712; (c) K. Juhl, N. Gathergood, K. A. J^orgensen, Angew. Chem. 113 (2001) 3083

APPENDIX-I

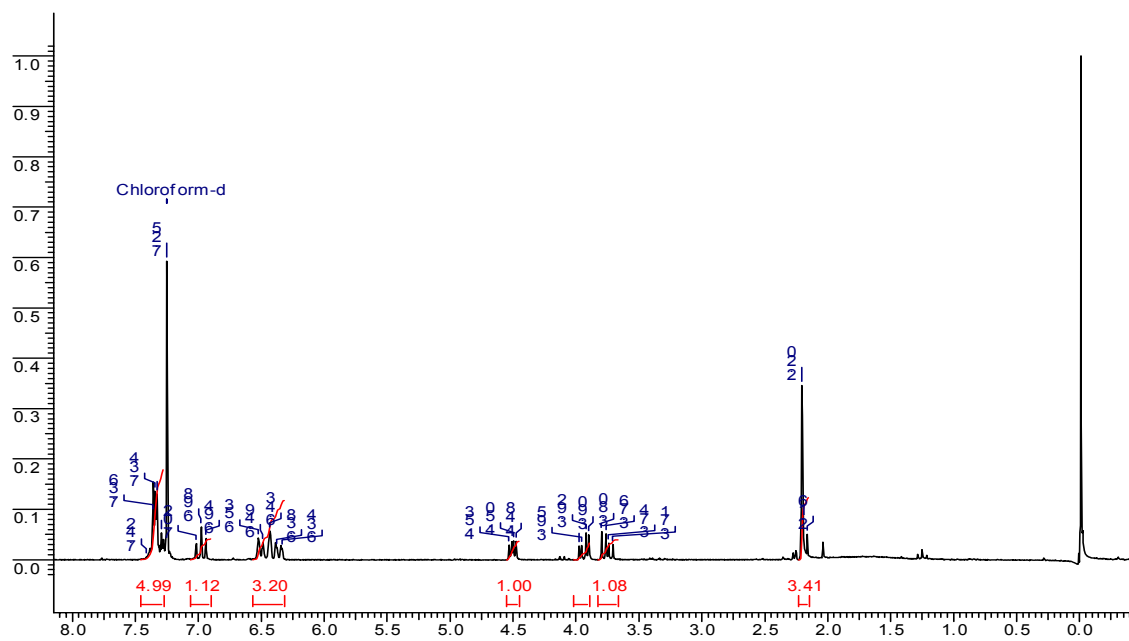
¹H NMR of 2-(2-Methylphenylamino)-2-phenyl ethanol



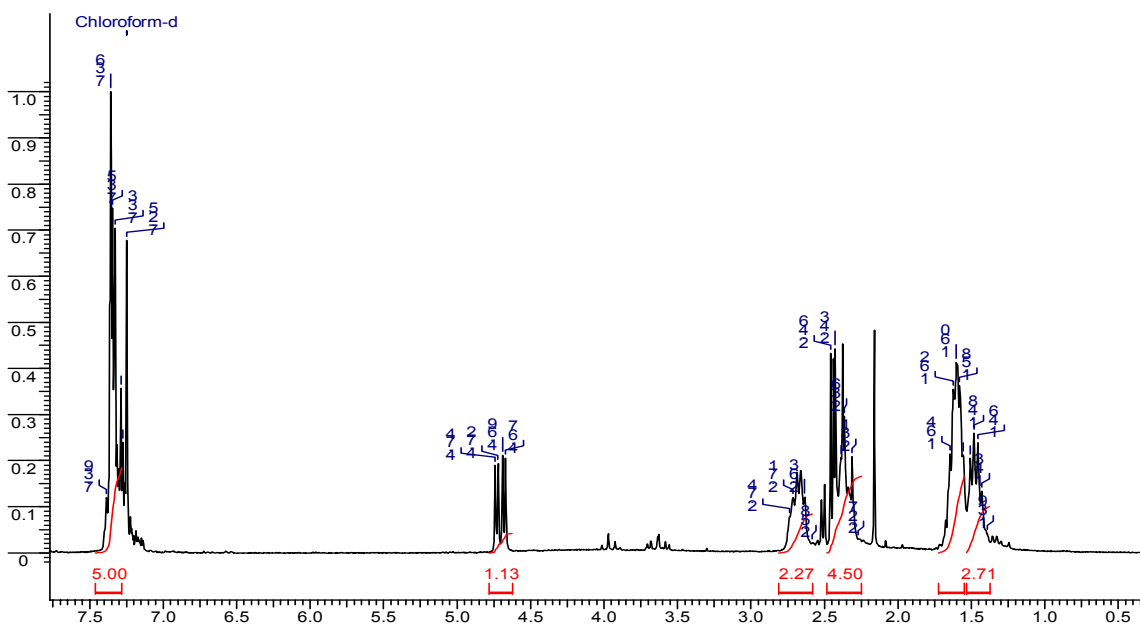
¹H-NMR of 2-(4-Chlorophenylamino)-2-phenyl ethanol



¹H-NMR of 2-(3-Methylphenylamino)-2-phenyl ethanol



¹H-NMR of 2-(1-Piperidino)-1-phenyl ethanol



CHAPTER – 4

Chemo-, Regio- and Stereoselective Oxidation of Terpenes over Mn Complexes Grafted on SBA-15

4.1. Introduction

The direct oxidation of hydrocarbons is a field of both academic and industrial importance. Epoxidation reaction is important in organic synthesis because epoxides are intermediates for various products of pharmaceutical, agrochemical, perfumery and food additives. Terpenes are a large and varied class of hydrocarbons, produced primarily by a wide variety of plants, particularly conifers, and also by some insects such as swallowtail butterflies, which emit terpenes from their osmeterium. They are the major components of resin, and of turpentine produced from resin. The name "terpene" is derived from the word "turpentine". When terpenes are modified chemically, such as by oxidation or rearrangement of the carbon skeleton, the resulting compounds are generally referred to as terpenoids. Some authors use the term terpene to include all terpenoids. Terpenes and terpenoids are the primary constituents of essential oils of many types of plants and flowers. Essential oils are used widely as natural flavor additives for food, as fragrances in perfumery, and in traditional and alternative medicines such as aromatherapy. Synthetic variations and derivatives of natural terpenes and terpenoids also greatly expand the variety of aromas used in perfumery and flavors used in food additives. Vitamin A is an example of a terpene. Monoterpenes are a class of terpenes that consist of two isoprene units and have the molecular formula $C_{10}H_{16}$. Monoterpenes may be linear (acyclic) or contain rings. Biochemical modifications such as oxidation or rearrangement produce the related monoterpenoids.

Monoterpenes, such as limonene, pinene, carene etc. are commonly available chemicals. Oxidation of these molecules either at double bonds or at allylic positions leads to formation of important chemicals of pharmaceutical, agrochemical products and food additives. The conventional synthesis of their epoxide or allylic products

involves the use of hazardous chemicals or gives organic waste formed as byproduct. Limonene epoxide is a key raw material in the synthesis of pharmaceuticals, fragrances, perfumes and food additives [1]. Conventionally, it is manufactured by oxidation of limonene with stoichiometric amounts of peracids. As this process is non-ecofriendly, attempts are in progress to develop efficient solid catalysts for this reaction [2-12]. Limonene is one of the molecules of choice to study chemo-, regio- and stereoselective catalytic oxidation. Oxidation of limonene, in general, yields a variety of products. Epoxides will be the selective products if oxidation occurs at olefinic positions. If the oxidation takes place at allylic positions, the products will be carveol and carvone. In addition, limonene has two olefinic bonds (1,2 and 8,9) and the oxidation can take place at either or both of these sites. Further, two types of diastereomers (*endo* and *exo*) are expected for each of the epoxide products. Most of the known solid catalysts (Ti-MCM-41 [2], carbon anchored Co(acac)₂ [10], supported Keggin heteropoly compounds [3], for example) show significantly low limonene conversions and epoxide selectivities (20 – 30%); carveol, carvone and polymeric products are formed in large quantities. They require expensive oxidants such as alkyl hydroperoxides and H₂O₂. When using air as oxidant, sol-gel prepared Co/SiO₂ [6] yields large amounts of allylic oxidation products. Mn complexes are known to be efficient in Mukaiyama-type of epoxidation of terpenes at mild conditions in the presence of molecular oxygen (oxidant), *iso*-butyraldehyde (co-reagent) and N-containing bases (additive) [13]. Schuster and Hölderich [7] reported the application of modified faujasite encapsulated Mn and Co complexes of (*R,R*)-(*N,N'*)-bis(3,5-di-*tert*-butylsalicylidene)-1,2-diphenylethylene-1,2-diamine for this reaction (epoxide selectivity \cong 50% and diastereomeric excess (*de*) = 36%). Bhattacharjee *et al* [11] reported the use of chiral sulfonato-salen-Mn(III) complexes

entrapped in layered double hydroxide hosts ($de = 31\%$) [11]. Similarly oxidation of α -pinene, carene, β -pinene etc. has been oxidized with various homogeneous and heterogeneous catalyst systems.

In this chapter, the aerial oxidation of *R*-(+)-limonene, α -pinene and 3-carene over Mn(Salen)Cl and Mn(TPP)Cl complexes immobilized on amine, thiol and sulfonic acid-functionalized, mesoporous SBA-15 molecular sieves has been investigated. These catalysts are superior to zeolite-Y encapsulated complexes (Mn(Salen)-Y) and “neat” Mn(Salen)Cl as well as other solid catalysts hitherto investigated for this reaction. Functionalization of the solid surface with acidic groups enhanced the catalytic performance significantly. Synthesis, detailed characterization and catalytic activities of these novel, solid catalysts have been investigated. The causes for the enhanced activity of the grafted metal complexes are discussed.

4.2. Experimental

4.2.1. Material synthesis and characterization

Mn(Salen)Cl and Mn(TPP)Cl grafted on propyl amine, propyl thiol and propyl sulfonic acid functionalized SBA-15 (SBA-15-*pr*-X-Mn(Salen)Cl and SBA-15-*pr*-X-Mn(TPP)Cl, where X = NH₂, SH and SO₃H, respectively) were prepared as described in Chapter 2; here, Salen²⁻ = N,N'-ethylenebis(salicylideaminato) and TPP²⁻ = *Meso*-tetraphenylporphyrinato. The materials were characterized (Chapter 2) by using atomic absorption spectroscopy (AAS), elemental analysis (C, H, N & S; Carlo-Erba 1106 analyzer), X-ray diffraction (Philips-X'Pert Pro; Cu K α radiation), transmission electron microscopy (TEM; JEOL-model 1200 EX), surface area analysis (BET; NOVA 1200 Quanta Chrome instrument), thermal analysis (Seiko DTA-TG 320), FTIR spectroscopy (Shimadzu 8201 PC), diffuse-reflectance UV-visible spectroscopy (DRUV-vis; Shimadzu UV-2500 PC) and electron paramagnetic resonance (EPR)

spectroscopy techniques. EPR spectra were recorded on a Bruker EMX spectrometer operating at X-band ($\nu = 9.42$ GHz) frequency and a 100 kHz field-modulation. The spectra were recorded at 80 K using a Bruker BVTB 3500 variable temperature controller. The magnetic field was calibrated with a Bruker ER 035M NMR Gaussmeter. The microwave-frequency was calibrated with a frequency counter fitted in a Bruker ER 041 XG-D microwave bridge unit. Cyclic voltammetric studies were conducted at 298 K as detailed in Chapter 2 using a three-electrode system (Solatron SI-1287 electrochemical interface).

4.2.2. Reaction procedure – aerial oxidation of monoterpenes

The Mukaiyama-type aerial oxidation of monoterpenes (R(+)-limonene, α -pinene and 3-carene) was studied at 298 K and atmospheric pressure using Mn(Salen)Cl and Mn(TPP)Cl complexes grafted on functionalized SBA-15 as catalysts. The reactions were conducted (Chapter 2) in the presence of a nitrogen-containing compound like N-methyl imidazole (N-MeIm), 2-methyl imidazole (2-MeIm) or imidazole (Im) as an additive and iso-butyraldehyde as a co-reagent. The products were analyzed by gas chromatography and identified using standard samples and GC-MS. The influence of catalyst support, ligand structure, reaction parameters and additives/co-reagent on catalytic activity/selectivity was investigated. The advantage of using an ordered silica SBA-15 instead of an amorphous silica material is also been examined. By means of in-situ spectroscopic studies the factors controlling catalytic activity and product selectivity have been probed.

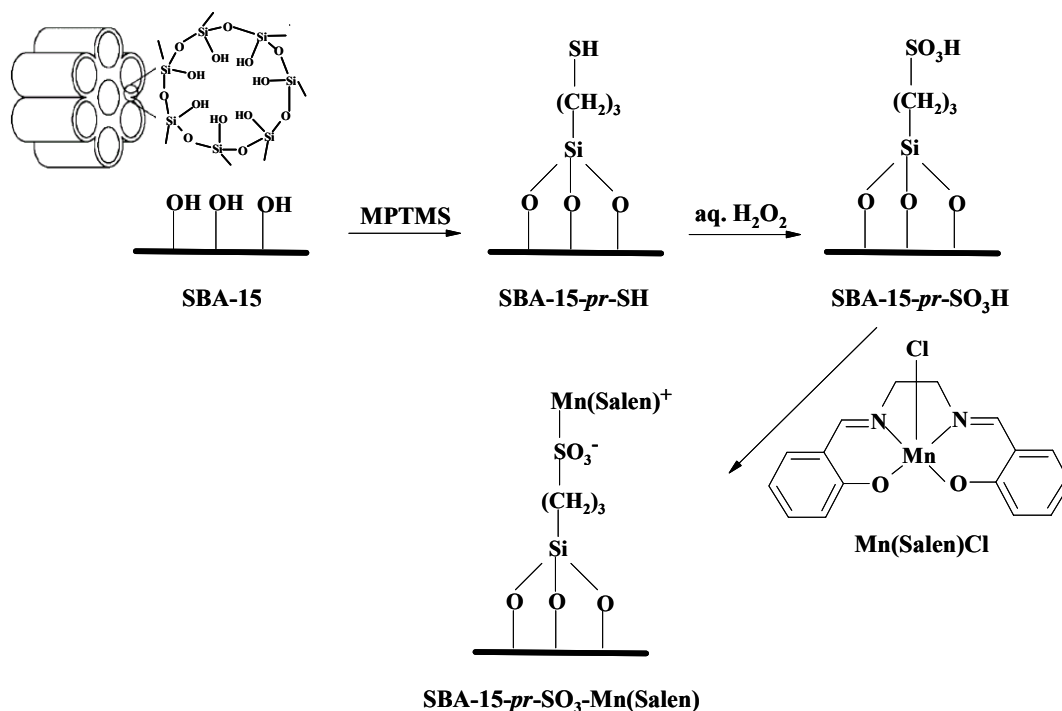
4.3. Results and Discussion

4.3.1. SBA-15-grafted Mn(Salen)Cl complexes

4.3.1.1. Chemical analysis

Propyl-amine and propyl-thiol functionalized SBA-15 molecular sieves (SBA-15-*pr*-NH₂ and SBA-15-*pr*-SH) were prepared by condensing the surface silanol groups of SBA-15 with 3-aminopropyltrimethoxysilane (APTMS) and 3-mercaptopropyltrimethoxysilane (MPTMS), respectively [14]. Oxidation of the thiol groups in SBA-15-*pr*-SH yielded the propyl-sulfonic acid-functionalized SBA-15 (SBA-15-*pr*-SO₃H) [15]. Mn complexes were then immobilized on those functionalized SBA-15 surfaces. Chemical analysis (Table 4.1) reveals that SBA-15-*pr*-SO₃H contained 0.31 mmol of -*pr*-SO₃H groups per g.silica. Out of that, 0.16 mmol participated in coordination with Mn(Salen)⁺ ions (AAS). Mn(Salen)Cl could also be immobilized directly on “bare” SBA-15 surfaces. However, the amount immobilized was very low (0.07 mmol/g.catalyst) compared to that on the functionalized surfaces (2.1, 0.9 and 0.31 mmol/g.catalyst in the case of SBA-15-*pr*-NH₂-Mn(Salen)Cl, SBA-15-*pr*-SH-Mn(Salen)Cl and SBA-15-*pr*-SO₃H-Mn(Salen)Cl, respectively); even this low amount directly immobilized on the pristine SBA-15 surface had leached out completely during the oxidation reactions. The organic functional groups have three potential sites (-Si(OCH₃)₃) that can bind to the silica surface. While all three -Si-OCH₃ can, in principle, react with surface silanol groups to form Si-O-Si bonds, as suggested in Scheme 4.1, it is also possible that only one or two of the alkoxy groups would react with surface silanol groups. In addition, two of the SH-propyltrimethoxysilane molecules may also react with each other, forming direct Si-O-Si bonds between the organic functional molecules. However, at the low concentration of functional groups utilized in the study, such a possibility of

formation of disulfide bonds is unlikely. In fact, spectral analysis did not indicate the presence of such disulfide bonds.



Scheme 4.1. Procedure for immobilization of Mn(Salen)^+ complexes on sulfonated SBA-15.

4.3.1.2. Low-angle XRD

SBA-15 and its functionalized derivatives showed XRD peaks in the 2θ range of $1 - 2.3^\circ$ (Fig. 4.1) attributable to 2D hexagonal $p6mm$ symmetry [14, 16]. The well-resolved (110) and (200) reflections reveal long-range, mesopore ordering typical of SBA-15. Upon Mn complex immobilization, the XRD peaks broadened and shifted marginally to higher 2θ values. The d spacing (d_{100}) and unit cell parameters, estimated from the position of the intense, low-angle (100) peak, are in the range of 9.1 - 9.9 nm and 10.6 - 11.5 nm, respectively. These values are in good agreement with those reported by others [14, 16]. Transmission electron micrographs have also confirmed the 2D hexagonal pore arrangement and long-range mesoporous

architecture. Organic functionalization and metal complex immobilization, thus, have little effect on the long-range mesoporous ordering.

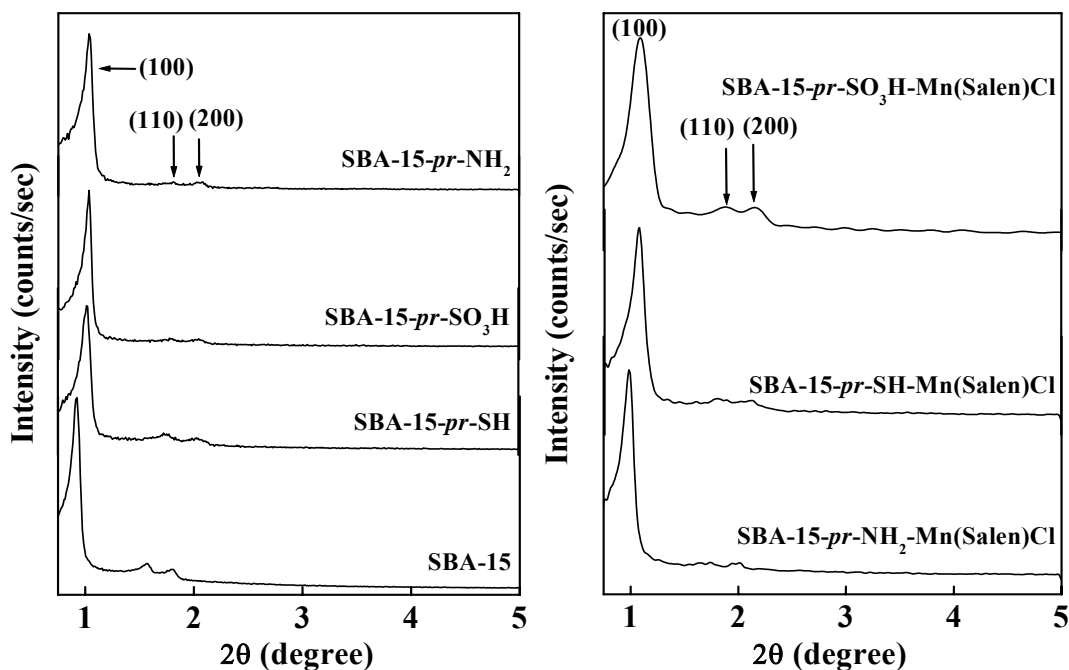


Fig. 4.1. XRD patterns of organo-functionalized SBA-15 and Mn(Salen)Cl-SBA-15 materials

4.3.1.3. N_2 adsorption/desorption

SBA-15 was characterized by type-IV nitrogen adsorption-desorption isotherms with H1 hysteresis (Fig. 4.2). Upon organic functionalization, marked decrease in BET surface area (from 539 to 289 m^2/g) and total pore volume (from 0.64 to 0.47 cm^3/g) (Table 4.1) was observed. The pore diameters were in the range of 5.1 – 6.7 nm, corresponding to those of mesoporous materials.

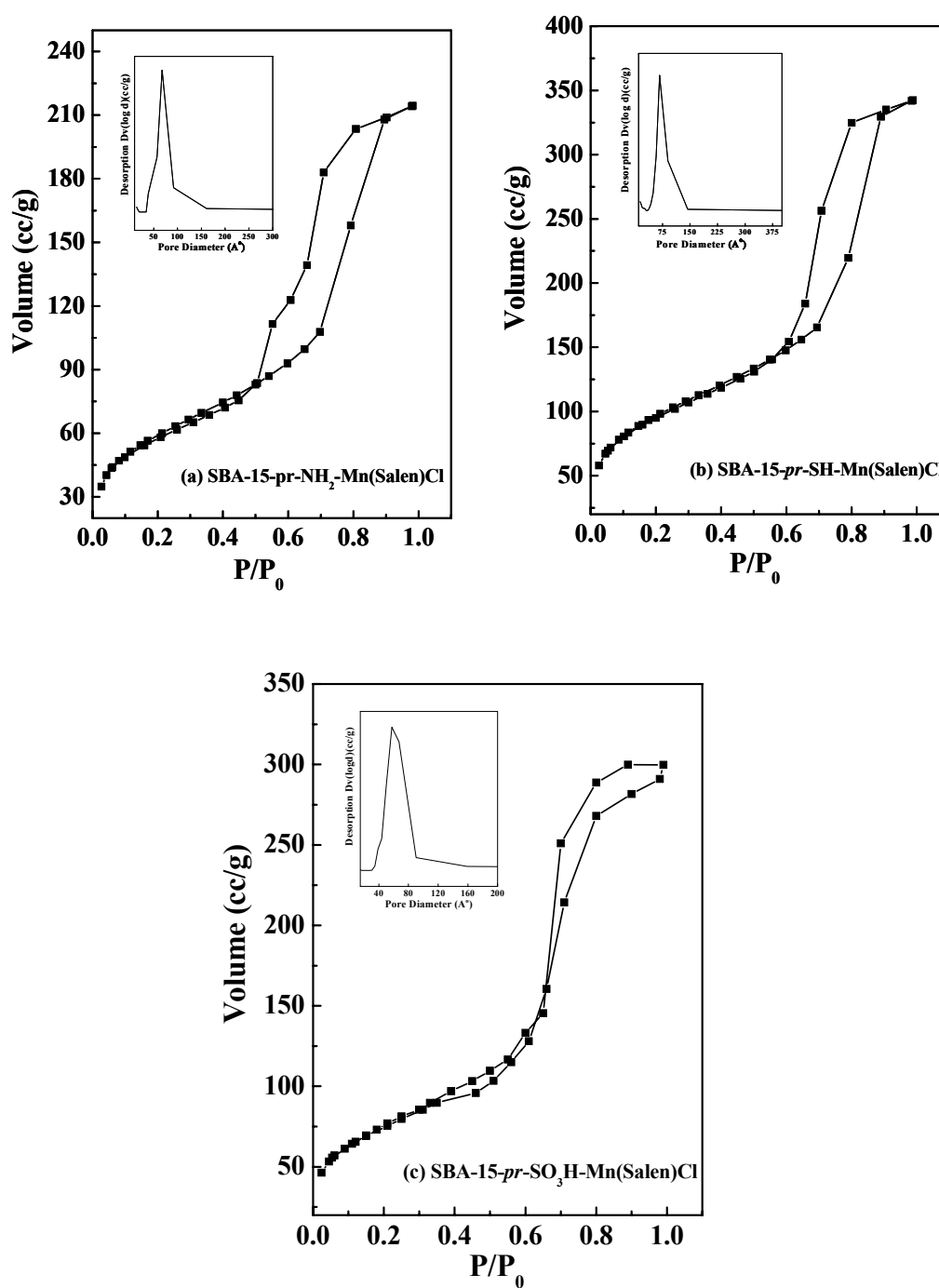


Fig. 4.2. N_2 -adsorption/desorption profiles of SBA-15-grafted Mn(Salen)Cl complexes

Table 4.1. Chemical composition and structural properties of immobilized Mn(Salen)Cl complexes

System	Chemical composition (wt%) ^a					Organic functional group (mmol/g. solid catalyst) ^{b,c}	Immobilized Mn(Salen)Cl complex (mmol/g. solid catalyst) ^{c,d}	XRD		N ₂ adsorption			Wall thickness (nm)
	C	H	N	S	Mn			d ₁₀₀ (nm)	Unit cell parameter (nm)	Pore diameter (nm)	S _{BET} (m ² /g)	Total pore volume (cm ³ /g)	
SBA-15	0.4	0.9	0	-	-	0	-	9.5	11.0	5.1	769	0.98	5.8
SBA-15- <i>pr</i> -NH ₂	10.9	2.8	3.6	-	-	2.5 (2.1)	-	9.9	11.4	5.9	258	0.4	5.5
SBA-15- <i>pr</i> -SH	6.3	1.8	0	4.7	-	1.5 (1.7)	-	9.9	11.5	5.2	440	0.57	6.3
SBA-15- <i>pr</i> -SO ₃ H	4.8	1.8	0	1.8	-	0.56 (0.7)	-	9.7	11.3	6.7	539	0.64	4.5
SBA-15- <i>pr</i> -NH ₂ -Mn(Salen)Cl	10.8	2.9	2.9	-	0.6	2.1	0.1 (0.41)	9.1	10.5	-	176	-	-
SBA-15- <i>pr</i> -SH-Mn(Salen)Cl	9.5	1.7	0.7	3.0	0.3	0.9	0.05 (0.21)	9.6	11.1	-	278	-	-
SBA-15- <i>pr</i> -SO ₃ H-Mn(Salen)Cl	7.9	2.2	1.1	1.0	0.9	0.31	0.16 (0.34)	9.1	10.6	6.7	289	0.47	3.9
“Neat” Mn(Salen)Cl	53.0	4.6	8.5	-	2.6	-	-	-	-	-	-	-	-

^aC, H, N and S compositions were estimated from the elemental analyses. The Mn content was determined from the AAS measurements.

^bDetermined from the S/N-contents.

^cDetermined from the Mn-content.

^dValues in the parentheses are those estimated from the thermogravimetric analyses data.

Table 4.2 . FT-IR and UV-Vis spectroscopic data of the immobilized Mn(Salen)Cl complexes

System	FT-IR data (cm ⁻¹) ^a								UV-Vis data (nm) ^b		
	From pendent arm				From Mn(Salen)Cl complex				Ligand-centered bands	LMCT	d-d
	$\nu(\text{C-H})$	$\nu(\text{N-H})$	$\nu(\text{S-H})$	$\nu(\text{SO}_3\text{H})$	$\nu(\text{C=N})$	$\nu(\text{C=C})$	Ring	$\nu(\text{C-O})$			
SBA-15- <i>pr</i> -NH ₂	2928, 2852	1547	-	-	-	-	-	-	-	-	-
SBA-15- <i>pr</i> -SH	2928, 2852	-	2575	-	-	-	-	-	-	-	-
SBA-15- <i>pr</i> -SO ₃ H	2928, 2852	-	-	1060, 650	-	-	-	-	-	-	-
SBA-15- <i>pr</i> -NH ₂ -Mn(Salen)Cl		1547	-	-	1636, 1607	1540	1452, 1444, 758	1285	248, 279, 314, 340	390, 483	570
SBA-15- <i>pr</i> -SH-Mn(Salen)Cl		-	-	-	1641, 1599	1540	1452, 757	1306	243, 285, 313, 353	402, 475	533, 604
SBA-15- <i>pr</i> -SO ₃ H-Mn(Salen)Cl		-	-	1060, 650	1631, 1602	1541	1446, 757	1306	243, 285, 313, 353	402, 474	523, 603
Mn(Salen)Cl-Neat		-	-	-	1627, 1615	1538	1468, 1440, 760	1287	240, 283, 315, 350	420, 487	564, 723

^aAs KBr pellets.^bData for “neat” Mn(Salen)Cl are those for its CH₂Cl₂ solution. For the rest of the samples measurement were made in diffused reflectance mode using spectral grade BaSO₄ as the reference material.

4.3.1.4. TEM and SEM

TEM and SEM pictures of bare SBA-15, organofunctionalized SBA-15 and grafted Mn(Salen) complexes (Fig 4.3 and 4.4, respectively) showed hexagonal honeycomb architecture and long rang order of the materials. Grafting of metal complexes didn't alter the morphology of mesoporous materials.

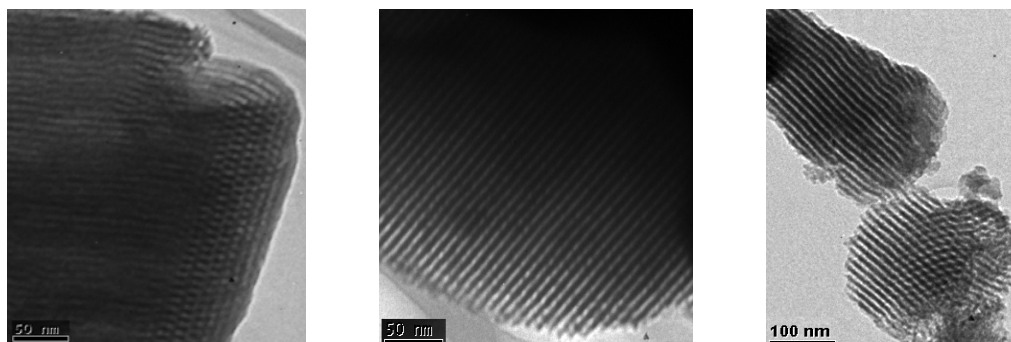


Fig. 4.3. TEM (from Left to right) of SBA-15-*pr*-NH₂-Mn(Salen)Cl, SBA-15-*pr*-SH-Mn(Salen)Cl and SBA-15-*pr*-SO₃H-Mn(Salen)Cl

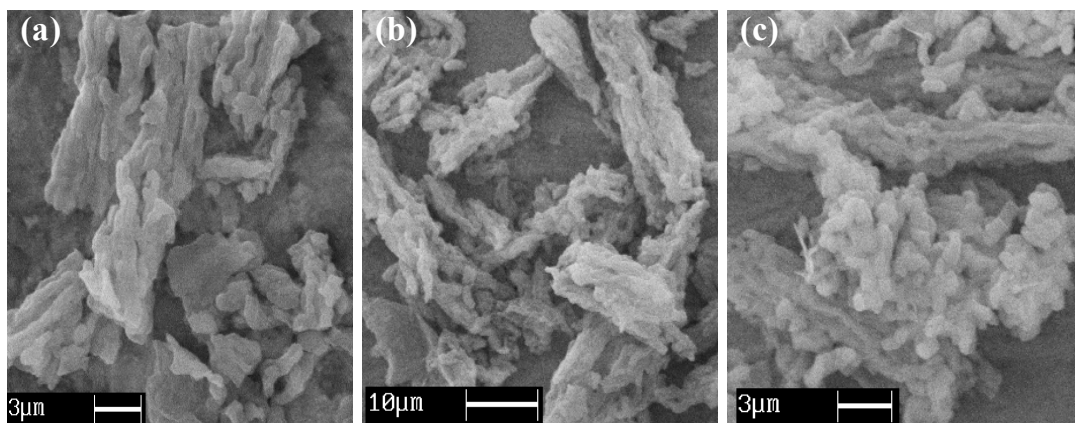


Fig. 4.4. SEM of (a) SBA-15-*pr*-SO₃H-Mn(Salen), (b) SBA-15-*pr*-SH-Mn(Salen) and (c) SBA-15-*pr*-NH₂-Mn(Salen)

4.3.1.5. FTIR Spectroscopy

SBA-15 showed characteristic FTIR peaks at 2900 – 3800, 1040 – 1260, 820 and 500 cm⁻¹ due to O-H of the silanols, adsorbed water molecules and Si-O-Si

stretching vibrations, respectively. Propylamine-functionalized SBA-15 showed an additional peak at 1547 cm^{-1} due to the N-H bonds in the amine group and 2928 and 2852 cm^{-1} due to C-H stretching modes of the propyl spacer (Fig. 4.5). Propylthiol-functionalized SBA-15 showed a characteristic peak at 2776 cm^{-1} due to S-H stretching vibrations. The sulfonic acid-functionalized SBA-15 showed typical peaks at 1060 and 650 cm^{-1} due to the $-\text{SO}_3\text{H}$ moiety (Fig. 4.5).

The peaks due to the azomethine group ($\nu(\text{C}=\text{N})$) of the Salen Schiff base ligand shifted from 1627 and 1615 cm^{-1} for the “neat” Mn-complex [17] to 1641 and 1599 cm^{-1} for the immobilized Mn(Salen) complex (Fig.4.5, Table 4.2). Similarly, the peak due to $\nu(\text{C}-\text{O})$ shifted from 1287 cm^{-1} for the “neat” complex [17] to 1306 cm^{-1} for the immobilized Mn-complex.

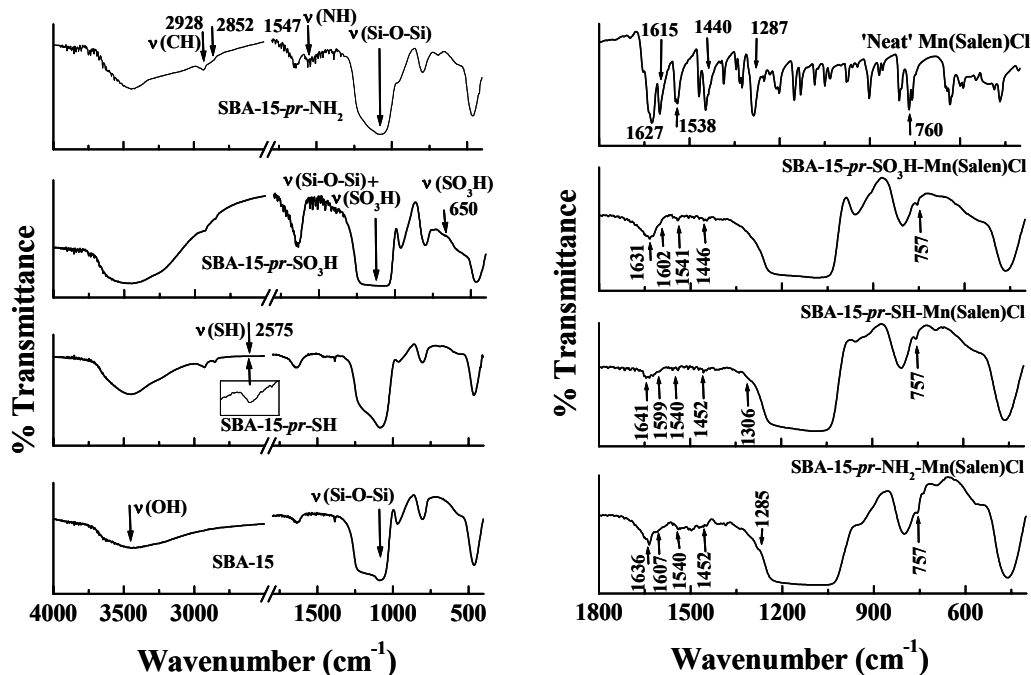


Fig. 4.5. FT-IR spectra of organo-functionalized SBA-15 and immobilized Mn(Salen)Cl.

4.3.1.6. DRUV-vis

“Neat” Mn(Salen)Cl showed weakly intense d-d bands at 420, 487, 564 and 723 nm (Fig. 4.6). These bands for Mn(Salen)Cl immobilized on propylamine-functionalized SBA-15 appeared at 483 and 570 nm. For the complex immobilized on propylthiol and propylsulfonic acid-functionalized SBA-15, the d-d bands were shifted to 475, 533 and 604 nm (for SBA-15-*pr*-SH-Mn(Salen)Cl) and 474, 523 and 603 nm (for SBA-15-*pr*-SO₃H-Mn(Salen)Cl) (Fig. 4.6). Diffuse reflectance UV-vis spectroscopic studies, thus, suggest that grafting/immobilization has modified the geometry and electronic structure of the immobilized Mn-complex.

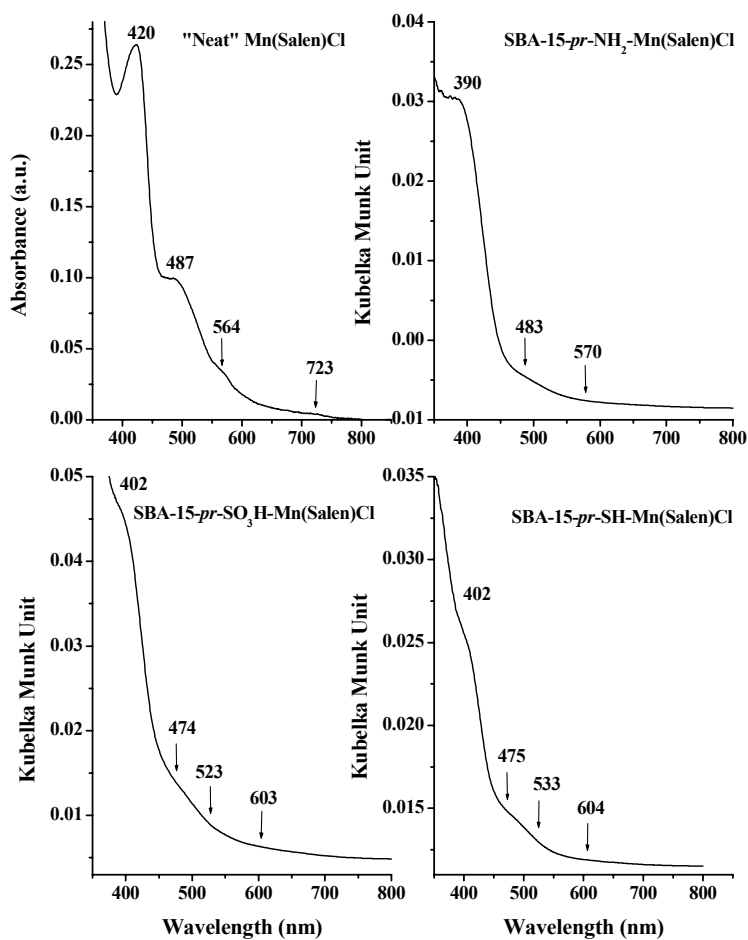


Fig. 4.6. DRUV-vis spectra of ‘neat’ and grafted Mn(Salen)Cl complexes.

4.3.1.7. EPR

“Neat” Mn(Salen)Cl was EPR-silent in both polycrystalline state and in solution consistent with the +3 oxidation state of the Mn ions. Upon immobilization, the Mn-complexes became EPR-active and showed a sextet-line Mn-hyperfine pattern (Fig. 4.7). The intensity of the Mn signals increased to some extent with the acidity of the organo-functional group in the following order: SBA-15-*pr*-NH₂-Mn(Salen)Cl < SBA-15-Mn(Salen)Cl < SBA-15-*pr*-SO₃H-Mn(Salen)Cl < SBA-15-*pr*-SH-Mn(Salen)Cl. While the g-values of these systems are about the same ($g_{av} = 2.0010$), the values of the hyperfine coupling constant (A) representing the electron density at the site of manganese were modified on immobilization; The A value for SBA-15-*pr*-NH₂-Mn(Salen)Cl is 88.4 G while that for SBA-15-*pr*-SH-Mn(Salen)Cl is 96 G. The appearance of these EPR signals, characteristic of Mn²⁺, indicates that, at least, part of the Mn ions is reduced from +3 to +2 oxidation state upon immobilization on the functionalized SBA-15 surface. In SBA-15-*pr*-SH-Mn(Salen)Cl, wherein the electron density at Mn is higher ($A_{Mn} = 96$ G), such a reduction from +3 to +2 oxidation state is more favored and, as a consequence, more intense EPR signals were detected (Fig. 4.7). For further confirmation that the acidity of the support indeed influences the oxidation state, “neat” Mn(Salen)Cl complex was dissolved in sulfuric acid and the EPR spectrum was recorded. Mn(Salen)Cl which was EPR-silent became EPR-active ($g = 2.0027$, $A_{Mn} = 98$ G) when dissolved in sulfuric acid. DRUV-vis and FTIR spectra revealed that the Schiff base Salen ligand was unaffected and was not decomposed upon coordination to the organo-functional groups. The charge transfer bands (at 240, 285 and 350 nm) (Fig. 4.6, region not shown), the stretching frequency (at 1627 - 1641 cm⁻¹) (Fig. 4.5 and Table 4.2), elemental analyses (Table 4.1) clearly

confirmed that the Schiff base ligand and C=N groups were not affected or destroyed on immobilization on the functionalized SBA-15.

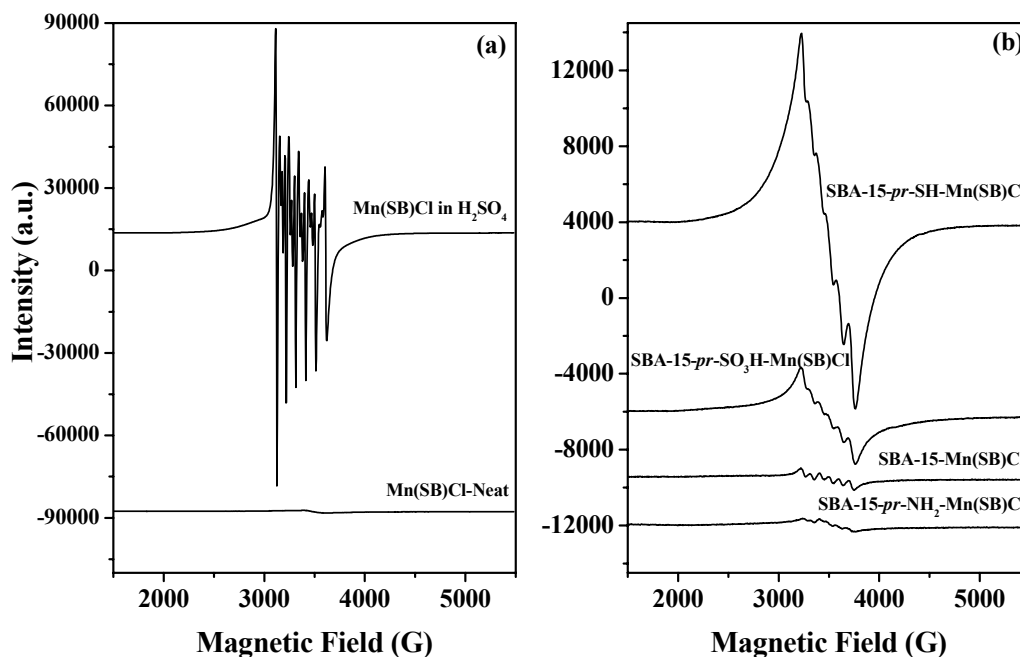


Fig. 4.7. X-band EPR spectra at 77 K. (a) Mn(SB)Cl as polycrystalline sample and in H₂SO₄. (b) Mn(SB)Cl immobilized on different SBA-15 supports. SB = Salen.

4.3.1.8. Cyclic voltammetry

The solid immobilized catalysts showed a distinct redox couple in the cyclic voltammogram attributable to Mn⁺⁴/Mn³⁺ transitions (Fig. 4.8) [18]. The $E_{1/2}$ value of this couple for different Mn-catalysts increased in the following order: SBA-15-*pr*-SH-Mn(Salen) (+0.697 V) < SBA-15-*pr*-SO₃H-Mn(Salen)Cl (+0.728 V) < SBA-15-*pr*-NH₂-Mn(Salen)Cl (+0.752 V). Lower $E_{1/2}$ values are indicative of more facile oxidation and reduction. Hence, a Mn-complex immobilized on propylthiol-functionalized support is more easily oxidized / reduced than that supported on propylsulfonic acid or propylamine-functionalized SBA-15 support. These results agree well with the observations from EPR spectroscopy. The Mn ions are in a

reduced +2 state in SBA-15-*pr*-SH-Mn(Salen)Cl. Such Mn centers can be easily oxidized either by electrochemical means (by applying a small positive potential) or by reacting with oxidant molecules. All the above experiments clearly reveal that the acidity of the support influences the electronic structure and redox behavior of the immobilized complex.

4.3.1.9. Thermal stability

Thermal analysis (TG-DTA) of SBA-15 (Fig. 4.9) showed three stages of weight loss, in agreement with the earlier reports [19]. Stage I (313 – 475 K; exothermic) corresponds to the loss of physically held water; stage II (475 – 815 K, exothermic) corresponds to the loss of water present within the micropore walls. Stage III (815 – 1273 K, endothermic) is due to silanol condensation ($2 \text{ Si-OH} \rightarrow \text{Si-O-Si} + \text{H}_2\text{O}$). SBA-15-*pr*-SH and SBA-15-*pr*-SO₃H showed four stages of weight loss: stages I, IIA, IIB and III, respectively. Stages IIA (475 – 661 K) and IIB (661 – 815 K) are due to desorption of water from the micropore walls as well as decomposition of the organic functional group (-*pr*-SH and -*pr*-SO₃H) [19]. SBA-15-*pr*-SO₃-Mn(Salen), on the other hand, showed five stages of weight losses: stages I, IIA, IIB, IIIA and IIIB, respectively. The additional weight losses in stages IIB and IIIA, IIIB (Table 4.3) are due to decomposition of the immobilized Salen complex.

4.3.2. Grafted Mn(TPP)Cl complexes

The chemical composition and structural and textural properties of grafted Mn(TPP)Cl complexes are listed in Table 4.4. As found in the case of Mn(Salen)Cl, even with Mn(TPP)Cl complexes, their grafting onto the silica surface did not disturb the long-range ordering of SBA-15 (Fig. 4.10). Organo-functionalization and grafting

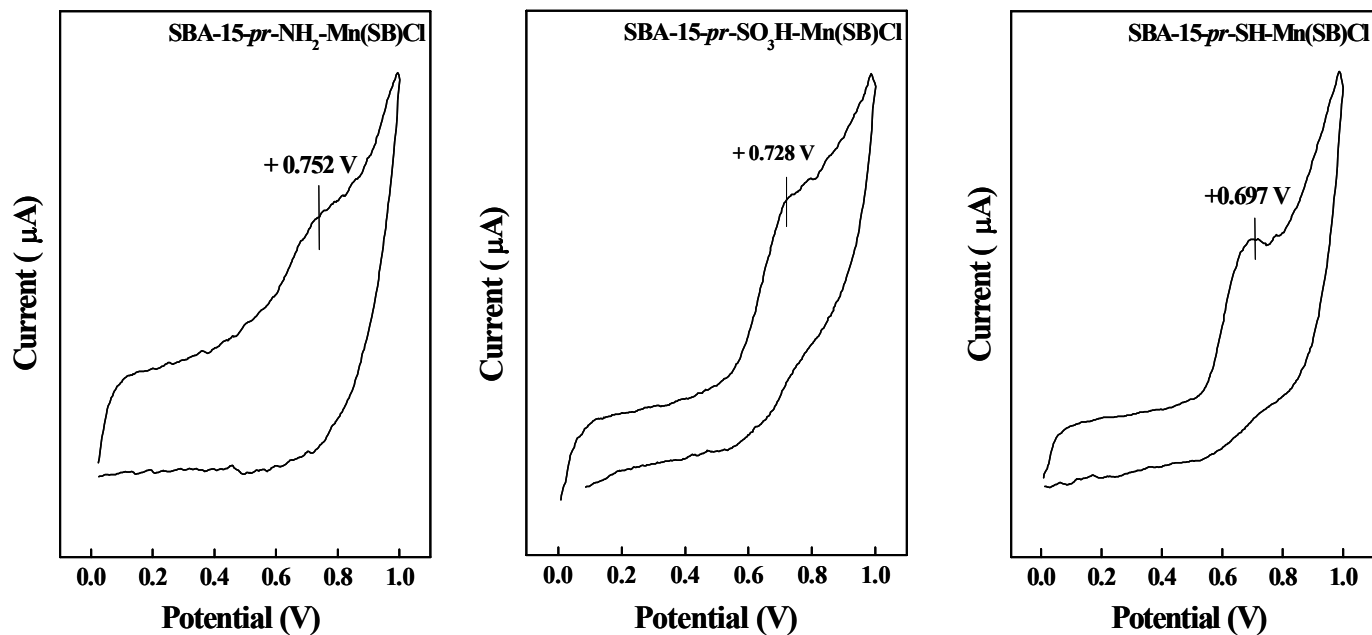
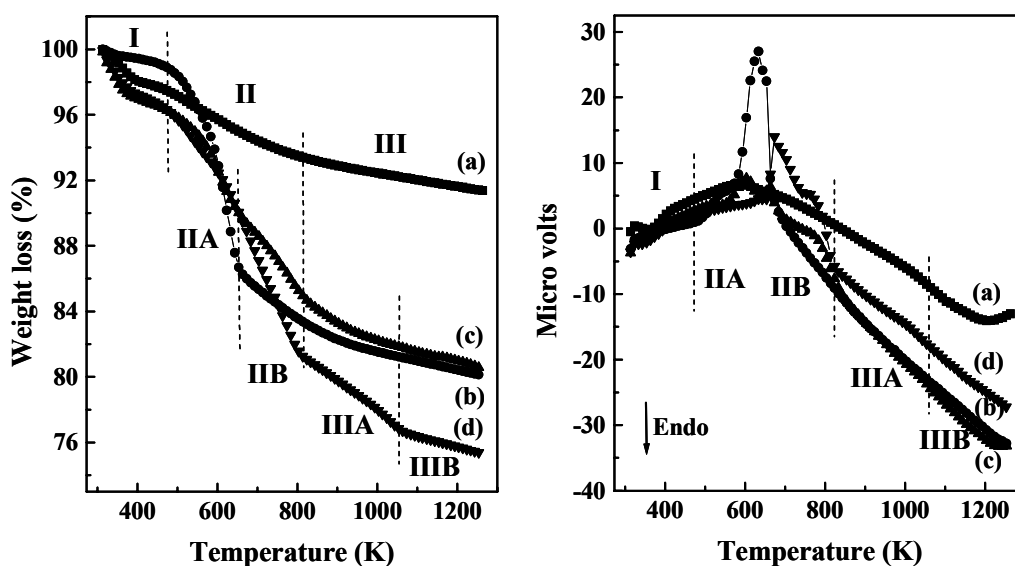


Fig. 4.8. Cyclic voltammograms of (a) SBA-15-*pr*-NH₂-Mn(SB)Cl, (b) SBA-15-*pr*-SO₃H-Mn(SB)Cl, and (c) SBA-15-*pr*-SH-Mn(SB)Cl.

The value of the anodic peak potential (Mn³⁺ to Mn⁴⁺) is indicated. SB = Salen.

Table 4.3. Thermal analysis of immobilized Mn(Salen)Cl

System	TG - DTA (Weight loss, %)		
	Stage I 313 – 475 K (Exo)	Stage II (A/B) 475 – 660 K & 660 – 815 K (Exo)	Stage III (A/B) 815 – 1064 K & 1064 – 1273 K (Endo)
SBA-15	2.35	4.14	2.09
SBA-15- <i>pr</i> -SH	1.08	12.62, 2.94	3.28
SBA-15- <i>pr</i> -SO ₃ H	3.71	6.46, 4.96	4.34
SBA-15- <i>pr</i> -SO ₃ -Mn(Salen)	3.71	6.46, 8.73	4.44, 1.39

Fig. 4.9. TGA and DTA profiles: (a) SBA-15, (b) SBA-15-*pr*-SH, (c) SBA-15-*pr*-SO₃H, and (d) SBA-15-*pr*-SO₃-Mn(Salen).

of the Mn-complex led to a reduction in the specific surface area (S_{BET}) and pore volume (Table 4.4). This reduction in S_{BET} on functionalization with a few molecules of modifier (*-pr*-NH₂, *-pr*-SH and *-pr*-SO₃H as well as Mn(TPP)Cl) is, rather, surprising. The value of the C constant of the BET equation decreased from 1.05×10^2 (for SBA-15) to 0.78×10^2 and 0.83×10^2 for SBA-15-*pr*-SH and SBA-15-*pr*-SO₃H, respectively. This is because of the elimination of acidic surface OH upon silylation. In such a case, the BET theory does not apply. However, the surface area

determined by BJH theory using the cumulative area of the pores also showed a similar decrease as a consequence of organo-functionalization (S_{BJH} (m^2/g): 686, 554 and 546 for SBA-15, SBA-15-*pr*-SH and SBA-15-*pr*-SO₃H, respectively). Apparently, some reconstruction of the solid, which could not be detected, is possibly occurring. Acid and base functionalities affected the surface properties to different extents with the latter affecting to a larger extent than the former. Moreover, concentration of organofunctional group on the surface is another factor affecting the surface modification.

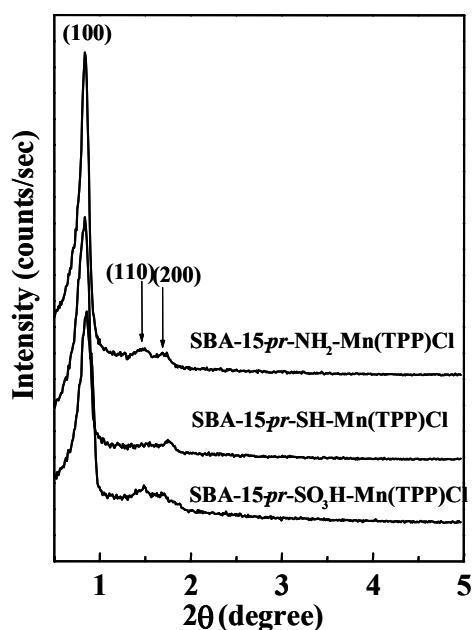


Fig. 4.10. XRD pattern of grafted Mn(TPP)Cl complexes.

The characteristic UV-visible spectra provided a reliable evidence for the presence of grafted Mn-porphyrin complexes in the catalysts of the present investigation (Fig. 4.11; left panel). “Neat” Mn(TPP)Cl showed an intense Soret band at 483 nm and Q-bands in the region of 537–618 nm. Upon grafting on the functionalized SBA-15 surfaces, marked changes were observed in the spectra of the

Table 4.4. Chemical composition and structural properties of Mn(TPP)Cl grafted on functionalized SBA-15

Catalyst	Chemical composition (wt%) ^a					Organic functiona l group (mmol/g. catalyst) ^b	Grafted Mn(TPP) Cl (mmol/g. catalyst) ^c	XRD		N ₂ adsorption			Wall thick ness (nm)
	C	H	N	S	Mn			d ₁₀₀ (nm)	Unit cell parameter (nm)	Pore diameter (nm) ^d	S _{BET} (m ² /g)	Total pore volume (cm ³ /g)	
SBA-15	0.4	0.9	0	0	0	0	0	9.5	11.0	6.5	692	1.13	5.8
SBA-15- <i>pr</i> -SH	6.3	1.8	0	4.7	0	1.5	0	9.9	11.5	6.5	534	0.87	6.3
SBA-15- <i>pr</i> -SO ₃ H	4.8	1.8	0	1.8	0	0.56	0	9.7	11.3	6.2	533	0.83	4.5
SBA-15- <i>pr</i> -NH ₂	10.9	2.8	3.6	0	0	2.5	0	9.9	11.4	5.9	258	0.4	5.5
SBA-15- <i>pr</i> -SH- Mn(TPP)Cl	3.3	3.4	0.7	-	0.06	-	0.011	10.6	12.3	5.7	549	0.66	6.5
SBA-15- <i>pr</i> -SO ₃ H- Mn(TPP)Cl	2.2	2.7	0.6	-	0.09	-	0.016	10.3	12.3	5.8	517	0.72	6.1
SBA-15- <i>pr</i> -NH ₂ - Mn(TPP)Cl	6.2	2.8	2.3	0	0.05	-	0.009	10.6	11.9	6.6	323	0.51	6.5
“Neat” Mn(TPP)Cl	75.4	4.1	8.1	0	2.6	0	-	-	-	-	-	-	-

^aC, H and N-contents were estimated by elemental analysis. Mn-content was determined by AAS technique. ^bDetermined based on S/N contents.

^cDetermined based on Mn-content. ^dDetermined using the BJH model.

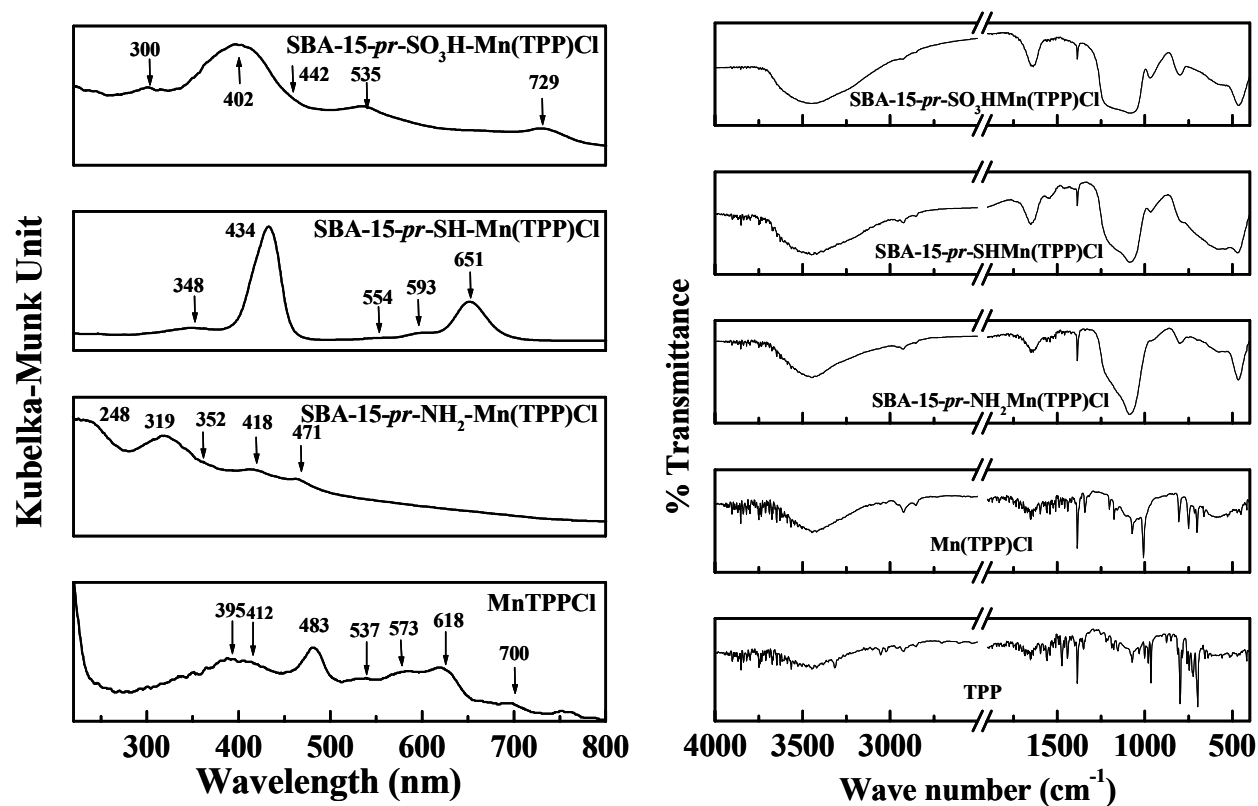


Fig. 4.11. Diffuse reflectance UV-visible (left) and FT-IR (right) spectra of ‘neat’ and SBA-15-grafted Mn(TPP)Cl complexes.

Mn complexes (Fig. 4.11; left panel). The spectral pattern of Mn(TPP)Cl was different on different supports. The Soret band had undergone a blue-shift (from 483 nm for “neat” Mn(TPP)Cl) to 418, 434 and 402 nm for SBA-15-*pr*-NH₂-Mn(TPP)Cl, SBA-15-*pr*-SH-Mn(TPP)Cl and SBA-15-*pr*-SO₃H-Mn(TPP)Cl, respectively). On the contrary, the Q-bands exhibited a red-shift, which is apparently more evident in the spectra of SBA-15-*pr*-SH-Mn(TPP)Cl and SBA-15-*pr*-SO₃H-Mn(TPP)Cl. Such shifts in the Soret and Q-bands positions correspond to a change in the conformation of the porphyrin to an S₄-ruffling geometry [20, 21]. ‘Neat’ Mn(TPP)Cl exhibits a weak d-d band at around 395 nm due to +3 oxidation state of the Mn. This band is absent in the spectra of SBA-15-*pr*-SH-Mn(TPP)Cl and SBA-15-*pr*-SO₃H-Mn(TPP)Cl. The shifts in the UV-visible band positions and absence of d-d band indicate that the oxidation state of Mn in SBA-15-*pr*-SH-Mn(TPP)Cl and SBA-15-*pr*-SO₃H-Mn(TPP)Cl decreases from +3 to +2. In the FTIR spectra, the peaks corresponding to the support SBA-15 have masked those of Mn(TPP)Cl (Fig. 4.11; right panel).

“Neat” Mn(TPP)Cl is EPR-silent at 80–298 K and X-band frequency consistent with the +3 oxidation of Mn ions. However, the SBA-15-grafted Mn(TPP)Cl complexes are EPR-active and showed a sextet-line hyperfine pattern centered at $g_{av} = 2.0027$ (Fig. 4.12). The spectra correspond to an Mn²⁺ species. For a known amount of the material, the intensity of the EPR signal indicative of the concentration of Mn²⁺ ions decreased in the following order: SBA-15-*pr*-SO₃H-Mn(TPP)Cl > SBA-15-*pr*-SH-Mn(TPP)Cl > SBA-15-*pr*-NH₂-Mn(TPP)Cl. Upon grafting, a part of the Mn³⁺ ions in Mn(TPP)Cl got reduced to an EPR-active Mn²⁺ species. Such a reduction in the oxidation state is more favored on acid-functionalized supports like SBA-15-*pr*-SO₃H and SBA-15-*pr*-SH than on base-functionalized supports like SBA-15-*pr*-NH₂ (EPR signal is more intense for the former than the

latter complexes; Fig. 4.12). In other words, the acido-basic properties of the support play a crucial role in fine-tuning the oxidation state and molecular electronic structure of the grafted Mn complexes.

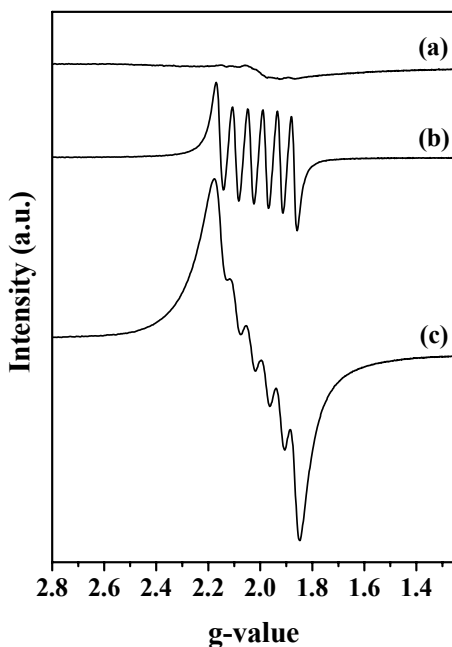


Fig. 4.12. EPR spectra of Mn(TPP)Cl grafted on (a) propylamine, (b) propylthiol and (c) propylsulfonic acid functionalized SBA-15.

We had also found a similar observation in the case of grafted Mn(Salen)Cl. In those materials, the extent of Mn^{3+} reduction decreased in the order: SBA-15-*pr*-SH-Mn(Salen)Cl > SBA-15-*pr*-SO₃H-Mn(Salen)Cl > SBA-15-*pr*-NH₂-Mn(TPP)Cl. The extent of Mn ions reduction was more in the case of TPP than in Salen complexes. This indicates that not only the support but the nature of the ligand too influences the redox properties of the Mn complexes. Porphyrins (metalloenzyme and photosystem-II, for example) are known to oxidize or reduce readily by chemical, electro chemical or photochemical means forming the corresponding cationic and anionic radical species during the reactions [22]. Such a facile redox behavior of porphyrins and

ability to act as an electron-sink makes them versatile to develop efficient redox catalysts. It is known from the electrochemical studies that porphyrin complexes exhibit a more facile redox behavior than the Schiff base-Salen complexes [20, 21]. This point once again clarifies the differences in the reducibility of Mn-TPP and Salen complexes on SBA-15 supports.

In the case of Mn(Salen)Cl complexes grafted on acidic SBA-15 supports, the $\text{Mn}^{4+}/\text{Mn}^{3+}$ redox couple occurred at less positive $E_{1/2}$ values (+0.697 to +0.728 V) than those grafted on basic propyl-amine support (+0.752 V) [23]. Lower $E_{1/2}$ value is indicative of more facile oxidation and reduction. Hence, Mn-complex grafted on propyl-thiol/sulfonic acid-functionalized SBA-15 is more easily oxidized/reduced than that grafted on propyl-amine-functionalized SBA-15. Possibly the acidic protons of thiol/sulfonic acid groups facilitate the oxidation/reduction processes. These results agree well with the observations from EPR spectroscopy. Mn(TPP)Cl is dark green in color. Propyl-amine, thiol and sulfonic acid functionalized Mn(TPP)Cl are of light pink, green and brown colored. The differences in the colors of the complexes are due to variations in their structure and electronic properties. Hence, the acido-basic properties of the support and ligand structure influence the electronic structure and redox behavior of the immobilized Mn complexes.

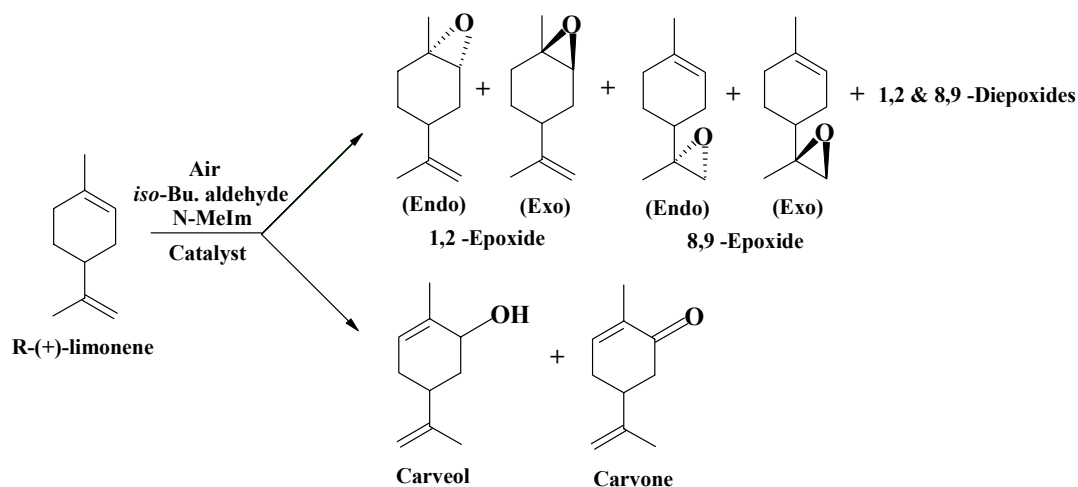
4.3.3. Catalytic activity studies

4.3.3.1. Oxidation of limonene

4.3.3.1.1. SBA-15-grafted Mn(Salen)Cl complexes

Limonene has two olefin bonds, one is acyclic and the other one is exocyclic double bond. The oxidation can take place at either or both the olefinic bonds (1,2 and 8,9). Two types of diastereomers (*endo* and *exo*) are expected for each of the epoxide

products. Additionally it has an allyl group. Hence, oxidation of limonene, in general, yields a variety of products including carveol and carvone (due



Scheme 4.2. Limonene and its oxidation products

to oxidation at allylic C-H bond) and 1,2-epoxide, 8,9-epoxide and 1,2 & 8,9-diepoxydes (due to oxidation of the olefinic bond) (Scheme 4.2). Thus, limonene happens to be the molecule of choice for studying the chemo-, regio- and stereoselective oxidations.

Novelty of the complexes: Most of the known solid catalysts [2-12] yielded significantly low limonene conversions and epoxide selectivities (20 – 30%); carveol, carvone and polymeric products are formed in large quantities. However, the Mukaiyama-type aerial oxidation over Mn(Salen)Cl complexes conducted in the presence of an additive like N-methyl imidazole (N-MeIm) and iso-butyraldehyde, a co-reagent yielded mainly the epoxide product; the allylic oxidation products formed only in minor amounts (Table 4.5). Among the various epoxides, 1,2-epoxide formed with higher (regio-) selectivity. This could be possibly due to differences in the electron density of the olefinic (C₁ – C₂) versus the (C₈ – C₉) double bonds. The former is more electron-rich due to the neighboring methyl group than the latter. The

grafted Mn(Salen)Cl complexes exhibited enhanced chemoselectivities than the “neat” complex especially in toluene (Table 4.5). However, such differences are not significant in CH₃CN indicating that the solvent plays a major role. It may be noted that unlike toluene, CH₃CN can form weak coordination to Mn complex and thereby change the electronic properties.

The selectivity for 1,2-epoxide over different immobilized Mn-complexes in toluene medium increased in the following order: SBA-15-*pr*-NH₂-Mn(Salen)Cl (80.2%) < SBA-15-*pr*-SO₃H-Mn(Salen)Cl (82.0%) < SBA-15-*pr*-SH-Mn(Salen)Cl (100%). Interestingly, this variation in epoxide selectivity follows the variation in electron density (hyperfine coupling constant – A; EPR studies) and oxidizability (cyclic voltammetric studies) of the Mn ions (Fig. 4.8). Mn-complexes immobilized on propylthiol-functionalized SBA-15 exhibited higher catalytic activity (turnover frequency; TOF) than those immobilized on propylsulfonic acid and propylamine-functionalized SBA-15 supports (Table 4.5). Apparently, the supports that keep Mn ions in an easily oxidizable environment lead to more efficient selective oxidation catalysts.

Influence of additives. The reaction did not occur in the absence of a catalyst or when *iso*-butyraldehyde (co-oxidation reagent) or the nitrogen-containing base (additive) was not used. With different N-containing bases, the catalytic activity of SBA-15-*pr*-SO₃-Mn(Salen) decreased in the order: N-MeIm > Im > 2-MeIm, in parallel with the decreasing electron donor capability of the nitrogen containing bases.

Table 4.5. Aerial oxidation of R-(+)-limonene over “neat” and immobilized Mn(Salen)Cl complexes^a

Catalyst	R-(+)- limonene conversion (mol%)	TOF (h ⁻¹) ^b	Diasterio meric excess (<i>de</i>) ^c	Product selectivity (mol%)				
				1,2- Epoxide	8,9- Epoxide	1,2 & 8,9- Diepoxide	Carve ol	Carvo ne
“Neat” Mn(Salen)Cl ^b	69.2	7.0	35.8	74.2	7.2	6.2	5.2	7.2
SBA-15- <i>pr</i> -NH ₂ -Mn(Salen)Cl	75.9	35.4	-	80.2	6.4	7.2	4.0	2.2
SBA-15- <i>pr</i> -SO ₃ H-Mn(Salen)Cl	60.0	17.8	39.8	82.0	8.0	2.6	3.7	3.7
SBA-15- <i>pr</i> -SH-Mn(Salen)Cl	64.1	58.9	-	100	0.0	0.0	0.0	0.0
SBA-15-Mn(Salen)	21.1	14.8	27.4	100	0	0	0	0
Mn(Salen)-Y	36.8	5.6	35.8	97.7	2.3	0	0	0

^aReaction conditions: R-(+)-limonene = 3.75 mmol; catalyst = 0.0165 g (“neat”) or 100 mg (“immobilized”); iso-butyraldehyde = 9 mmol; N-MeIm = 1.7 mmol; oxidant – air = 1 atm (2 ml/min); solvent = 20 ml; reaction temperature = 298 K; reaction time = 8 h.

^bTurnover frequency (TOF) = Moles of R-(+)-limonene converted per mole of Mn per hour.

^cDiastereomeric excess (*de*) = (% selectivity of endo 1,2-epoxide - % selectivity of exo 1,2-epoxide) x 100 / (% total 1,2-epoxide selectivity).

Effect of immobilization. Grafted Mn(Salen)Cl complexes are considerably more active than Mn(Salen)-Y (TOF = 5.6 h⁻¹) as well as the “neat” Mn(Salen)Cl (Table 4.5). The sulfonated catalysts yielded a higher diastereomeric excess (*de*) of 39.8% compared to 27.4% for the non-sulfonated analogs. The zeolite-Y-encapsulated Mn(Salen)⁺ (Mn(Salen)-Y), was prepared according to reported procedures [24] employing the flexible ligand synthesis method. Mn content (AAS) = 0.31 mmol/g.

Influence of solvent. The catalytic activity of SBA-15-*pr*-SO₃H-Mn(Salen)Cl in different solvents decreased in the order: toluene > acetonitrile > acetone > dichloromethane (Table 4.6). The reaction did not proceed when alcohols (methanol and *tert*-butanol) were used as solvent. Alcoholic solvents probably compete with the nitrogen bases for coordination to Mn ions and thereby, retard the catalytic activity.

Influence of reaction time. Conversion of limonene increased with time and reached a maximum at 8 h. 1,2-Epoxyde was the only product at lower conversions. At conversions above 20%, 8,9-epoxyde and 1,2 & 8,9-diepoxydes were also formed. At conversions above 50%, carveol and carvone formed in smaller quantities in addition to the epoxyde. At similar conversions, the encapsulated complexes yielded the *endo*-1,2-epoxyde more selectively (Fig. 4.13).

Hot-filtration and catalyst reusability studies. The solid catalysts were hot-filtered at 2.5 h and the reaction was continued (Fig. 4.14). We found that limonene oxidation continued even after the catalyst was separated out. Analysis of the filtrate for metal ions by atomic absorption spectroscopy revealed that leaching of a part of the Mn ions had occurred.

Table 4.6. Influence of solvent on aerial oxidation of *R*-(+)-limonene over SBA-15-*pr*-SO₃-Mn(Salen)^a

Solvent	Conversion of <i>R</i> -(+)-limonene (mol%)	TOF (h ⁻¹) ^c	Product selectivity (%)				
			1,2- epoxide	8,9- epoxide	1,2- & 8,9- diepoxide	Carveol	Carvone
Toluene ^b	60.0	17.8	82.0	8.0	2.6	3.7	3.7
Dichloromethane	9.4	2.8	100	0	0	0	0
Acetonitrile	39.2	11.8	100	0	0	0	0
Acetone	27.1	8.1	100	0	0	0	0

^aReaction conditions: *R*-(+)-limonene = 3.75 mmol; *iso*-butyraldehyde = 9 mmol; Additive - *N*-MeIm = 1.7 mmol; catalyst = 0.1 g; solvent = 20 ml; oxidant = air (1 atm); reaction temperature = 298 K; reaction time = 12 h.

^bReaction time = 8 h.

^cTurnover frequency (TOF) = Moles of *R*-(+)-limonene converted per mole of Mn per hour.

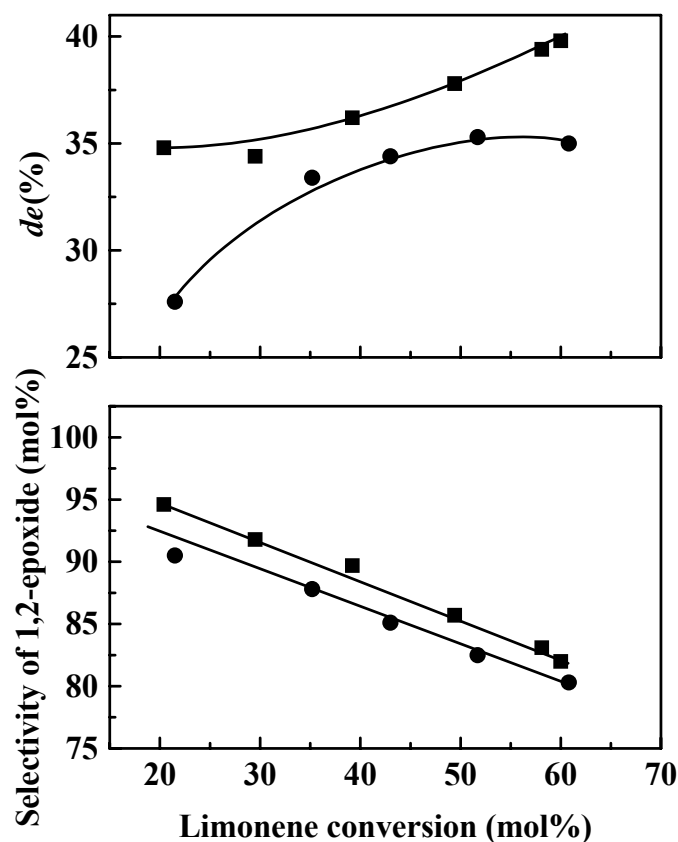


Fig. 4.13. Diastereomeric excess (*de*) and 1,2-epoxide selectivity as a function of limonene conversion over “neat” Mn(Salen)Cl (●) and SBA-15-*pr*-SO₃-Mn(Salen) (■).

The solid catalyst was filtered and reused after washing with toluene and dichloromethane, followed by drying at 353 K for 2 - 4 h. While the diastereomeric selectivity (*de* value) was unaffected, limonene conversion decreased in catalyst recyclability studies (Fig. 4.15). For SBA-15-*pr*-SO₃-Mn(Salen) the decrease in catalytic activity is from 60% (for a “fresh” catalyst) to 44% in the 5th recycle. In the case of Mn(Salen)-Y, this decrease was from 36.8% to 20.3%. Mn(Salen) immobilized directly on “bare” SBA-15 became completely inactive in the 3rd recycle itself. The extent of this decrease at the end of fourth recycle is lower for SBA-15-*pr*-

SH-Mn(Salen)Cl (18%) than for SBA-15-*pr*-SO₃H-Mn(Salen)Cl (25%) and SBA-15-*pr*-NH₂-Mn(Salen)Cl (28%). Hence, based on the observed conversions it can be concluded that the extent of Mn leaching into the solution decreased in different catalysts in the order: SBA-15-*pr*-NH₂-Mn(Salen)Cl > SBA-15-*pr*-SO₃H-Mn(Salen)Cl > SBA-15-*pr*-SH-Mn(Salen)Cl.

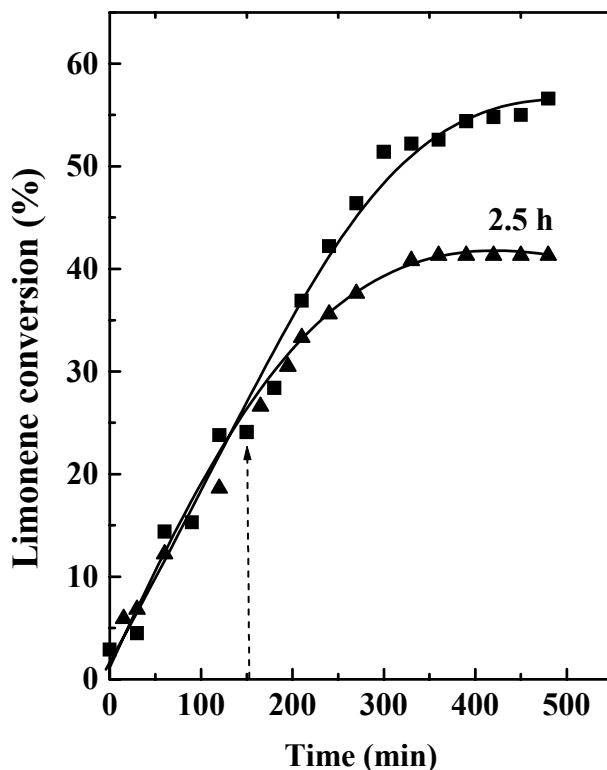


Fig. 4.14. Catalyst stability studies in limonene oxidation: catalyst - (SBA-15-*pr*-SO₃-Mn(Salen)).

4.3.3.1.2. SBA-15-grafted Mn(TPP)Cl complexes: Oxidation of limonene

The grafted Mn(TPP)Cl complexes are also highly efficient for the oxidation of limonene at mild conditions with molecular oxygen as oxidant (Table 4.7). Epoxide is the main product; the allylic oxidation products formed only in minor amounts. Among the epoxides, the 1,2-epoxide formed with higher (regio-) selectivity.

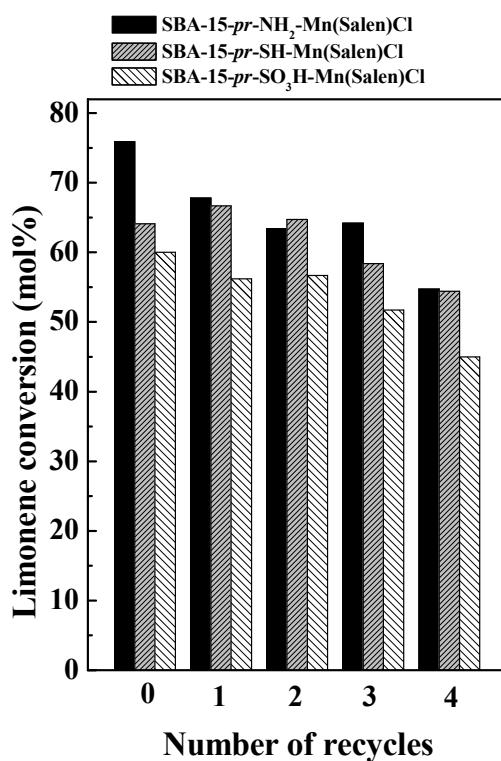


Fig. 4.15. Stability and reusability of immobilized Mn(Salen) complexes in limonene oxidation with air.

The grafted complexes showed enhanced catalytic activities than the “neat” complex (Table 4.7). The conversion of limonene increased with the temperature (Fig. 4.16). However, there was a marginal drop in the 1,2-epoxide selectivity from ca., 94 to 84 mol%; 8,9-epoxide and small percentage of carveol and carvone formed at higher temperatures. The grafted TPP complexes were found to be catalytically more efficient than the corresponding Salen complexes. Turnover frequencies are higher by an order of magnitude for Mn(TPP)Cl than for Mn(Salen)Cl complexes (compare Tables 4.5 and 4.7). The complexes grafted on the acidic supports showed higher catalytic activity and regioselectivity than those grafted on the basic support.

Table 4.7. Oxidation of R-(+)-limonene over SBA-15 grafted Mn(TPP)Cl complexes^a

Catalyst	R-(+)-limonene conversion (mol%)	TOF (h ⁻¹)	Product selectivity (mol%)				
			1,2- Epoxide	8,9- Epoxide	1,2 & 8,9- Diepoxide	Carveol	Carvon e
“Neat” Mn(TPP)Cl	12.1	34.0	100	-	-	-	-
SBA-15- <i>pr</i> -NH ₂ -Mn(TPP)Cl	30.6	319	88.4	8.1	0.9	1.2	1.4
SBA-15- <i>pr</i> -SO ₃ H-Mn(TPP)Cl	62.1	364	95.0	5.0	-	-	-
SBA-15- <i>pr</i> -SH-Mn(TPP)Cl	47.4	346	93.2	5.1	0.9	-	0.8

^aReaction conditions: R-(+)-limonene = 3.75 mmol; catalyst: MnTPP - 0.036 g (“neat”) or 0.05 g (“grafted”), Mn(Salen)Cl – 0.0165 g (“neat”) or 0.1 g (“grafted”); iso-butyraldehyde = 9 mmol; N-MeIm = 1.7 mmol; oxidant – air = 1 atm (2 ml/min); toluene = 20 ml; reaction temperature = 298 K; reaction time = 8 h.

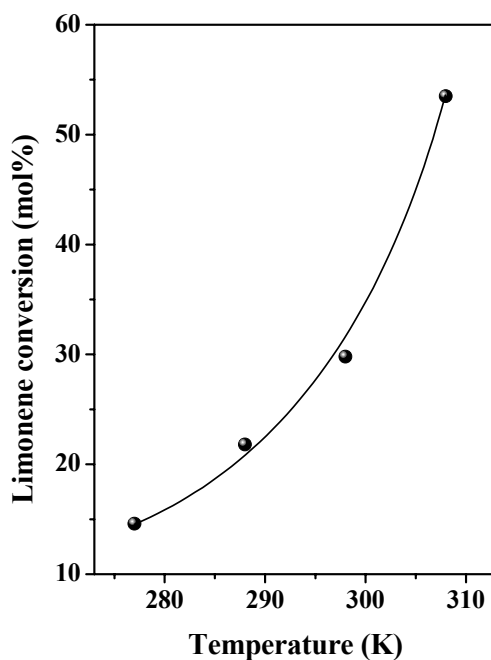
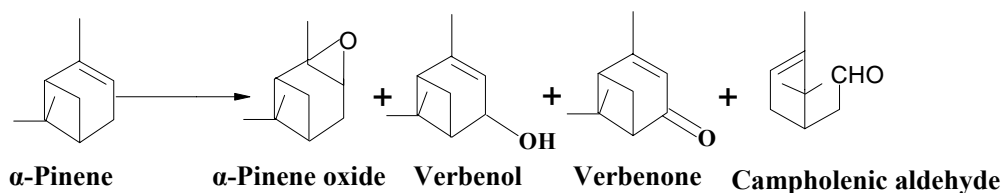


Fig. 4.16. Influence of temperature on the catalytic activity of SBA-15-*pr*-SH-Mn(TPP)Cl. Reaction conditions: catalyst = 25 mg; R-(+)-limonene = 3.75 mmol; iso-butyaldehyde = 9 mmol; N-MeIm = 1.7 mmol; oxidant – air = 1 atm (2 ml/min); toluene = 20 ml; reaction time = 8 h.

4.3.3 2. Oxidation of α -pinene and carene

Oxidation of α -pinene gives various products as shown in Scheme 4.3. The major product of oxidation of α -pinene over Mn(Salen)Cl complexes is α -pinene oxide; in addition small quantities of allylic oxidized products are also formed.



Scheme 4.3. Oxidation products of α -pinene.

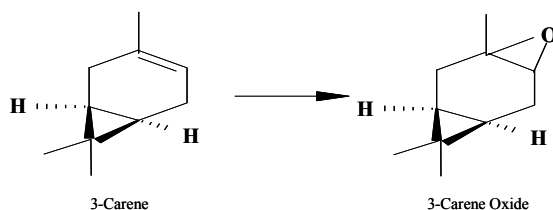
Oxidation of α -Pinene over grafted Mn(Salen) complexes was conducted in different solvents. Solvent has a marked effect on conversion and epoxide selectivity (Table 4.8)

Table 4.8. Oxidation of α -Pinene over grafted Mn(Salen)Cl complexes

Catalyst	Solvent	Conv. (mol%)	TOF (h ⁻¹)	α -Pinene oxide selectivity
SBA-15- <i>pr</i> -NH ₂ -	Toluene	35.9	16.8	99.0
Mn(Salen)Cl	Acetonitrile	100	46.9	82.1
	Acetone	58.2	27.3	88.3
SBA-15- <i>pr</i> -SH-	Toluene	47.9	45.0	80.6
Mn(Salen)Cl	Acetonitrile	92.2	86.4	41.1
	Dichloromethane	36.0	33.8	95.0
SBA-15- <i>pr</i> -SO ₃ H-	Acetonitrile	16.7	5.0	100
Mn(Salen)Cl				

Reaction Conditions: α -Pinene = 3.75 mmol; catalyst = 0.1g; iso-butyraldehyde = 9 mmol; N-MeIm = 1.7 mmol; oxidant – air = 1 atm (2 ml/min); solvent = 20 ml; reaction time = 8 h.

The major product of oxidation of 3-carene is its corresponding oxide (Scheme 4.4). Formation of other products like hydroxylated carene, allylic oxidized products were also observed (Table 4.9).



Scheme 4.4. Oxidation product of 3-carene.

Table 4.9. Oxidation of 3-carene over grafted Mn(salen)Cl complexes

Catalyst	Conversion (mol%)	3-Carene oxide selectivity	TOF (h ⁻¹)
SBA-15-pr-NH ₂ -MnSB	33.4	15.7	100
SBA-15-pr-SH-MnSB	46.5	43.6	100
SBA-15-pr-SO ₃ H-MnSB	54.0	15.8	100

Reaction conditions: Carene = 3.75 mmol; catalyst = 0.1g; iso-butyraldehyde = 9 mmol; N-MeIm = 1.7 mmol; oxidant – air = 1 atm (2 ml/min); Acetonitrile = 20 ml; reaction temperature = 298 K; reaction time = 8 h.

4.3.4. Structure-activity correlations

N-MeIm and iso-butyraldehyde were used as additive and co-reagent during the Mukaiyama-type selective oxidation of monoterpenes. The reaction didn't occur when either of them were absent. The role of additive (N-MeIm) and co-reagent (iso-butyraldehyde) in the epoxidation reactions was investigated using in-situ EPR spectroscopy. Mn(Salen)Cl was dissolved in CH₃CN and different reagents were added. EPR spectra were recorded after each addition. When N-MeIm was added, the solution became EPR-active and resolved Mn²⁺ hyperfine signals were observed (Fig. 4.17(a)). Addition of iso-butyraldehyde and exposure to air made the solution EPR-silent (Fig. 4.17(b)). Exposure of Mn²⁺ ions to O₂ gave rise to high-valent oxo-Mn species which were EPR-inactive. These reactive oxo-species transfer oxygen atom to limonene and undergo self-reduction back to EPR-active Mn²⁺ species (Fig. 4.17(c)). This redox cycle continues and epoxide is produced selectively. Hence, surface modification and use of additives (N-MeIm) and co-reagents (iso-butyraldehyde) led to a greater concentration of Mn²⁺ species.

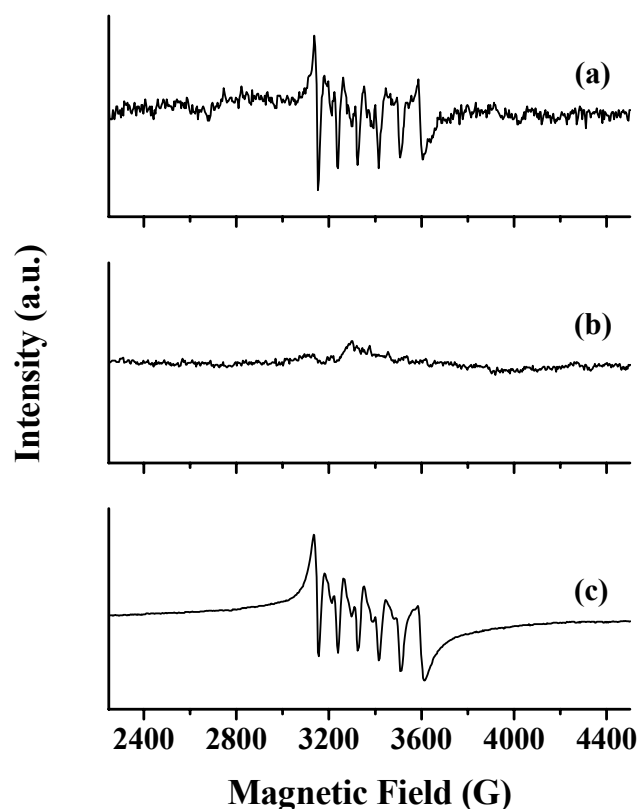


Fig. 4.17. EPR spectra at 102 K of Mn(Salen)Cl dissolved in CH₃CN (a) after adding N-MeIm, (b) addition of iso-butylaldehyde to solutions in (a) and exposed to air, and (c) addition of limonene to solution in (b) and exposed to air.

From the electrochemical studies the $E_{1/2}$ value for Mn(Salen)Cl complex grafted on thiol functionalized material was found to be +0.697 V, which is lower than that of other two grafted complexes. Lower value of $E_{1/2}$ facilitate oxidation/reduction behavior, as a consequence the Mn(Salen)Cl complex grafted on thiol functional material easily reduces Mn^{+3} to Mn^{+2} in higher amount which facilitates the oxidation of limonene. This result can be correlated with the hyperfine coupling constant value for the grafted materials, higher value of hyperfine coupling constant value means electron density surrounding the metal centre is more which is observed in thiol functionalized material. As a result Mn(Salen)Cl complex grafted on

thiol functionalized SBA-15 gives better selectivity towards the oxidation of limonene to 1,2 limonene oxide (Fig. 4.18).

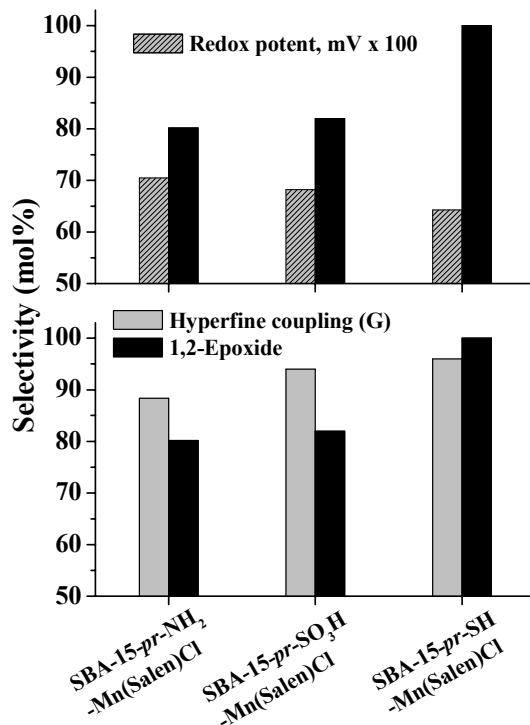


Fig. 4.18. Correlation between hyperfine coupling constant (A) and redox potential ($E_{1/2}$) with catalytic activity and epoxide selectivity.

A correlation was found between the intensity of the EPR signal i.e., concentration of the Mn^{2+} species and the catalytic activity (Fig. 4.19). Higher the concentration of Mn^{2+} complex species the higher was the catalytic activity (turnover frequency) for limonene oxidation. This correspondence, apparently, reveals that supports that keep Mn ions in an easily oxidizable environment lead to more efficient selective oxidation catalysts. Thus, by a proper fine-tuning of the support surface with acidic and basic moieties as well by choosing a right kind of the ligand system (porphyrin, for example) one could design highly selective oxidation catalysts.

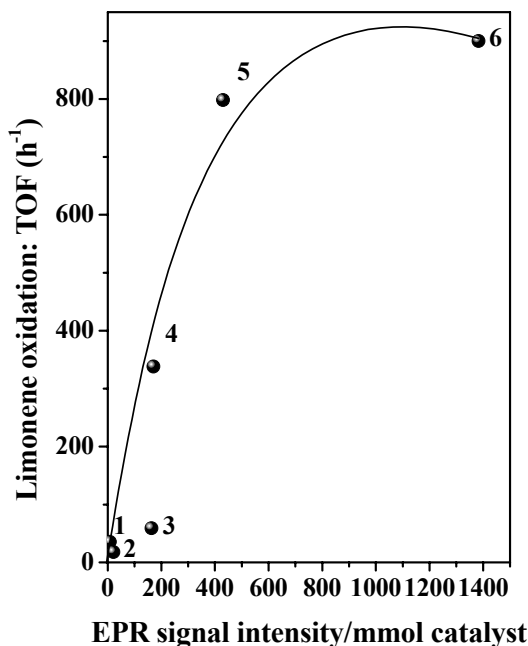


Fig. 4.19 Correlation between the limonene oxidation activity and Mn^{2+} species concentration (EPR signal intensity) in SBA-15-grafted Mn complexes. (1) SBA-15-*pr*- NH_2 -Mn(Salen)Cl, (2) SBA-15-*pr*- SO_3H -Mn(Salen)Cl, (3) SBA-15-*pr*-SH-Mn(Salen)Cl, (4) SBA-15-*pr*- NH_2 -Mn(TPP)Cl, SBA-15-*pr*-SH-Mn(TPP)Cl, (5) SBA-15-*pr*- SO_3H -Mn(TPP)Cl

Based on the magnitude of Mn hyperfine coupling constants, which is an indication of the electron density at the site of Mn, the metal-ligand (sulfur/oxygen/nitrogen) bond strength in different grafted Mn(Salen) complexes would decrease in the order: SBA-15-*pr*-SH-Mn(Salen)Cl > SBA-15-*pr*- SO_3H -Mn(Salen)Cl > SBA-15-*pr*- NH_2 -Mn(Salen)Cl (Fig. 4.20). Due to trans-axial lability, the Mn-O₂ bond strength (in the oxygen adduct) should increase in the reverse order. Thereby, the O-O bond strength of the activated oxygen should follow the same order while the electron density on oxygen orbitals follows the reverse trend: SBA-15-*pr*-SH-Mn(Salen)Cl < SBA-15-*pr*- SO_3H -Mn(Salen)Cl < SBA-15-*pr*- NH_2 -Mn(Salen)Cl.

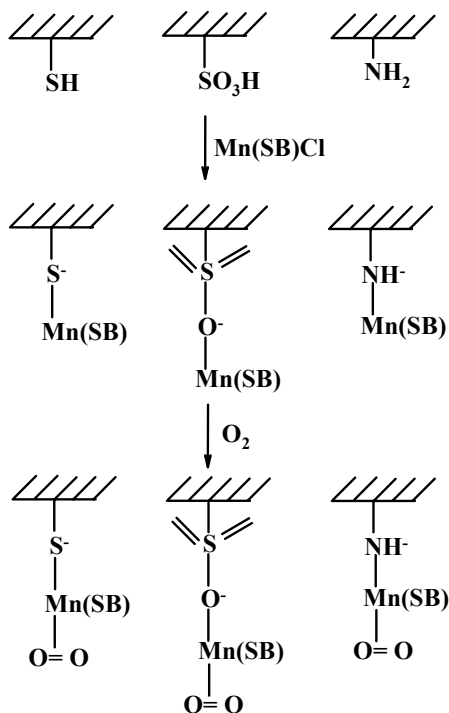


Fig. 4.20. Schematic representation of activation of molecular oxygen over grafted Mn(Salen)Cl complexes.

Heterolytic O-O bond cleavage, formation of reactive Mn=O and the consequent epoxide selectivity are therefore expected to be higher in SBA-15-*pr*-SH-Mn(Salen)Cl than in SBA-15-*pr*-SO₃H-Mn(Salen)Cl and SBA-15-*pr*-NH₂-Mn(Salen)Cl. Thus, higher electron density at manganese (due to reduction from +3 to +2 state) and consequent lower redox potential of grafted Mn complex enhance catalytic activity. The ability to fine tune redox potential of grafted metal complexes (and thereby, their catalytic oxidation properties) by modifying surface charge/potential is a powerful tool in the design of solid oxidation catalysts. In [Table 4.5](#), the first and the fourth entries for the “neat” and SBA-15-*pr*-SH-grafted Mn(Salen)Cl, have similar limonene conversions but the turnover frequency (TOF) values are different by almost an order of magnitude. Further the selectivity for 1,2-epoxide over SBA-15-*pr*-SH-Mn(Salen)Cl is remarkably high (100%). This is

primarily because of the difference in the oxidation states of Mn in the “neat” and grafted complexes. As mentioned before, Mn is in a +3 oxidation state in the “neat” complex. Upon grafting on surface thiol groups, the electronic structure is modified and the oxidation state of Mn is reduced from +3 to +2. This is an example where the support has shown a definite influence on the electronic structure, and, thereby on the catalytic activity/selectivity of the grafted Mn complexes.

4.4. Conclusions

Efficient, chemo- and region- and stereoselective, mesoporous catalysts for the oxidation of R(+)-limonene, α -pinene and 3-carene were prepared by modifying the surface of SBA-15 molecular sieves with organo-functional groups and Mn Schiff base and TPP complexes. Mn(Salen)Cl and Mn(TPP)Cl were grafted on propylamine, propylthiol and propylsulfonic acid-functionalized SBA-15 molecular sieves. The modified SBA-15 support influenced the oxidation state and redox potentials of Mn ions and thereby, the oxidation activity. Upon grafting, a part of the Mn ions is reduced from +3 to +2 oxidation state. The extent of such a reduction in the oxidation state of Mn is more in the case of TPP than in Salen complexes and also when the complexes are grafted on acid functionalized SBA-15 molecular sieves (SBA-15-*pr*-SH and SBA-15-*pr*-SO₃H). A direct correlation between the concentration of the Mn²⁺ species and catalytic activity was observed. In case of Mn(Salen)Cl complexes, Mn(Salen)Cl supported on propylthiol-functionalized SBA-15 was found to be superior catalyst for limonene oxidation with aerial oxygen, at ambient conditions, yielding 1,2-limonene epoxide with 100% selectivity. Grafted Mn(TPP)Cl materials were found superior to grafted Mn(Salen)Cl and other known solid catalysts for this reaction. The ability to fine-tune the redox potential (and thereby the catalytic activity / selectivity) of supported metal ions by modification of the acidity of the underlying

support is a powerful tool in the design of catalysts. The nature of the support as well the ligand play a crucial role controlling the redox behavior, molecular electronic structure and thereby, the catalytic activity of the Mn complexes.

4.5. References

- [1] B. D. Mookherjee, R.A. Wilson, 4th Ed., Encyclopedia of Chemical Technology Kirk-Orthmer, Vol. 17, Wiley, New York, 1996, p. 603.
- [2] R. Hutter, T. Mallat, A. Baiker, *J. Catal.* 153 (1995) 177.
- [3] (a) M. V. Cagnoli, S.G. Casuscelli, A. M. Alvarez, J. F. Bengoa, N. G. Gallegos, N. M. Samaniego, M.E. Crivello, G.E. Ghione, C.F. Pérez, E.R. Herrero, S. G. Marchetti, *Appl. Catal.A: Gen.*, 287 (2005) 227. (b) M.V. Cagnoli, S. G. Casuscelli, A. M. Alvarez, J.F. Bengoa, N.G. Gallegos, M.E. Crivello, E.R. Herrero, S.G. Marchetti, *Catal. Today* 107 – 108 (2005) 397. (c) H. E. B. Lempers, R.A. Sheldon, *Appl. Catal. A: Gen.* 143 (1996) 137.
- [4] (a) L. S. Salles, J.-Y. Piquemal, R. Thouvenot, C. Minot, J.-M. Brégeault, *J. Mol. Catal. A: Chem.* 117 (1997) 375. (b) M. A. Armendia, V. Borau, C. Jiménez, J. M. Luque, J. M. Marinas, J.R. Ruiz, F. J. Urbano, *Appl. Catal. A: Gen.* 216 (2001) 256. (c) P.A.L. Villa, A.F. Taborda, C. Monte de Correa, *J. Mol. Catal. A: Gen.* 185 (2002) 269. (d) N.K. Kala Raj, V.G. Puranik, C. Gopinathan, A.V. Ramaswamy, *Appl. Catal. A: Gen.* 256 (2003) 265. (e) S.Casuscelli, E. Herrero, M. Crivello, C. Pérez, M.G. Egusquiza, C.I. Cabello, I.L. Botto, *Catal. Today* 107 – 108 (2005) 230.
- [5] (a) L.E. Firdoussi, A. Baqqa, S. Allaoud, B.A. Allal, A.Karim, Y. Castanet, A. Mortreux, *J. Mol. Catal A: Chem.* 135 (1998) 11. (b) A.D. Silva, M.L. Patitucci, H.R. Bizzo, E. D’Elia and O.A.C. Antunes, *Catal. Commun.* 3 (2002) 435. (c) J. Bussi, A. López, F. Peña, P. Timbal, D. Paz, D. Lorenzo, E.

- Dellacasa, *Appl. Catal. A: Gen.* 253 (2003) 177. (d) P.A. Robles-Dutenhefner, D.L. Nunes, J.A. Gonçalves, E.V. Gusevskaya, E.M.B. Sousa, *J. Non-Crystalline Solids*, 348 (2004) 195.
- [6] P. A. Robles-Dutenhefner, M.J. da Silva, L.S. Sales, E.M.B. Sousa, E.V. Gusevskaya, *J. Mol. Catal. A: Chem.* 217 (2004) 139.
- [7] (a) C. Schuster and W. F. Hölderich, *Catal. Today* 60 (2000) 193. (b) W.F. Hölderich, *Catal. Today* 62 (2000) 115.
- [8] F.C. Skrobot, A.A. Valente, G. Neves, I. Rosa, J. Rocha, J.A.S. Cavaleiro, *J. Mol. Catal. A: Chem.* 201 (2003) 211.
- [9] S.Tangestaninejad, M. Moghadam, V. Mirkhani, H. Kargar, *Ultrasonics Sonochemistry* 13 (2006) 32.
- [10] P. Oliveira, A.M. Ramos, I. Fonseca, A. Botelho do Rego, J. Vital, *Catal. Today* 102 – 103 (2005) 67.
- [11] S. Bhattacharjee, T.J. Dines, J.A. Anderson, 225 (2004) 398.
- [12] (a) P.C. Bakala, E. Briot, L. Salles, J.M. Bregeault, *Appl. Catal. A: Gen.* 300 (2006) 91. (b) R. Raja, G. Sankar, J. M. Thomas, *Chem. Commun.* (1999) 829.
- [13] (a) S. Borocci, F. Marotti, G. Mancini, D. Monti, A. Pastorini, *Langmuir* 17 (2001) 7198. (b) L.F. Lima, L. Cardozo-Filho, P.A. Arroyo, H. Márquez-Alvarez, O.A.C Antunes, *React. Kinet. Catal. Lett.* 84 (2005) 69. (c) B.B. Wentzel, P.L. Alsters, M.C. Feiters, R.J.M. Nolte, *J. Org. Chem.* 69 (2004) 3453. (d) M.F.T. Gomes, O.A.C. Antunes, *Catal. Lett.* 42 (1996) 213.
- [14] W.M. Van Rhijn, D.E. De Vos, B.F. Sels, W.D. Bossaert, P.A. Jacobs, *Chem. Commun.* (1998) 317
- [15] (a) F. Feng, G.E. Fryxell, L.-Q. Wang, A.Y. Kim, K.M. Kemner, *Science* 276

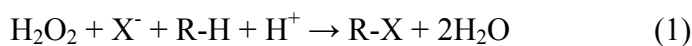
- (1997) 923. (b) L. Mercier, T.J. Pinnavaia, *Adv. Mater.* 9 (1997) 500. (c) A. Stein, B.J. Melde, R.C. Schroden, *Adv. Mater.* 12 (2000) 1403 (d) C.M. Crudden, M. Sateesh, R. Lewis, *J. Am. Chem. Soc.* 127 (2005) 10045.
- [16] (a) T. Kang, Y. Park, J.C. Park, Y.S. Cho, J. Yi, *Stud. Surf. Sci. Catal.* 146 (2003) 527. (b) T. Kang, Y. Park, J. Yi, *Ind. Eng. Chem. Res.* 43 (2004) 1478.
- [17] K. Srinivasan, P. Michaud, J.K. Kochi, *J. Am. Chem. Soc.* 108 (1986) 2309
- [18] A. Domenech, P. Formentin, H. Garcia, M.J. Sabater, *J. Phys. Chem.* 106 (2002) 574.
- [19] (a) B. Sow, S. Hamoudi, M.H. Zahedi-Niaki, S. Kaliaguine, *Microporous Mesoporous Mater.* 79 (2005) 129. (b) L.M. Yang, Y.J. Wang, G.S. Luo, Y.Y. Dai, *Microporous Mesoporous Mater.* 84 (2005) 275.
- [20] K.S. Suslick, R.A. Watson, S.R. Wilson, *Inorg. Chem.* 30 (1991) 2311.
- [21] A.D.Q. Ferreira, F.S. Vinhado, Y. Iamamoto, *J. Mol. Catal. A: Chem.* 243 (2006) 111.
- [22] Metal sites in proteins and models: Iron centers, H.A.O. Hill, P.J. Sadler, A.J. Thomson (eds.), *Structure & Bonding* (Springer-Verlag, Berlin), Vol. 88, 1997.
- [23] L.Saikia, D. Srinivas, P. Ratnasamy, *Micropor. Mesopor. Mater.* 104 (2007) 225.
- [24] (a) T.H. Bennur, D. Srinivas, P. Ratnasamy, *Microporous Mesoporous Mater.* 48 (2001) 111. (b) S.P. Varkey, C. Ratnasamy, P. Ratnasamy, *J. Mol. Catal. A: Chemical* 135 (1998) 295. (c) C.R. Jacob, S.P. Varkey, P. Ratnasamy, *Microporous Mesoporous Mater.* 22 (1998) 465.

CHAPTER – 5

Regiospecific Oxyhalogenation of Aromatics over SBA-15-supported Nanoscopic Metal Oxides

5.1. Introduction

Halogen-containing compounds constitute an important segment of fine and specialty chemicals, dyes, flame-retardants, pharmaceuticals and agrochemicals [1-3]. Halogenated arenes are extensively used as precursors in the preparation of various bioactive molecules and pharmaceuticals [4, 5] and play a vital role in metal-catalyzed coupling reactions [6]. The classical halogenation reaction uses molecular halogen, despite the fact that it is a pollutant and a safety and health hazard [7]. Perbromide (Br_3^-) exchanged polymers are safer to handle and are commercially available. Nevertheless, their preparation still involves direct contact with Br_2 and like most supported stoichiometric reagents they lack adequate process productivity [8]. In contrast to Br_2 , stoichiometric brominating reagents such as *N*-bromosuccinimide (NBS), *N*-bromoacetamide (NBA) and bromodimethylsulfonium bromide do not produce HBr in bromination of organic molecules, but are expensive and generate organic waste [9]. In this context, oxyhalogenation, a bio-mimetic approach, is safer and greener since it avoids the hazardous X_2 by replacing with a halide salt in the presence of an oxidizing agent under acidic conditions (Eq. (1)).



Bio-catalytic approaches offer clear advantages, such as high chemo- or even enantioselectivity and superior catalytic activity at mild, physiological conditions. In biocatalysts, the protein matrix surrounding the active center has been optimized during the process of evolution to maximize the catalyst performance. Such concepts of supramolecular organization have been used in bio-inspired catalysts. Raja and Ratnasamy had reported [10] the application of zeolite-encapsulated copper

phthalocyanines as chloroperoxidase mimics. There was an enhancement in catalytic activity for substrate conversion when the complexes were encapsulated in the cavities of zeolites X, Y and L. There was, however, no regioselectivity among the products. In the oxidation of anisole and toluene, both ortho (predominant) and para-halogenated products were formed. Significant quantities of di- and tri-halogenated products were also detected. Sels et al [11] reported the application of transition metal anion exchanged layered double hydroxides in oxyhalogenations.

The application of SBA-15-supported Group IV-VI metal oxides (TiO_x , VO_x , MoO_x and WO_x) for oxyhalogenation of a range of aromatic compounds is reported in this chapter for the first time. The supported metal oxide catalysts were prepared by the post-synthesis methods and characterized by FTIR, diffuse reflectance UV-visible, laser Raman and X-ray photoelectron spectroscopies. These catalysts are reusable and operate at room temperature. Interestingly, these catalysts show very high selectivity for para-halogenated products. In addition, the reactions over SBA-15-supported metal oxides, unlike other solid catalysts, occur at moderate acidic conditions.

5.2. Experimental

Nanoscale titanium, vanadium, molybdenum and tungsten oxides supported on mesoporous SBA-15 have been prepared as described in Chapter 2. All the catalyst materials were prepared by the post synthetic impregnation technique. The catalysts were characterized using various physicochemical techniques. Procedure for catalytic reaction is provided in Chapter 2.

5.3. Results and Discussion

5.3.1. Structural and spectroscopic characterization

5.3.1.1. XRD

SBA-15 materials showed XRD peaks in the 2θ range of $1 - 2.3^\circ$ (Fig. 5.1; left panel) attributable to 2D hexagonal $p6mm$ symmetry [13-18]. The well-resolved (110) and (200) reflections reveal that incorporation of metal oxides did not alter the long-range mesoporous ordering of the host SBA-15. However, a marginal shift (by 0.06°), peak broadening and decrease in peak intensity were observed to different extents in different metal oxide supported on SBA-15. These differences could be attributed to variations in dispersion and crystallite sizes of metal oxides. This was further confirmed by recording XRD in higher 2θ range as well as investigating the optical spectral characteristics.

$WO_x(n)$ -SBA-15 showed distinct, additional peaks in the 2θ range of $20 - 70^\circ$ typical of nanocrystalline WO_3 (Fig. 5.1; right panel). Intensity of these peaks increased with increasing WO_x loading (5 – 20 wt%). Similar such peaks due to crystalline metal oxides were not detected in the case of TiO_x , VO_x and MoO_x supported on SBA-15. The d spacing (d_{100}) and unit cell parameters, estimated from the position of low-angle (100) peak (Table 5.1) agree well with those reported by others [13-18].

5.3.1.2. N_2 adsorption/desorption

All the materials under investigation exhibited type IV nitrogen adsorption-desorption isotherms with a H_1 -type broad hysteresis loop (Fig. 5.2), corresponding to a large pore mesoporous material with one dimensional cylindrical channels. Capillary condensation of nitrogen with uniform mesopores occurred, causing a sudden step increase in nitrogen uptake in the characteristic relative pressure (P/P_0) range of 0.6 to 0.8,

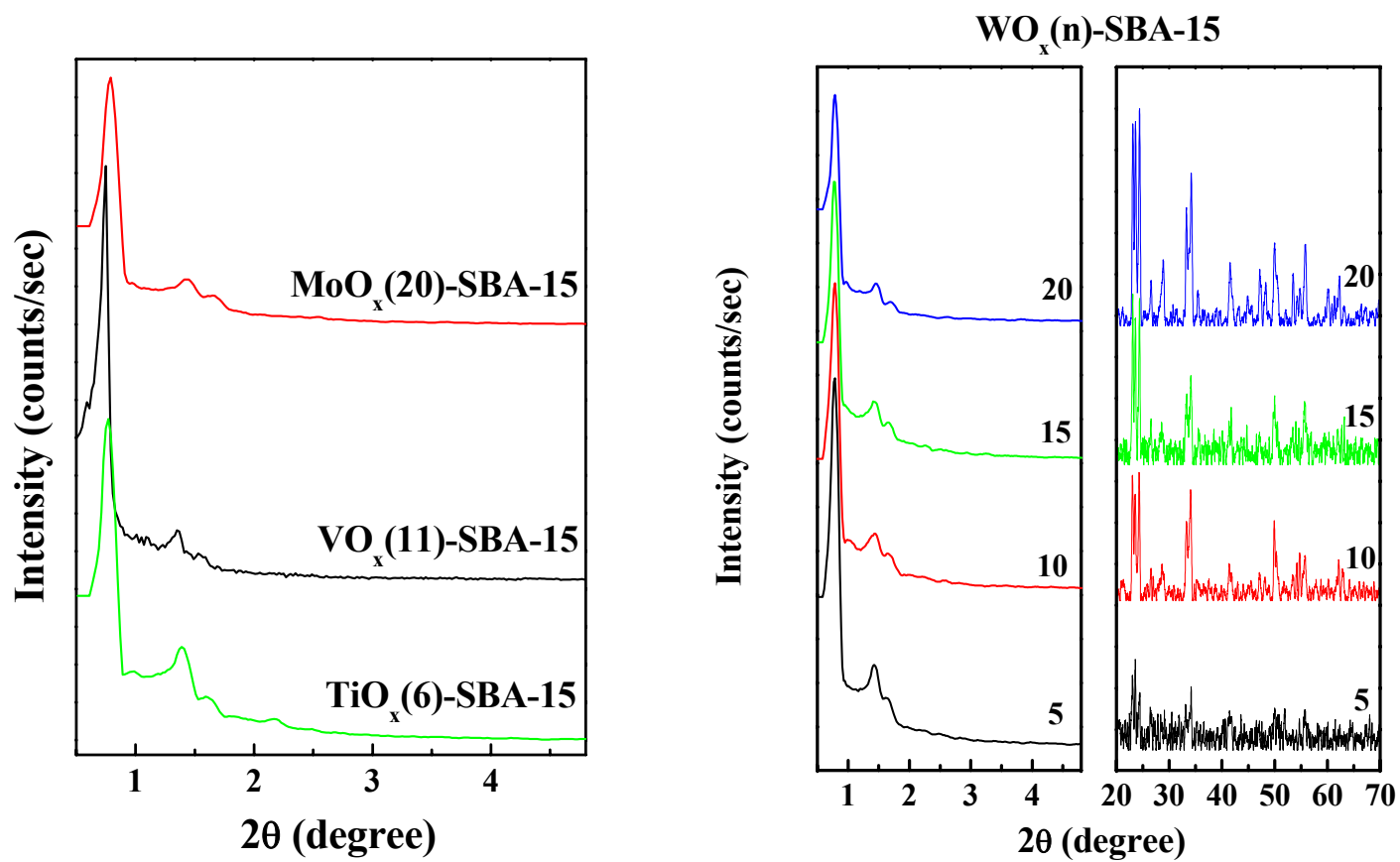


Fig. 5.1. XRD pattern of SBA-15-supported metal oxides.

Table 5.1. Structural and textural properties of SBA-15-supported metal oxide catalysts

Catalyst	XRD		N ₂ physisorption			Wall thickness (nm)	EDAX – Si/Metal At.% (wt.%)
	d ₁₀₀ (nm)	Unit cell parameter (nm)	Pore diameter (nm)	S _{BET} (m ² /g)	Total pore volume (cc/g)		
WO _x (5)-SBA-15	11.0	12.7	7.2	432	0.77	5.5	47.2 (7.2)
WO _x (10)-SBA-15	11.0	12.7	7.2	419	0.76	5.5	23.1 (3.5)
WO _x (15)-SBA-15	11.1	12.8	7.1	391	0.70	5.7	18.2 (2.8)
WO _x (20)-SBA-15	11.0	12.7	8.5	322	0.68	4.2	10.1 (1.5)
MoO _x (20)-SBA-15	11.3	13.1	6.6	452	0.75	6.5	10.9 (3.2)
TiO _x (6)-SBA-15	11.4	13.2	9.5	452	1.08	3.7	11.2 (6.2)
VO _x (11)-SBA-15	11.7	13.5	6.0	349	0.52	7.5	8.8 (4.8)
SBA-15	9.5	11.0	6.9	766	1.33	4.5	-

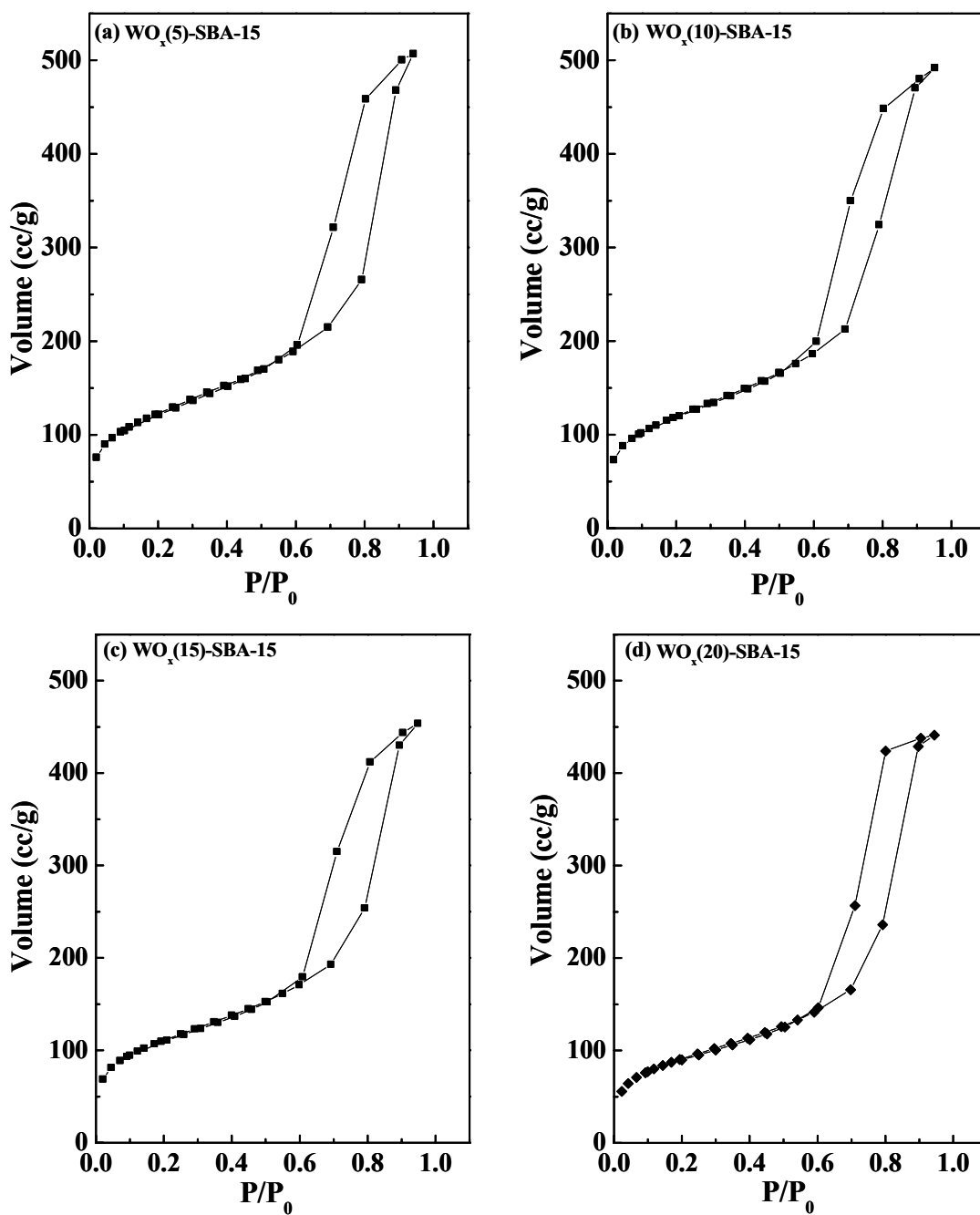


Fig. 5.2. N₂ adsorption-desorption isotherms of WO_x(n)-SBA-15; n = 5 (a), 10 (b), 15 (c) and 20 (d).

suggesting typical mesoporous structure with uniform pore diameters [19]. The amount of nitrogen adsorbed decreased for SBA-15-supported metal oxides as compared to bare SBA-15. The decrease in BET surface area (from 766 to 322 m²/g) and pore volume (from 1.33 to 0.52 cc/g) of the modified SBA-15 materials compared to “bare” SBA-15 (Table 5.1) is a clear indication of metal oxide incorporation in SBA-15.

5.3.1.3. HRTEM and SEM

High resolution transmission electron micrographs (HRTEM) of MoO_x(20)- and WO_x(20)-SBA-15 recorded from different orientations are shown in Fig. 5.3. The high magnification images reveal the highly ordered hexagonal arrays of mesopores of the characteristic SBA-15 support. No separate, bulk metal oxide phase was detected. HRTEM images confirm the conclusions drawn from XRD measurements that mesoporosity of SBA-15 is intact even after modification with metal oxides. The pore diameter value (9.2 nm) calculated for WO_x(20)-SBA-15 from TEM matches well with that determined from the nitrogen physisorption measurements (8.5 nm).

Scanning electron microscopes (SEM) (Fig. 5.4) revealed that the particles of WO_x(20)-SBA-15 have an elliptical morphology while those of MoO_x(20)-SBA-15 contained also some spherical shaped particles.

5.3.1.4. FTIR

Bare SBA-15 showed FTIR peaks at 2900 – 3800, 1040 – 1260, 820 and 500 cm⁻¹ due to O-H of the silanols, adsorbed water molecules and Si-O-Si stretching vibrations, respectively [12]. SBA-15-supported metal oxides showed additional peaks in the spectral range of 800 – 964 cm⁻¹ (Fig. 5.5). While the bands observed at 958 – 964 cm⁻¹ are attributed to that of M-O-Si vibrational modes, that around 910 cm⁻¹ in the case of

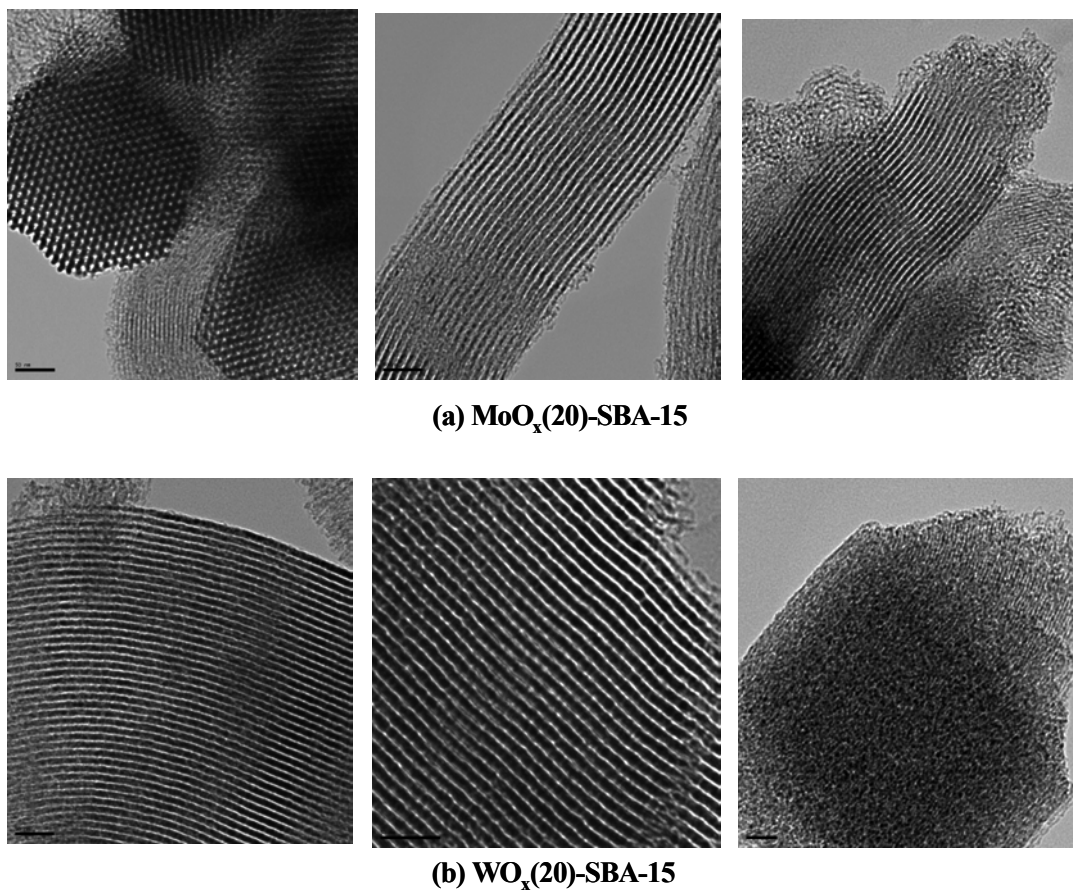


Fig. 5.3. Transmission electron micrographs of the catalysts.

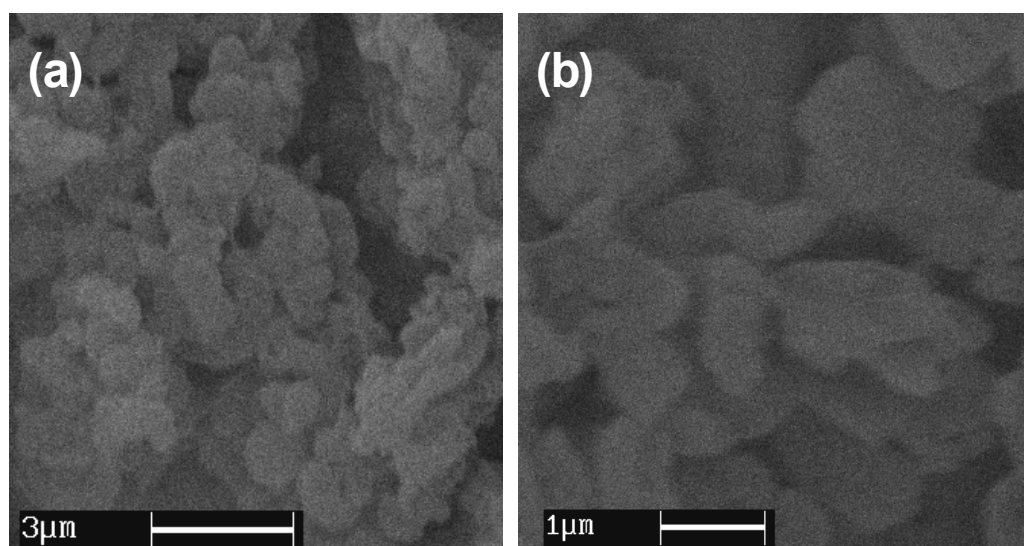


Fig. 5.4. Scanning electron micrographs: (a) WO_x(20)-SBA-15 and (b) MoO_x(20)-SBA-

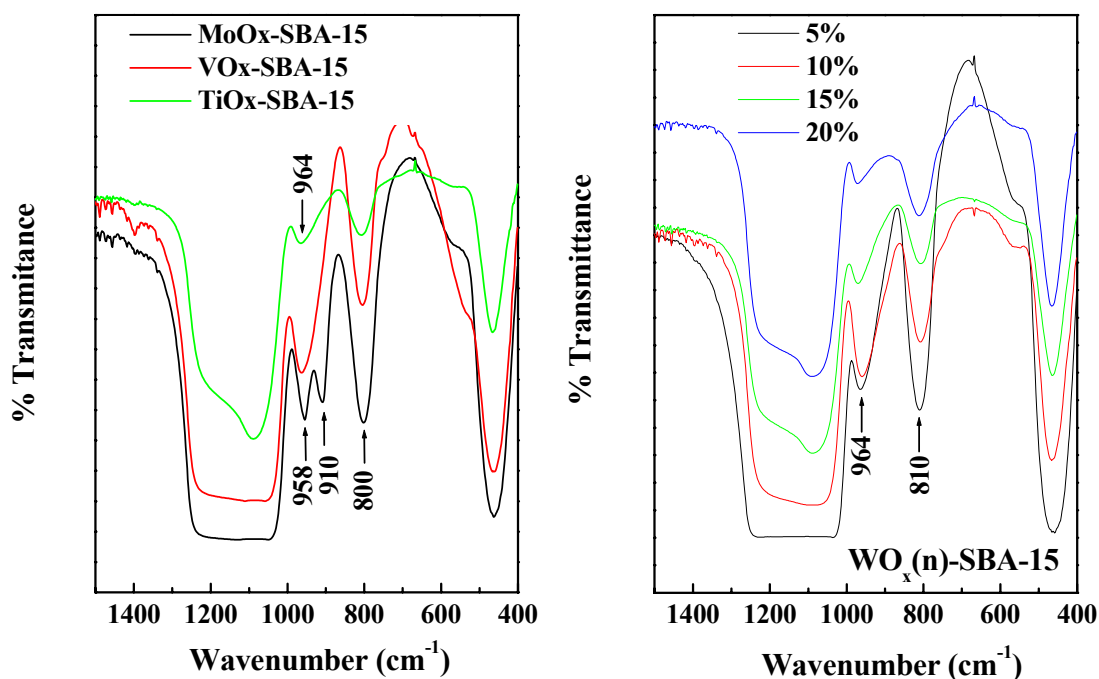


Fig. 5. 5. FTIR spectra of SBA-15-supported metal oxides.

MoO_x is due to Mo-O-Mo vibrations [19]. Further, the absence of bands at 929, 879 and 774 suggest the absence of Keggin-type units in the corresponding mesopores [20]. Intensity of these additional peaks increased with an increase in WO_x loading indicating that they truly originated from the supported the metal oxide species.

5.3.1.5. DRUV-vis

Diffuse reflectance UV-visible (DRUV-vis) spectroscopy can differentiate the dispersed metal oxides from the bulk-phase metal oxides. Bulk titania, vanadia, molybdenum oxide and tungsten oxide show O₂⁻ → Mⁿ⁺ charge transfer band above 380 nm [20]. In the case of dispersed metal oxides this band shifts to higher energy side (blue shift) [20]. In fact, TiO_x(6)-SBA-15 and MoO_x(20)-SBA-15 showed an intense asymmetric

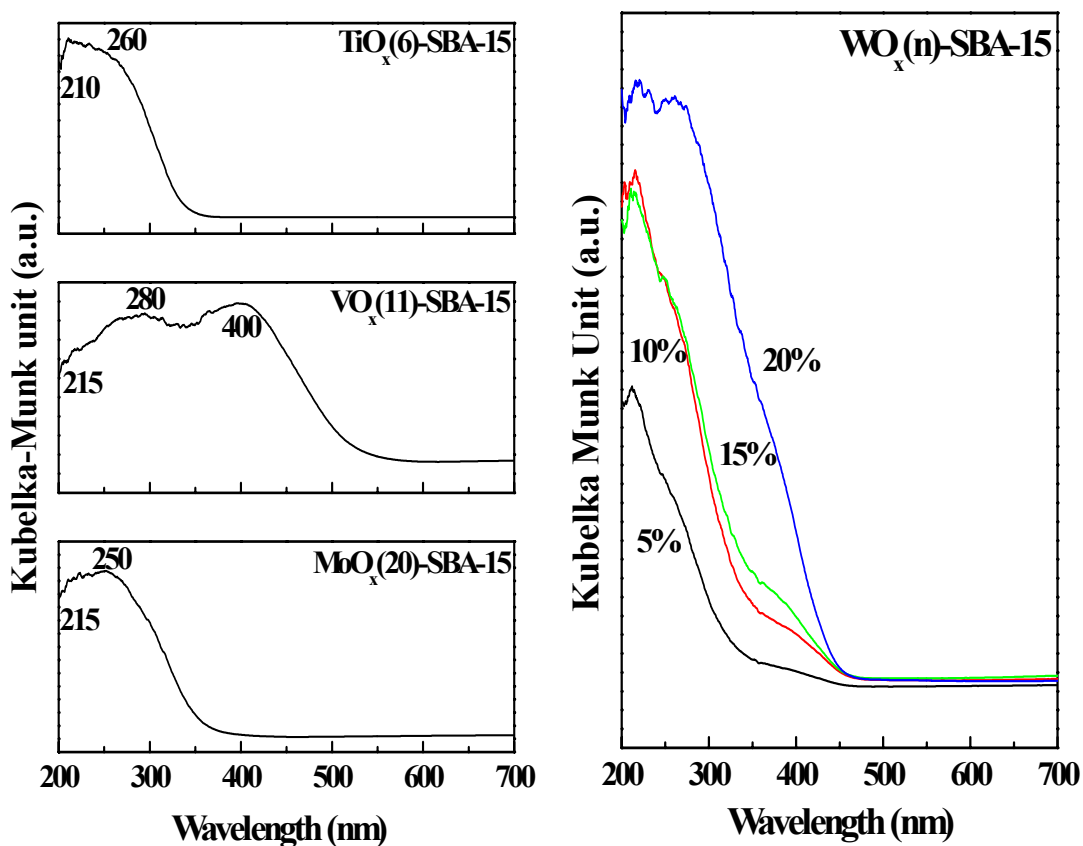


Fig. 5.6. DRUV-vis spectra of SBA-15-supported metal oxides

band below 300 nm indicative of isolated metal oxide species (Fig. 5.6). $\text{VO}_x(11)\text{-SBA-15}$ and $\text{WO}_x(20)\text{-SBA-15}$ showed additionally bands due to bulk-like (400 and 385 nm) metal oxide species. Intensity of the band at 400 nm increased with increasing metal oxide content in $\text{WO}_x(n)\text{-SBA-15}$. A blue shift of absorption edge in all these materials with respect to the bulk-phase indicates formation of a spatially confined, dispersed metal oxide [20].

5.3.1.6. Laser Raman spectroscopy

Laser Raman spectroscopy has been found to work best for crystalline oxides. Amorphous oxides have wide distribution of bond angles leading to broadening of peaks and more featureless spectrum [21]. Raman spectroscopy is very sensitive to the coordination environment of metal species [21]. Anatase has Raman scattering properties showing intense bands at 150, 395, 515 and 640 cm^{-1} . $\text{TiO}_x(6)$ -SBA-15 showed very weak Raman spectrum. No trace of 150 cm^{-1} band, a sensitive indicator, revealed the absence of anatase-like phase in $\text{TiO}_x(6)$ -SBA-15 (Fig. 5.7). On the other hand there clearly are titanium-dependent bands at 955 and 1100 cm^{-1} , corresponding to a syn- and antisymmetric stretch, respectively. Antisymmetric stretch of Ti-O-Si species and the asymmetric stretching mode of T_d framework titania in TS-1 occurs at 1125 cm^{-1} . A shift to lower frequency has been attributed to loosely coordinated Ti species in the framework [21-23]. The diffused spectral pattern and the absence of 150 cm^{-1} band (Fig. 5.7) indicates titania in a highly dispersed state in $\text{TiO}_x(6)$ -SBA-15.

Based on literature reports, isolated vanadia centers in T_d coordination show Raman bands at 1042 cm^{-1} . Cluster-type VO_x species show bands at 994, 697, 286 and 147 cm^{-1} . Undistorted VO_6 octahedron exhibits a strong and sharp band at 870 – 890 cm^{-1} . V_2O_5 phase exhibits typical spectral bands at 994, 701, 526, 284, 144 cm^{-1} [25-27]. Absence of this band in $\text{VO}_x(11)$ -SBA-15 (Fig. 5.7) reveals a different local environment for vanadium in $\text{VO}_x(11)$ -SBA-15. Raman band associated with V=O usually appears at 900 – 1000 cm^{-1} . The weak band at 1034 cm^{-1} in the spectrum of $\text{VO}_x(11)$ -SBA-15 may be corresponded to this stretching vibration. Intense well-resolved Raman shifts were observed in the case of $\text{MoO}_x(20)$ - and $\text{WO}_x(20)$ -SBA-15 (Fig. 5.7).

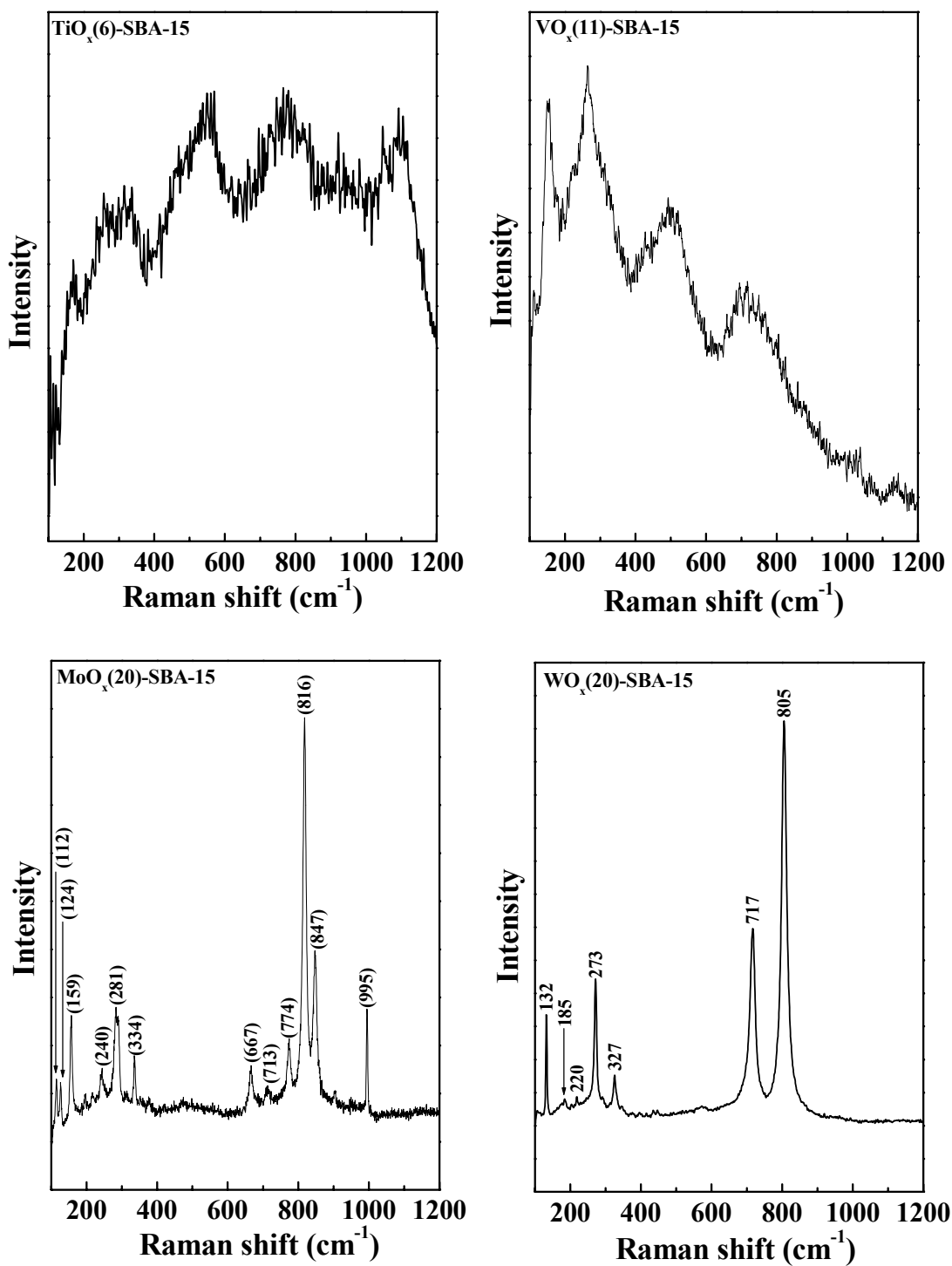


Fig. 5.7. Laser Raman spectra of SBA-15-supported metal oxides.

While the band at 995 cm^{-1} in $\text{WO}_x(20)$ -SBA-15 corresponds to $\text{Mo}=\text{O}$ of two dimensional polymolybdate (octahedral MoO_6 species) that at 816 cm^{-1} corresponds to MoO_5 type species [21]. The intense sharp bands at 805, 717, 273, 137 cm^{-1} for $\text{WO}_x(20)$ -SBA-15 reveals the presence of octahedral WO_6 units as in WO_3 phase [21]. The Raman spectra, therefore, reveal that the supported metal oxides are in a dispersed state and the extent of dispersion differs in different SBA-15-supported metal oxides.

5.3.1.7. XPS

The oxidation state of W and Mo was +6 and that of V was +5 (Fig. 5.8). The peaks corresponding to $4f_{7/2}$ and $4f_{5/2}$ of W in $\text{WO}_x(20)$ -SBA-15 appeared at 26 and 36.8 eV, respectively. The binding energies of Mo 3d levels in $\text{MoO}_x(20)$ -SBA-15 appeared at 235.8 and 233.1 eV. Vanadium showed binding energies at 512.4 and 515.6 eV for $2p_{3/2}$. In all the cases the peaks shifted compared to the corresponding bulk oxides indicating dispersion of metal oxide species on SBA-15. The acidity of the catalysts was determined using NH_3 as probe molecule. NH_3 -TPD confirmed the presence of weak Lewis acidic sites. The amount of NH_3 desorbed in the temperature 373 – 573 K from different supported catalysts decreased in the order: $\text{WO}_x(20)$ -SBA-15 (1.63 mmol/g) > $\text{MoO}_x(20)$ -SBA-15 (0.224 mmol/g) > $\text{TiO}_x(6)$ -SBA-15 (0.201 mmol/g).

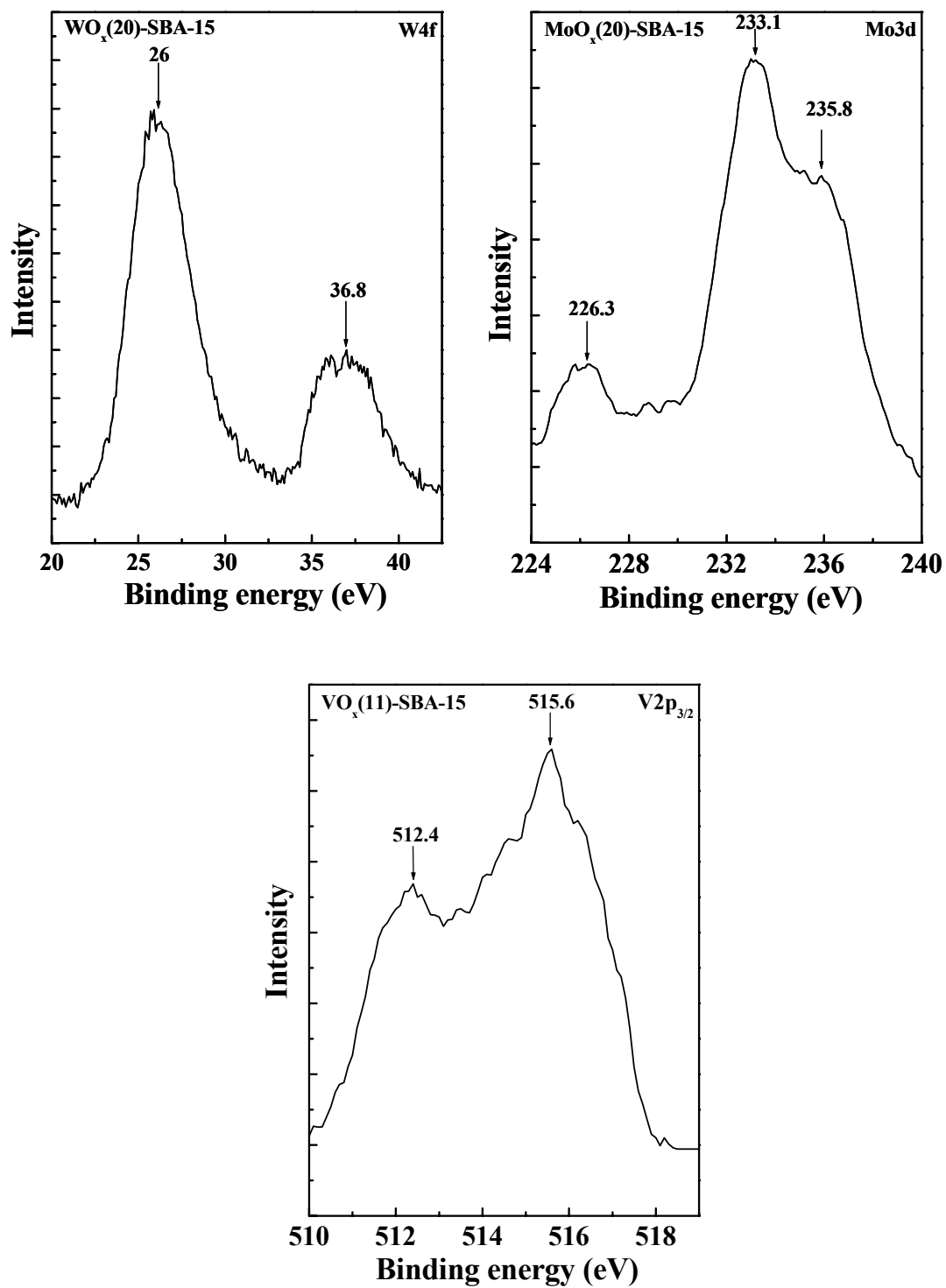
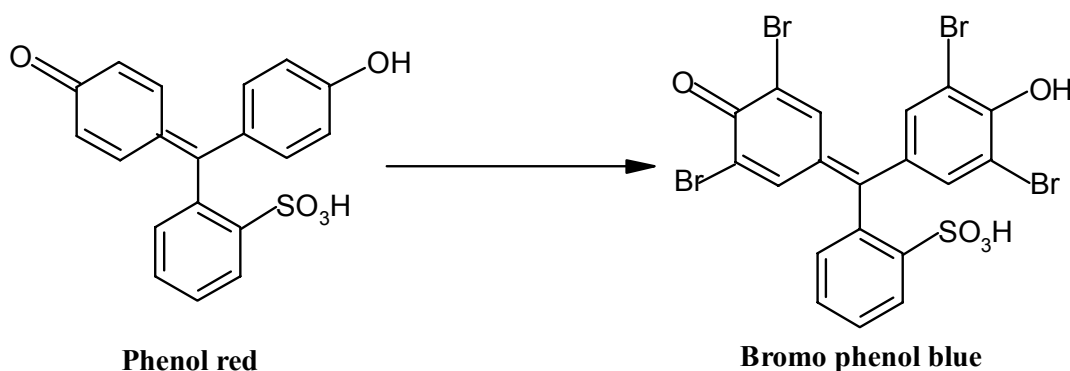


Fig. 5.8. XPS of SBA-15-supported metal oxides in specific regions.

5.3.2. Catalytic activity studies

5.3.2.1. Oxybromination of phenol red

Phenol red (phenolsulfonephthalein) is a conjugated system, which shows a visible band at 430-450 nm in aqueous solution. Bromination of phenol red at mild acidic conditions yields bromophenol blue (tetrabromophenolsulfonephthalein) (Scheme 5.1). The conversion of phenol red to bromophenol blue is a common test to monitor bromination activity under peroxidative conditions. The widespread use of this dye stems from its ability to undergo rapid and stoichiometric bromination and from the ease with which this can be monitored using UV-vis spectroscopy [11].



Scheme 5.1. Oxidative bromination of Phenol red to Bromo phenol blue.

Oxybromination of phenol red to bromo-phenol blue was performed over nanoscopic tungsten oxide, molybdenum oxide, titanium oxide and vanadium oxide supported on SBA-15. In a typical reaction, 20 ml of 0.05 M phenol red solution ($\text{H}_2\text{O} + \text{CH}_3\text{OH}$, 4 : 1) was taken in a double-necked round bottom flask. To it, 2 mmol of KBr and 2 mmol of H_2O_2 (30% aqueous) were added. After addition of 0.025 g of catalyst, the pH of the reaction mixture was adjusted to ~5 by adding HEPES (4-(2-hydroxyethyl)-1-piperazineethanesulfonic acid) buffer drop-wise. The progress of the reaction (298 K)

was monitored by taking out small aliquots of the samples at equal interval (15 min), separating the catalyst by centrifugation and then by recording the UV-vis spectrum which showed a decrease in absorbance at $\lambda_{\text{max}} = 430\text{-}450$ nm corresponding to phenol red and concomitant increase in absorbance at $\lambda_{\text{max}} = 590 - 600$ nm due to bromo phenol blue. The reaction was also carried out with different loadings of tungsten oxide under similar conditions. Effect of temperature on the conversion of phenol red was studied over $\text{WO}_x(20)\text{-SBA-15}$ catalyst.

When SBA-15-supported nanoscopic metal oxides were allowed to react with phenol red in the presence of H_2O_2 and KBr in aqueous medium under mild acidic conditions the yellow color of the reaction mixture rapidly changed to deep-blue. Electronic absorption spectra (Fig. 5.9) recorded as a function reaction time provided clear evidence for the disappearance of phenol red ($\lambda_{\text{max}} = 434$ nm) and formation of bromophenol blue ($\lambda_{\text{max}} = 595$ nm). The initial rate of the bromination over different supported oxide catalysts decreased (Table 5.2) in the order: $\text{WO}_x(20)\text{-SBA-15}$ (3.42×10^{-4}) > $\text{MoO}_x(20)\text{-SBA-15}$ (2.61×10^{-4}) > $\text{TiO}_x(6)\text{-SBA-15}$ (2.24×10^{-4}) > $\text{VO}_x(11)\text{-SBA-15}$ ($1.65 \times 10^{-4} \text{ mM}\cdot\text{min}^{-1}$). Controlled experiments revealed that oxybromination does not occur in the absence of catalyst. The supported metal oxides exhibited higher catalytic activity than the corresponding bulk oxides. The catalytic activity (turnover frequency (TOF) – moles of substrate converted per mole of metal per min) of tungsten oxide has enhanced by 5 orders of magnitude when dispersed and supported on SBA-15 (Table 5.2, compared rows 2 and 9).

Temperature and bromide ion concentration exhibited a marked effect on the rate of oxybromination which increased with temperature (Table 5.2). Conversion of phenol

red increased with bromide ion concentration up to 2 mmol and beyond that it decreased with further increase in bromide ion concentration (Fig. 5.10). MgAl-WO₄²⁻ and MgAl-MoO₄²⁻ exhibited TOF of about 0.3 min⁻¹ [11]. TOF values of 32 and 16 min⁻¹ observed for WO_x(20) and MoO_x(20) supported on SBA-15 indicate that nature of the support influences the activity of the metal oxide species.

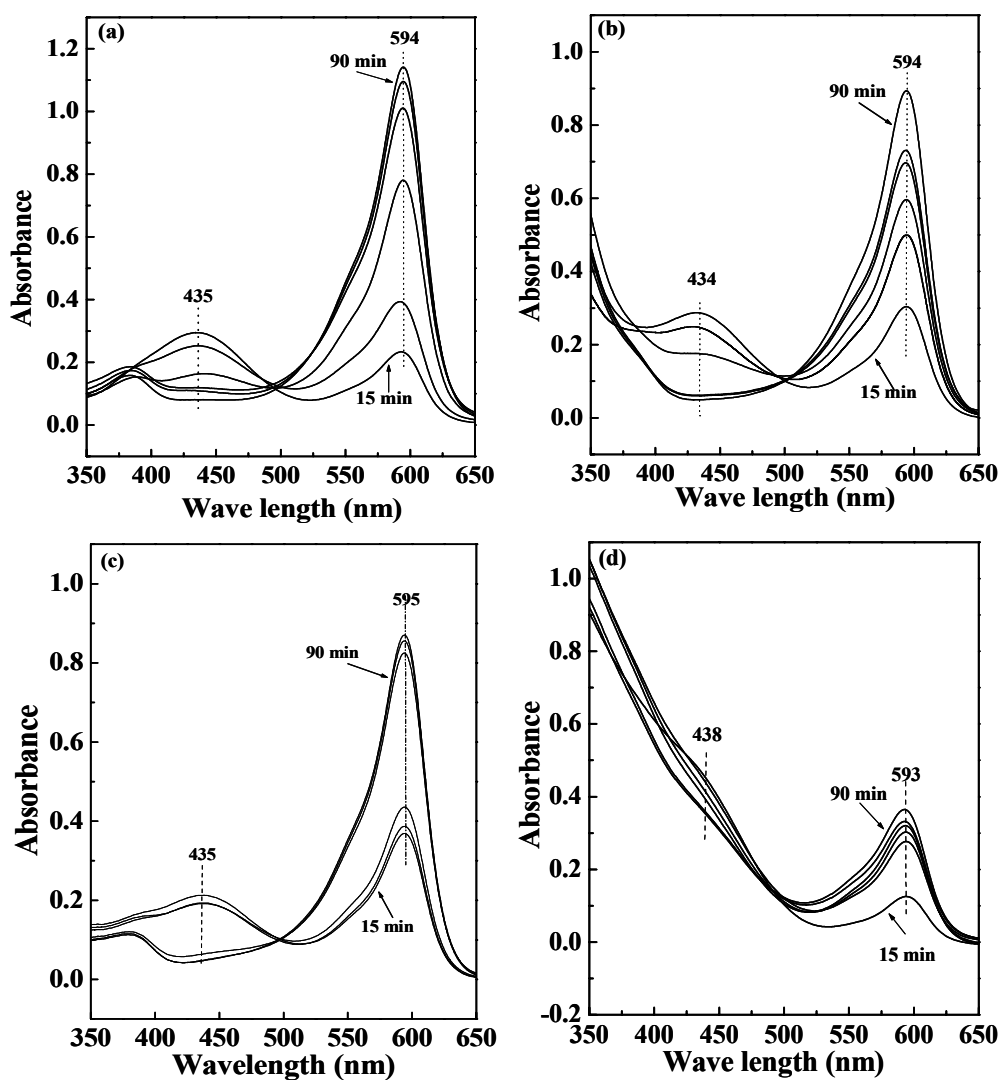


Fig 5.9. UV-Vis spectrum of progress of oxybromination of Phenol red to bromophenol blue with (a) WO_x-SBA-15 (20%), (b) MoO_x-SBA-15 (20%), (c) TiO₂-SBA-15 (6%) and (d) VO_x-SBA-15 (11%) catalysts.

Table 5.2. Oxybromination of phenol red over SBA-15-supported nanocrystalline metal oxides

Catalysts	Temperature (K)	Phenol red conversion (mol%)	TOF (min^{-1})	Initial Rate (mM. min^{-1})
WO _x (20)-SBA-15	293	49.8	32	3.15×10^{-4}
	298	62.6	40	3.42×10^{-4}
	303	63.0	40	4.11×10^{-4}
	313	70.1	45	4.43×10^{-4}
	323	82.0	52	7.86×10^{-4}
MoO _x (20)-SBA-15	298	44.0	16	2.61×10^{-4}
TiO _x (6)-SBA-15	298	42.0	10	2.24×10^{-4}
VO _x (11)-SBA-15	298	12.0	2	1.65×10^{-4}
NH ₄ WO ₃ .2H ₂ O	298	4.0	2×10^{-4}	
V ₂ O ₅	298	11.6	3.2×10^{-4}	

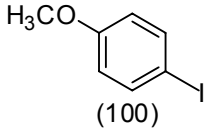
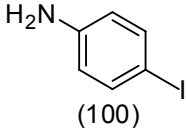
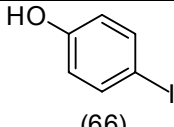
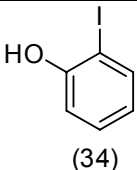
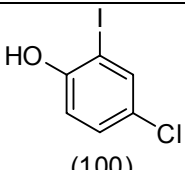
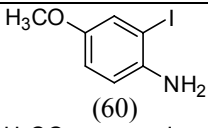
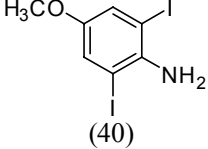
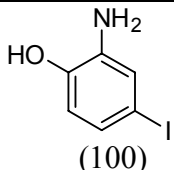
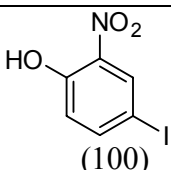
Reaction Conditions: Phenol red = 0.05 mM, catalyst = 0.025 gm (SBA-15 supported metal oxides) and 0.1 mmol (V₂O₅ and NH₄WO₃.2H₂O), KBr = 2 mmol, H₂O₂ (30% aq.) = 2 mmol, solvent (water + methanol (4:1)) = 20 ml, pH ~ 5 (adjusted with HEPES buffer), reaction time = 90 min. Turnover frequency (TOF) = moles of phenol red converted per mole of metal per min.

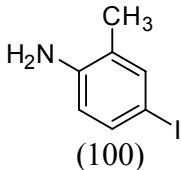
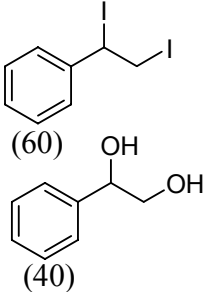
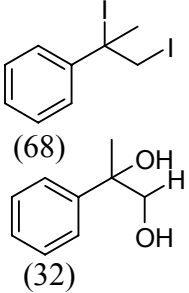
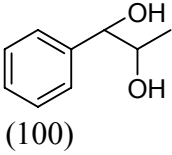
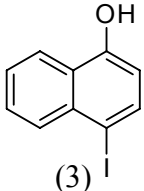
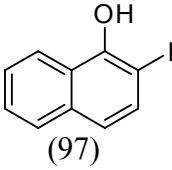
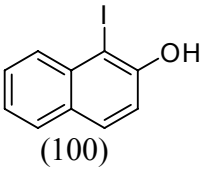
5.3.2.2. Oxyhalogenation of aromatics

5.3.2.2.1. Oxyiodination

Iodination of arenes (Table 5.3) was achieved at moderate pH (~ 4). The reaction occurred at room temperature (298 K) and atmospheric pressure. The iodinating agent used was KI/H₂O₂; pH of the medium was adjusted with HNO₃. Complete conversion of range of arenes into corresponding iodo products was achieved in just 4 h. Iodination of aniline and anisole can occur at both ortho- and para positions. However, only the para-isomer formed selectively over WO_x(20)-SBA-15. Iodination of p-Cl-phenol is more

Table 5.3. Oxyiodination of organics over WO_x(20)-SBA-15

Entry No.	Substrate	Conversion (mol%)	Product Selectivity	
			Para	Others
1.	Anisole	100	 (100)	(0)
2.	Aniline	100	 (100)	(0)
3.	Phenol	100	 (66)	 (34)
4.	<i>p</i> -Cl-phenol	100	(0)	 (100)
5.	<i>p</i> -Anisidine	100	(0)	 (60)  (40)
6.	<i>o</i> -Aminophenol	100	 (100)	(0)
7.	<i>o</i> -Nitrophenol	100	 (100)	(0)

8.	<i>o</i> -Toluidine	81.5	 (100)	(0)
9.	Styrene	100	(0)	 (60) (40)
10.	α -Methyl styrene	100	(0)	 (68) (32)
11.	β -Methyl styrene	17.8	(0)	 (100)
12.	α -Naphthol	100	 (3)	 (97)
13.	β -Naphthol	17.8	(0)	 (100)

Reaction Conditions: Catalyst = 0.050 g, substrate = 2 mmol, H₂O₂ (30% aq.) = 5 mmol, KI = 5 mmol, CH₃CN and H₂O = 5 mL each, pH was adjusted to ~3 by adding required quantity of conc. HNO₃ acid, temperature = 298 K, reaction time = 4 h.

facile than neat phenol. Ortho-iodo product formed in 100% selectivity in the former while phenol yielded selectively the para-product. In the case of styrene and methyl styrene the olefinic bond is preferentially attacked forming diiodo and iodohydrin compounds. Additionally, diol was also formed. Methyl substitution in methyl styrenes has a marked effect on product selectivity (Table 5.3). Iodination of aniline was performed at different reaction temperatures. Increase in aniline conversion beyond 298 K was marginal.

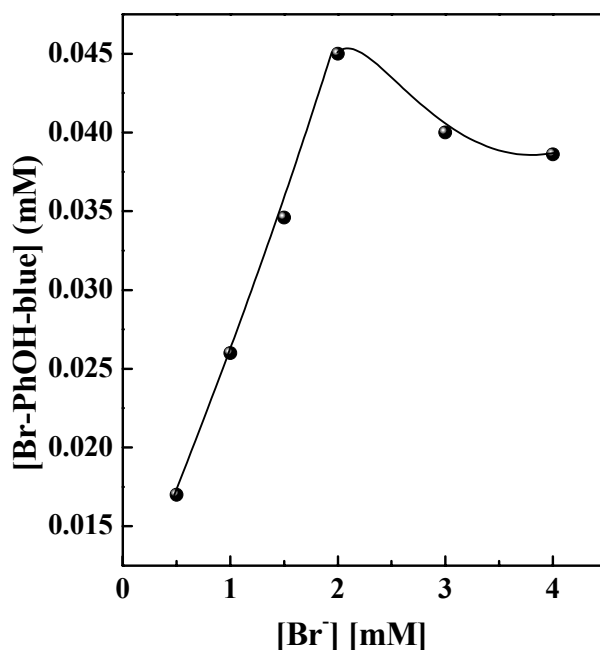
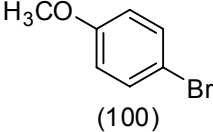
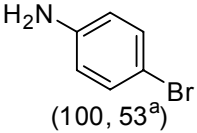
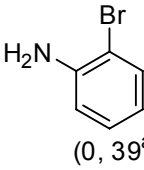
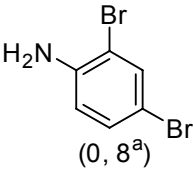
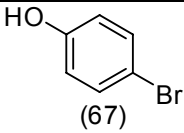
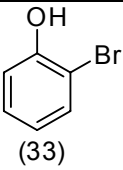
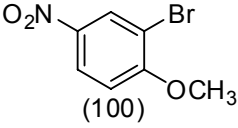
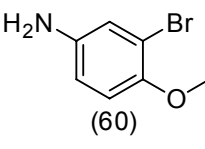
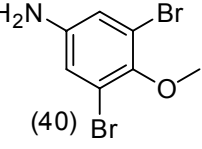
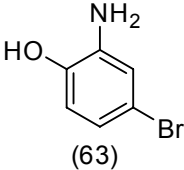
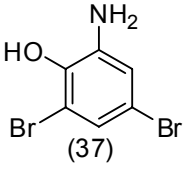
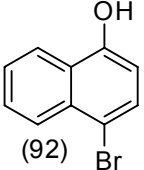
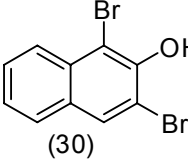
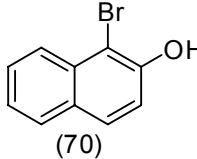


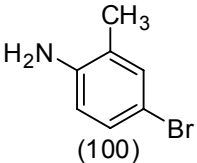
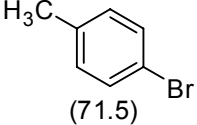
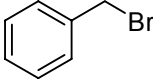
Fig. 5. 10. Influence of Br⁻ concentration on oxybromination of phenol red over WO_x(20)-SBA-15.

5.3.2.2.2. Oxybromination

The reaction was carried out at ambient temperature and pressure under mild acidic conditions (Table 5.4). Among various substrates investigated, substituted anilines, anisole, naphthol, phenol, 1, 3, 5-trimethyl benzene were found to be the most reactive

Table 5.4. Oxidative bromination of aromatics using WO_x-SBA-15 (20%)

Entry No.	Substrate	Conversion (mol %)	Product Selectivity (%)	
			Para	Others
1.	Anisole	100	 (100)	(0)
2.	Aniline	100 (69) ^a	 (100, 53 ^a)	 (0, 39 ^a)  (0, 8 ^a)
3.	Phenol	100	 (67)	 (33)
4.	<i>p</i> -nitro anisole	93.7	(0)	 (100)
5.	<i>p</i> -Anisidine	100	(0)	 (60)  (40)
6.	<i>o</i> -Aminophenol	100	 (63)	 (37)
7.	α -naphthol	100	 (92)	(8)
8.	β -naphthol	100	(0)	 (30)  (70)

9.	<i>o</i> -Toluidine	63	 (100)	(0)
10.	Toluene	14	 (71.5)	 (28.5)

Reaction Conditions: Catalyst WO_x-SBA-15(20%), Substrate, 2 mmol; H₂O₂-5 mmol; KBr- 5 mmol; HNO₃-0.180 g; acetonitrile 5 ml + water 5 ml as solvent; reaction temperature, 298 K; reaction time, 4 h, Atmospheric pressure.

^aValues in the parentheses are those corresponding to neat tungsten oxide.

(100% conversion). In case of phenol, aniline, anisole etc., *para*-brominated isomer formed with 100% selectively. In oxidative bromination, a mixture of acetonitrile and water was used as a solvent system. In the case of phenol, aniline, anisole the major product was the *para*-isomer, while in the case of *p*-chloroaniline, the *ortho*-bromo product formed with 100% selectivity. When naphthol was brominated under similar conditions, α -naphthol gave about 92% *para*-isomer and β -naphthol gave 70% *ortho*-product along with dibrominated product. Non-activated aromatics like toluene are weakly active compared to activated aromatics. In case of cyclohexane, a non-activated cyclic alkane, a conversion of 63% was observed; only one product was formed. Out of all these nanoscopic metal oxides investigated, WO_x(20)-SBA-15 was found more active than other three catalysts. Catalytic activity increased with tungsten oxide loading up to 20 wt% (Table 5.5).

Table 5.5. Oxybromination of anisole

Catalyst	Substrate	Conversion (mol%)	Selectivity of para- brominated product (%)
WO _x (20)-SBA-15	Anisole	100	100
WO _x (15)-SBA-15	Anisole	68.6	100
WO _x (10)-SBA-15	Anisole	51.2	100
MoO _x (20)-SBA-15	Anisole	96.3	100
TiO _x (6)-SBA-15	Anisole	62.8	100
VO _x (11)-SBA-15	Anisole	44.3	100

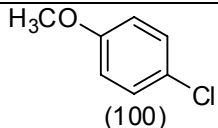
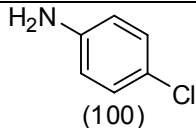
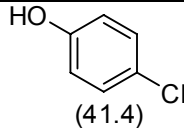
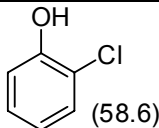
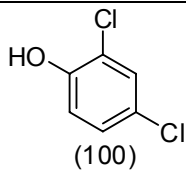
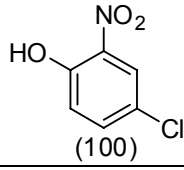
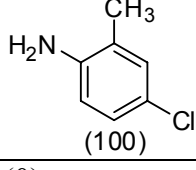
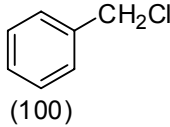
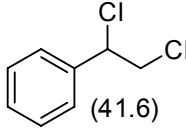
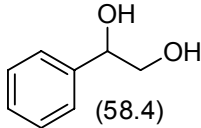
Reaction conditions: Substrate = 2 mmol, KBr = 5 mmol, 30%aq. H₂O₂ = 5 mmol, catalysts = 0.05 g, solvent (CH₃CN + H₂O) = 10 ml, HNO₃ = 2 mmol, time = 4 h.

5.3.2.2.3. Oxychlorination

Organic chlorinated compounds play an important role in synthetic organic chemistry. *p*-Chloroaniline is used as an intermediate in the manufacture of dyes, pigments, agricultural chemicals and pharmaceuticals. It is a persistent environmental degradation product of some herbicides and fungicides. And para-chloro anisole is used with formaldehyde for preparation of condensation polymers [27]. The chlorophenols make up an important class of industrial chemical compounds. They are used as either intermediate in the synthesis of agrochemicals, dyestuffs, and pharmaceuticals or directly in formulations [28].

Chlorination of various organic compounds was achieved at moderate pH conditions (pH ~ 3). Activated aromatics like anisole, phenol, aniline etc. gave very high conversion and chlorinated product selectivity (Table 5.6). Like bromination and

Table 5.6. Oxychlorination of organics over WO_x(20)-SBA-15

Entry No.	Substrate	Conversion (mol %)	Product Selectivity (%)	
			Para-	Others
1.	Anisole	100		(0)
2.	Aniline	100		(0)
3.	Phenol	5.3		
4.	<i>p</i> -Cl-Phenol	33.3	(0)	
5.	<i>o</i> -nitrophenol	100		(0)
6.	<i>o</i> -Toluidine	100		(0)
7.	Toluene ^a	8	(0)	
8.	α -Methyl styrene	54.3	(0)	 

Reaction Conditions: Catalyst = 0.050 g, substrate = 2 mmol, H₂O₂ (30% aq.) = 5 mmol, HCl = 5 mmol, pH of the reaction was adjusted to ~ 2.5. solvent (CH₃CN / H₂O) = 5 ml each, reaction temperature = 298 K, reaction time = 4 h.

^aReaction conducted at 343 K.

iodination substrates like aniline, anisole etc. gave para-chlorinated product regioselectively. Oxychlorination is a tougher reaction compared to oxybromination and iodination. It is interesting to note that SBA-15-supported tungsten oxide showed high activity even in the chlorination reaction and thereby a superior mimic for chloroperoxidase enzymes.

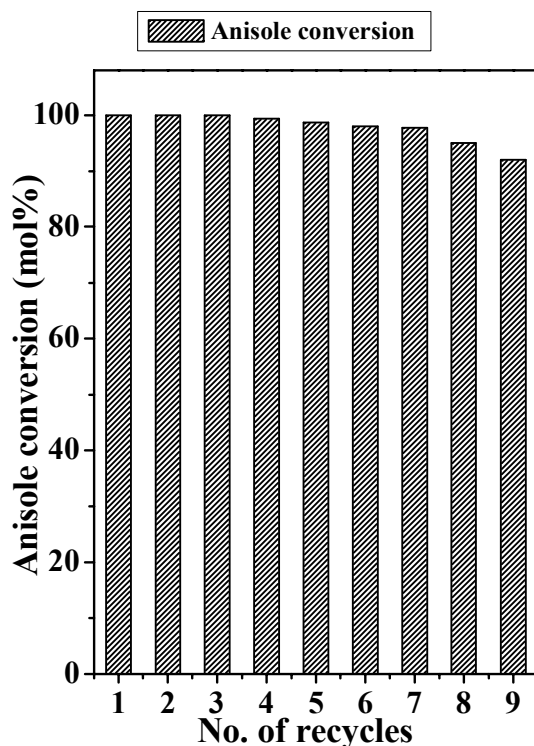


Fig. 5.11. Catalyst reusability: oxybromination of anisole over $\text{WO}_x(20)$ -SBA-15.

5.3.2.2.4. Catalyst reusability

The stability of the catalyst ($\text{WO}_x(20)$ -SBA-15) was confirmed by reusing it in several recycling experiments. In each run, after completion of the reaction, the catalyst was separated from the reaction mixture by filtration, washed with a solvent mixture containing dichloromethane and acetone and dried in air followed by activation at 473 K

for 2 h. The catalyst, thus, activated was then used next recycle. The results with the recycled catalyst invariably showed unaltered activity in para-bromination of anisole suggesting that $\text{WO}_x(20)$ -SBA-15 is a stable heterogeneous catalyst (Fig. 5.11). In this respect, it is important to stress that $\text{WO}_x(20)$ -SBA-15 catalyst, in contrast to enzymes, was not sensitive to oxidative destruction and thereby, showed superior performance over homogeneous catalyst systems. Reusability was also confirmed in oxyiodination reaction. $\text{WO}_x(20)$ -SBA-15 was reused in nine recycles with little loss in activity/product selectivity.

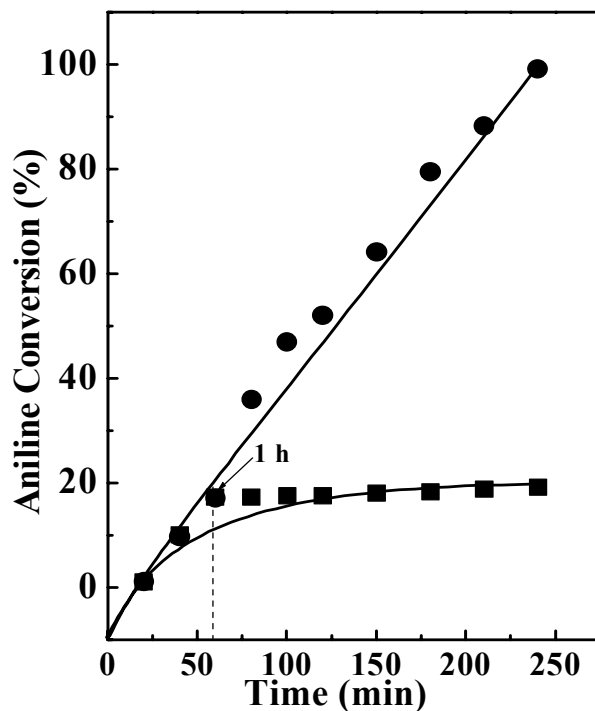


Fig. 5.12. Catalyst leaching test: Oxybromination of aniline over $\text{WO}_x(20)$ -SBA-15.

To check any leaching of active sites into the reaction medium during the reaction, the catalyst was filtered and separated at the end of 1 h and the reaction was continued for

another 3 to 7 hr without any catalyst. It may be noticed from Fig. 5.12 that the reaction did not proceed any further in the absence of catalyst. The conversion of aniline to *p*-bromoaniline remained the same.

The catalytic activity varied with the Lewis acidity (NH₃-TPD) of the catalyst in the order: WO_x(20)-SBA-15 > MoO_x(20)-SBA-15 > TiO_x(6)-SBA-15 > VO_x(11)-SBA-15. The dispersed metal oxides showed enhanced catalytic activity than the bulk oxides (Table 5.2 and 5.5).

5.3.2.2.5. Spectroscopic evidence for peroxidative mechanism

In-situ diffuse reflectance UV-visible spectroscopy (DRUV) was used to probe the mechanism of oxyhalogenation and the transient species formed during the interaction of SBA-15 supported metal oxides with H₂O₂/Br⁻ system (Fig. 5.13.). Upon addition of H₂O₂, the white colored solid rapidly turned to pale yellow. A new absorption band which was absent in bare catalysts was observed at around 364 nm. By analogy with the literature, this band at 364 nm is attributed to formation of metal-peroxo species [11]. The band at 260 nm corresponding to O²⁻ → W/Vⁿ⁺ charge transfer band had undergone a blue shift to 220 nm. When the catalyst was treated with H₂O₂ + KBr solution, there was a relative increase in overall intensity of the bands. In addition to the band at 364 nm due to metal-peroxo species, a new band was observed at 276 nm. This band was attributed to Br₃⁻ species [10]. So, in analogy to the active vanadium site in marine haloperoxidase enzymes, nanocrystalline metal oxides supported on SBA-15 transform into their peroxo form upon exposure of the solid catalyst to H₂O₂. This reactive peroxo intermediate in the presence of bromide ions produces perbromide species (Br₃⁻) which, then, participates in

the halogenation reactions. Hence, halogenation of arenes with H_2O_2 -KX system over metal oxides supported on SBA-15 probably proceeds via a peroxidative mechanism.

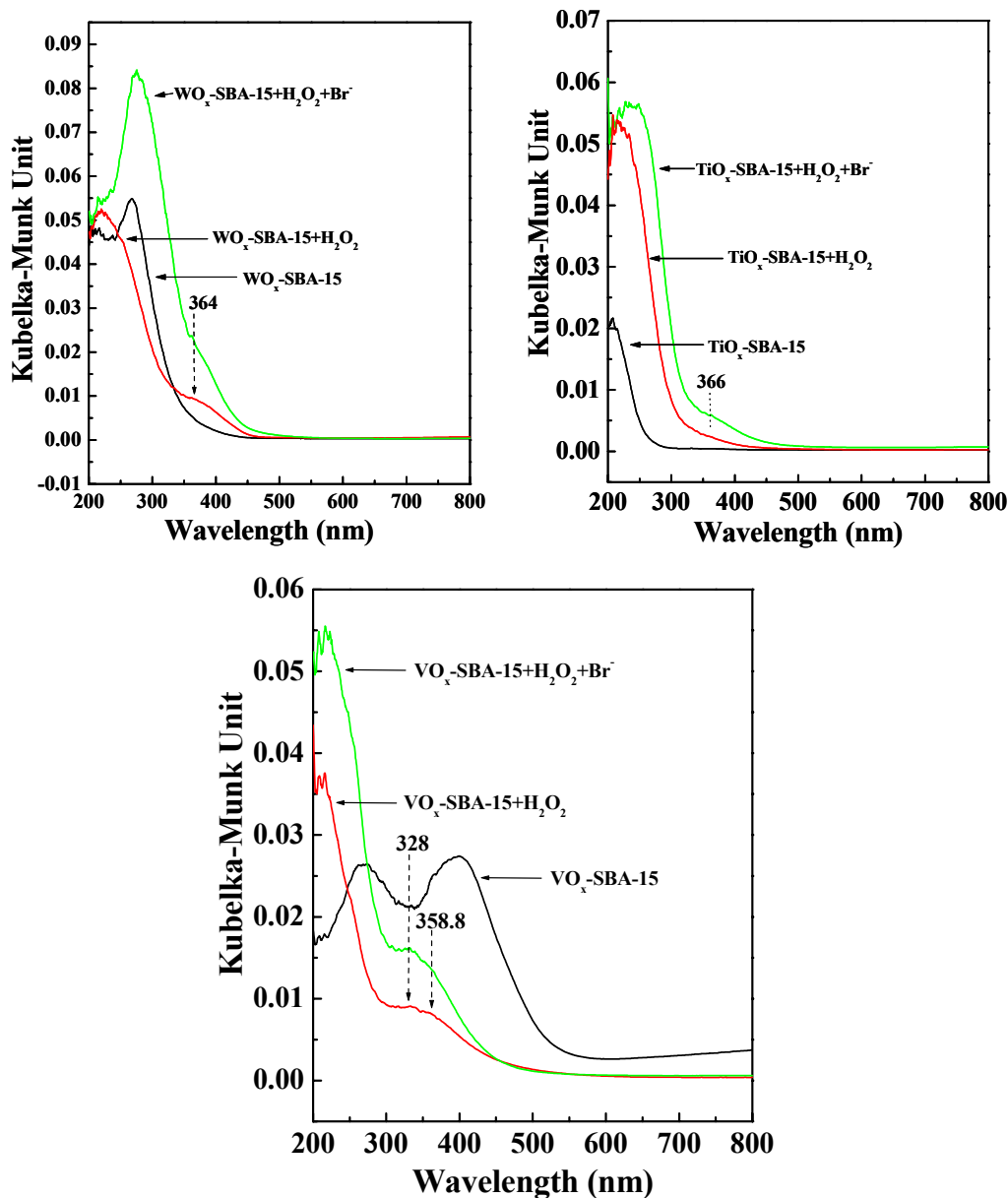


Fig. 5.13. SBA-15 supported metal oxides and their interaction with aq. H_2O_2 and $\text{H}_2\text{O}_2 + \text{KBr}$ system.

5.4. Conclusions

Titanium, vanadium, molybdenum and tungsten oxides supported on SBA-15 were prepared by the post-synthesis techniques. Structural and spectroscopic characterization studies revealed that the metal oxides on SBA-15 are highly dispersed. Several aromatic compounds have been quantitatively halogenated *at room temperature and moderate acidic conditions* over these catalysts with a H₂O₂-halide ion system. The para-isomer was formed with 100% selectivity. These catalysts are reusable and no leaching of metal ions into the reaction mixture was detected. The activity of these catalysts is higher than most of the hitherto known solid catalysts and neat metal oxides.

5.5. References

- [1] J. H. Dawson, Science 240 (1988) 433.
- [2] J. Littlechild, Curr. Opin. Chem. Biol. 3 (1999) 28.
- [3] D.C. Crans, J.J. Smee, E. Gaidamauskas, L. Yang, Chem. Rev. 104 (2004) 849.
- [4] J. K. Still, Pure Appl. Chem. 57 (1985) 1771.
- [5] (a) N. Miyauro, A. Suzuki Chem. Rev. 95 (1995) 2457, (b) I.P. Beletskaya, A.V. Cheprakov, Chem. Rev. 100 (2000) 3009.
- [6] W. Cabri, I. Canadiani, Acc. Chem. Res. 28 (1995) 2.
- [7] P. Ratnasamy, A.P. Singh, S. Sharma in Handbook of Heterogeneous Catalysis Ed. G. Ertl, H. Knözinger, J. Weitkamp, VCH Verlagsgesellschaft mbH, Weinheim, Vol. 5 (1997) 2348.
- [8] (a) S. Cacchi, L. Caglioti, Synthesis (1979) 64. (b) A. Bongini, G. Cainelli, M.

- Contento, F. Manescalchi, *Synthesis* (1980) 143.
- [9] (a) H. Fu, H. Kondo, Y. Ichikawa, G. C. Look, C. H. Wong, *J. Org. Chem.* 57 (1992) 7265. (b) M. C. Carrenõ, J. L. Garcí'a Ruano, G. Sanz, M. A. Toledo, A. Urbano, *J. Org. Chem.* 60 (1995) 5328. (c) A. Tenaglia, O. Pardigon, G. Buono, *J. Org. Chem.* 61 (1996) 1129. (d) G. Majetich, R. Hicks, S. Reister, *J. Org. Chem.* 62 (1997) 4321.
- [10] R. Raja, P. Ratnasamy, *J. Catal.* 170 (1997) 244.
- [11] (a) B.F. Sels, D.E. De Vos, M. buntinx, P.A. Jacobs, *J. Catal.* 216 (2003) 288. (b) B.F. Sels, D.E. De Vos, P.A. Jacobs, *J. Am. Chem. Soc.* 123 (2001) 8350.
- [12] L. Saikia, D. Srinivas, P. Ratnasamy, *Micropor. Mesopor. Mater.* 104 (2007) 225.
- [13] F. Feng, G.E. Fryxell, L.-Q. Wang, A.Y. Kim, K.M. Kemner, *Science* 276 (1997) 923.
- [14] L. Mercier, T.J. Pinnavaia, *Adv. Mater.* 9 (1997) 500.
- [15] A. Stein, B.J. Melde, R.C. Schrodin, *Adv. Mater.* 12 (2000) 1403.
- [16] W.M. Van Rhijn, D.E. De Vos, B.F. Sels, W.D. Bossaert, P.A. Jacobs, *Chem. Commun.* (1998) 317.
- [17] D. Das, J.-F. Lee, S. Cheng, *Chem. Commun.* (2001) 2178.
- [18] E. Cano-Serrano, J.M. Campos-Martin, J.L.G. Fierro, *Chem. Commun.* (2003) 246.
- [19] S. Razl Seyedmonlr, S. Abdo, and R. F. Howe, *J. Phys. Chem.* 86 (1982) 1233.
- [20] Z. Zhang, J. Suo, X. Zhang, S. Li, *Appl. Catal. A: Gen.* 179 (1999) 11.
- [21] X. Ming, *J. Phys. Chem.* 107 (2003) 8972.

- [22] Q. Yang, S. Wang, J. Lu, G. Xiong, Z. Feng, Q. Xin, C. Li, *Appl. Catal. A: Gen.* 194 (2000) 507.
- [23] W. Li, *Chem. Mater.* 17 (2005) 2241.
- [24] F. D. Hardcastle, I. E. Wasch, *J. Phys. Chem.* 95 (1991) 5031.
- [25] L.-X. Dai, K. Tabata, E. Suzuki, and T. Tatsumi, *Chem. Mater.* 43 (2001) 208.
- [26] P. Brandão, A. Philippou, N. Hanif, P. Ribeiro-Claro, A. Ferreira, M. W. Anderson, and J. Rocha, *Chem. Mater.* 14 (2002) 1053.
- [27] *Kirk-Othmer Encyclopedia of Chemical Technology* 11 (2004) 454.
- [28] (a) J. E. Bailey, M. Bohnet, J. Brinker (Eds.), *Ullmann's Encyclopedia of Industrial Chemistry*, 6th ed., Wiley-VCH, Weinheim, 1998. (b) L. Menini, E. V. Gusevskaya *Appl. Catal. A: Gen.* 309 (2006) 122.

CHAPTER - 6

Summery and Overall Conclusions

Designing of efficient and selective, solid catalyst is still a challenging task in catalysis research. Mesoporous silica materials have a major advantage, for example, the easy molecular diffusivity of bulk molecules of fine and pharmaceutical interest inside their pores compared to microporous zeolites. However, the former containing Al in their lattice exhibit weaker acidity than the latter. Modification of the mesoporous silica surfaces with acidic functionalities like thiol and sulfonic groups or transition metal oxides generates a new era of more efficient, solid acid catalysts. Further, these surface-modified, mesoporous silica can be used as supports for grafting/immobilizing active centers like homogeneous metal complex catalysts. The supported metal catalysts can in a way mimic the functionality of metalloenzyme and proteins in oxidation reactions. In view of the above, this thesis has reported the synthesis, characterization and catalytic activity studies of some functionalized, ordered, mesoporous silica materials.

Three-sets of surface-modified SBA-15 materials have been investigated in this work. The first-set consisted of SBA-15 modified with organo-acidic (propyl thiol and propyl sulfonic acid) moieties. The second-set consisted of Mn complexes grafted on propyl amine, thiol and sulfonic acid-functionalized SBA-15. The third-set composed of nanocrystalline metal oxides supported on SBA-15. Catalytic activities of the first-set have been investigated in several acid-catalyzed reactions viz., regio- and stereoselective ring-opening of epoxides with amines and alcohols, tert.-butylation of glycerol, esterification and three-component-Mannich reactions (Chapter 3). The second-set showed efficient performance in chemo-, regio- and stereoselective aerial oxidation of monoterpenes at ambient conditions (Chapter 4). TiO_x , VO_x , MoO_x and WO_x supported

on SBA-15 mimicked the functionality of haloperoxidase enzymes. Several arenes have been para-selectively oxyhalogenated under mild reaction conditions (Chapter 5).

Thiol, sulfonic acid and amine functionalized SBA-15 has been prepared by grafting the corresponding acidic and basic precursors to the surface silanol groups of SBA-15. Various amounts of sulfonic acid functionalized SBA-15 has also been prepared by the direct synthesis (co-condensation) technique. However, in certain reactions the materials prepared by the grafting technique showed superior catalytic performance than those by the direct synthesis technique. The composition, structure and texture properties of the materials were determined by C, H & N analysis, X-ray powder diffraction (XRD), transmission electron microscopy (TEM), N₂-adsorption & desorption, Fourier transform infrared (FTIR) and thermal analysis (TG-DTA). Acidic properties were determined by temperature-programmed desorption of NH₃ (NH₃-TPD) and ion-exchange techniques. The ion-exchange technique gave more reliable results compared to NH₃-TPD. The grafted moieties decomposed at higher temperature and so the results obtained by NH₃-TPD were not accurate. Sulfonic acid functionalized SBA-15 was found more acidic than the thiol functionalized and bare SBA-15. The sulfonic acid functionalized SBA-15 showed highly efficient, catalytic activity in opening of the oxirane ring with nitrogen (aromatic as well as aliphatic amines) and oxygen (alcohols)-containing nucleophiles. The reactions occurred at ambient temperatures and without any solvent. A range of β -amino alcohols was synthesized with high regio- and stereoselectivity. The mesoporous, solid acids of the present study were found reusable and exhibited significantly higher catalytic activities than the hitherto known acid catalysts. Adsorption studies revealed that both the epoxide and amine compete for adsorption on the acidic sites (-SO₃H) on

the catalyst surface. Epoxide adsorption and activation on acid sites were found to be essential. Catalytic activity decreased with increasing basicity of the amine/alcohol or the dielectric constant of the solvent. Polar solvent molecules, when present, also compete for adsorption with the reactant molecules. The sulfonic acid functionalized SBA-15 catalysts were found efficient also for etherification of glycerol with tert.-butanol. Di- and tri-tert.-butyl glycerol ethers, which can be used as oxygenates, have formed in good selectivity along with mono-tert.-butyl glycerol ether. Also good activity was shown by these catalysts for esterification of acetic acid with alcohols and three-component Mannich reaction at ambient temperatures.

SBA-15 molecular sieves were functionalized with propylamine, propylthiol and propylsulfonic acid groups. Mn(Salen)Cl and Mn(TPP)Cl complexes were grafted on these organo-functionalized SBA-15. The support and the type of organo-functional group influenced the electronic structure (oxidation state and redox behavior) and chemoselectivity of the Mn-complexes in the oxidation of limonene. The Mukaiyama-type oxidation reactions were carried out at ambient temperatures and using molecular oxygen as oxidant. The Mn ions were reduced from +3 to +2, the extent of this reduction on different supports decreasing in the case of Mn(Salen)Cl complexes in the order: SBA-15-*pr*-SH > SBA-15-*pr*-SO₃H > SBA-15-*pr*-NH₂. Mn(Salen)Cl supported on propylthiol-functionalized SBA-15 yielded the 1,2-limonene epoxide with 100% chemo- and regioselectivity. Higher electron density at the site of Mn ions and the consequent lower redox potential of the Mn-complexes on immobilization are the probable causes for their efficient and selective catalytic activity. Solvents, additives (N-MeIm) and co-reagents (iso-butyraldehyde), which facilitated formation of Mn²⁺ ions, enhance the

catalytic activity. A part of the Mn complexes was leached out of the solid phase during the reaction and the extent of this with different catalysts decreased in the order: SBA-15-*pr*-NH₂-Mn(Salen)Cl > SBA-15-*pr*-SO₃H-Mn(Salen)Cl > SBA-15-*pr*-SH-Mn(Salen)Cl. These catalysts showed selective activity for the epoxidation of α -pinene and 3-carene at ambient conditions. The nature of the support as well the ligand (Salen vs TPP) played a crucial role controlling the redox behavior, molecular electronic structure and thereby, the catalytic activity of the Mn complexes. The study thus revealed that the ability to fine-tune the redox potential (and thereby the catalytic activity / selectivity) of supported metal ions by modification of the acidity of the underlying support is a powerful tool in the design of catalysts.

TiO_x, VO_x, MoO_x and WO_x were supported on SBA-15 by the post synthesis technique. The materials were characterized by several physicochemical technique including FTIR, laser Raman and diffuse reflectance UV-visible. Acidic properties of the materials were determined by NH₃-TPD. Nanocrystallinity and dispersion of metal oxides was noted upon supporting on SBA-15. These SBA-15 modified with metal oxides mimicked the functionality of haloperoxidase enzymes. A range of arenes were oxyhalogenated (chlorination, bromination and iodination) with the H₂O₂-halide ion system. The reaction occurred at room temperature (298 K) and moderate acid pH (3 – 5). Unlike the hitherto known solid catalysts, these catalysts yielded the para-halogenated product (with 100% selectivity) in the case of substituted aromatics, like aniline, anisole, etc. Catalytic activity of these supported oxides is higher by several orders of magnitude than the corresponding “neat” bulk oxides. Catalytic activity decreases in the order: WO_x > MoO_x > TiO_x > VO_x, and with halide ions: I⁻ > Br⁻ > Cl⁻. The catalysts were reusable

and no leaching of metal ions was detected. In situ spectroscopic measurements revealed that oxyhalogenation over these modified SBA-15 catalysts occurs via the peroxidative mechanism proposed in the case of vanadium haloperoxidases.

By and large, this thesis reports a new class of organofunctionalized SBA-15 materials, their characterization and application as regio-, stereo and chemoselective catalysts in several organic transformations at moderate and solvent-free reaction conditions.

List of Publications

1. Chemo-, regio- and stereo-selective aerial oxidation of limonene to the endo-1,2-epoxide over Mn(Salen)-sulfonated SBA-15
L. Saikia, D. Srinivas, P. Ratnasamy
Applied Catalysis A: General 309 (2006) 144–154.
2. Comparative catalytic activity of Mn(Salen) complexes grafted on SBA-15 functionalized with amine, thiol and sulfonic acid groups for selective aerial oxidation of limonene
L. Saikia, D. Srinivas, P. Ratnasamy
Microporous and Mesoporous Materials 104 (2007) 225-235.
3. Regio- and stereoselective synthesis of β -amino alcohols over titanosilicate molecular sieves.
J.K. Satyarthi, **L. Saikia**, D.Srinivas, P. Ratnasamy
Applied Catalysis A: General 330 (2007) 145-151.
4. Activation and reactivity of Epoxides on Solid Acid Catalysts.
L. Saikia, J.K. Satyarthi, D.Srinivas, P. Ratnasamy.
Journal of Catalysis, 252 (2007) 148 - 160.
5. Redox and selective oxidation properties of Mn complexes grafted on SBA-15.
L. Saikia, D.Srinivas.
Catalysis Today (2008) (Accepted; Article in Press).
6. Double Metal Cyanides an efficient catalysts for synthesis of β -amino alcohols under solvent free conditions
L.Saikia, J. K. Satyarthi, R. Gonnade, D.Srinivas, P. Ratnasamy
Catalysis Letters (2008) (Accepted; Article in Press).
7. Funtionalized SBA-15 and its Catalytic Applications in Selective Organic transformation
D.Srinivas and **L.Saikia**
Catalysis Survey from Asia (Accepted; Review Article in Press).
8. Biomimetic Oxyhalogenation of Aromatics over SBA-15 supported Nanoscopic group IV-VI metal oxides
L.Saikia, M. Rajesh, D. Srinivas P.Ratnasamy
Appl. Catal. A. Gen. (Communicated)

PCT/Indian Patent filed

1. A process for the preparation of primary alkyl glycerol ethers useful as biofuel additive from glycerol (226NF2007; 2582DEL2006; NCL-2/2006)
D. Srinivas, P. Ratnasamy, **L. Saikia**